THE MECHANICS AND CONTROL OF ROBOTIC SYSTEMS EXPLOITING VISCOUS PHENOMENA FOR PLANAR LOCOMOTION

by

Peter Mikael Hassing

A dissertation submitted to the faculty of
The University of North Carolina at Charlotte
in partial fulfillment of the requirements
for the degree of Doctor of Philosophy in
Mechanical Engineering

Charlotte

2015

Approved by:

_____
Dr. Scott Kelly

_____
Dr. Peter Tkacik

_____
Dr. Russ Keanini

_____
Dr. Badrul Chowdhury

_____
Dr. Antonis Stylianou

ABSTRACT

PETER MIKAEL HASSING. The mechanics and control of robotic systems exploiting viscous phenomena for planar locomotion. (Under the direction of DR. SCOTT KELLY)

Viscous phenomena can be used to aid in the locomotion and control of robotic systems. With the aid of Lagrangian reduction techniques, it is shown that dissipation can be used to model nonholonomic, holonomic, and kinematically constrained systems. This is shown theoretically, analytically, and numerically for a class of robotic systems. Using techniques from geometric mechanics, control problems for novel planar robots that incorporate nonholonomic constraints, dissipation, and geometric phase are explored. A robotic fish is introduced, and experiments demonstrate it can harvest energy from fluid vortices to assist in propulsion, consistent with geometric models in the literature. Experimental fluid vortices are also generated and characterized with the aid of particle image velocimetry.

ACKNOWLEDGMENTS

I would like to thank Scott Kelly for his guidance and mentoring. It has truly been a privilege to be his student throughout the years. My deep gratitude goes to Dr. Peter Tkacik, along with Patrick Tkacik, Akshar Patel, and Daniel Barnhardt. Without their help, hard work, and long days in the lab, the experiments would have never happened. Jerry Zacharias' help in developing the original micro-controller code and electrical system was invaluable. I gratefully acknowledge my labmates Tapobrata Battacharya and Mike Fairchild for encouraging me to continue with my research and education amid the hardships of the degree, for lengthy discussions about geometric mechanics and more trivial topics, and for all the fun we had in the lab. Finally, many thanks to family and friends for being supportive during the many, many years of graduate school.

TABLE OF CONTENTS

LIST OF FIGURES

LIST OF TABLES

CHAPTER 1: INTRODUCTION

Mechanics is the paradise of the mathematical sciences, because by means of it one comes to the fruits of mathematics.

Leonardo da Vinci

1.1 Previous Work

Deepening understanding of mechanical systems is as important today as it was when the kinematics of motion were formalized in Galilei (1638), the motions of the planets were quantified in Kepler (1609), and the laws of motion were forumulated in Newton (1687). Much of the mathematics used today were developed in an effort to understand more about the mechanical nature of the universe. Because mechanics sits at the confluence of applied mathematics and engineering, its study often serves as the beginning for many rich mathematical theories into the foundations of the engineering sciences. The mathematical fervor affixed to the field lends to its richness and depth and allows for new developments in a field as old as the scientific method itself.

The mathematical discipline of differential geometry was pioneered in the works Gauss (1822, 1827, 1844), and Monge (1785a, 1785b) (see Struik (1933) for a historical overview). This discipline applied calculus to curves, surfaces, and other topological entities. In Lie (1891), the author developed continuous symmetry groups to account for the intuitive notion that an object's velocity was the same whether in a local

frame or a global frame. In Noether (1918), the author recognized these symmetries as inherent in Lagrangian systems and linked them to conservation laws. All these ideas were eventually tied together into the modern-day field of geometric mechanics (see Holm (2009), and Marsden and Ratiu (1998) for a thorough introductions to the field).

The topic of reduction for Lagrangian systems was approached in Routh (1884). In his work, he demonstrated that for systems with cyclic variables, the Lagrangian could be rewritten in a way that eliminated the cyclic variables. This was feasible because the the conjugate momenta corresponding to cyclic variables were conserved quantities. Routh's procedure worked well for systems with an Abelian symmetry group. The reduction method for the non-Abelian case was developed much more recently, with its origins in the work of Smale (1970), Marsden and Weinstein (1974), and Meyer (1973). In Marsden and Scheurle (1993a) and Marsden et al. (1990), the Lagrangian version of symplectic reduction explored in Marsden and Weinstein (1974) was derived. The work in Smale (1970), Abraham and Marsden (1978), and Kummer (1981) constructed a "mechanical connection" that maps tangent vectors of a system's internal configuration variables to the frame velocities on the reduced space. In Bloch et al. (1996), the authors extended reduction techniques to systems with nonholonomic constraints. Nonholonomic constraints, or simply, nonintegrable constraints, were studied extensively in Chaplygin (1911,1949), Cartan (1928), and were seen as fundamental objects in the field of analytical mechanics. Thus, their treatment in the context of Lagrangian reduction was seen as a natural and important topic. In Kelly and Murray (1996), the authors researched reduction for unconstrained

dissipative systems.

Techniques from differential geometry extend themselves well into the field of fluid mechanics. In Arnol'd (1966), the author addressed the evolution of an inviscid, incompressible fluid as a problem in geometric mechanics. In Marsden and Weinstein (1983), they revisited inviscid flow in the context of Hamiltonian reduction. See Arnol'd and Khesin (1998) for an exposition on the topic. The dynamics and stability of a rigid vehicle immersed in an irrotational field was studied in Leonard and Marsden (1996). In Ozcazanc (1994), the dynamical interaction of a finite vortical fluid and a free rigid container was studied. Coupled motion of vortices and planar rigid bodies were studied in Koiller (1987).

Techniques from differential geometry also extend themselves well into the field of control theory. The marriage of the fields is the subject area known as geometric control theory. Its development was driven by the realization that tools from differential geometry and Lie theory could be used to extend linear control theory into a nonlinear setting. The surveys of Brockett (1983c) and Brockett (2014) give a detailed account of the growth of the field. Significant work has since been carried out to apply geometric control techniques to a variety of robotics problems. In Kelly and Murray (1994), the authors calculated a mechanical connection for a two- wheeled kinematic robot. They gave a geometric interpretation of a theorem formalized in Chow (1949), and then applied it to the controllability analysis of a four-wheeled cart robot. They used the geometric phase of an inchworm robot to optimize gaits for locomotion. It was in Marsden et al. (1990) that geometric phase was introduced for coupled planar rigid bodies. In Bloch et al. (1996), a robotic snakeboard with

nonholonomic constraints was analyzed. Dissipation and drift was added to the snakeboard in Ostrowski (1998). Since the system possessed drift, a unique controllability analysis, developed in Sussman (1987), was necessary in analyzing the controllability of the system. In Osborne and Zenkov (2005), the authors worked out a problem that explored the modeling and steering of a nonholonomic system using a moving mass. The authors of Kelly et al. (2011) and Kelly et al. (2012) analyzed an underactuated nonholonomic system with a rotating mass.

The theoretical treatment of biological aquatic locomotion has seen much attention from the academic community. Works such as Lighthill (1975), Wu (1971), and Newman and Wu (1974) have made theoretical contributions across the full spectrum of aquatic locomotion. They discuss the energy efficiency, stealth, and maneuverability observed in such locomotion. The efficiency gains that fish can attain by swimming in schools was hypothesized in Belyayev (1969). The authors of Hemelrijk et al. (2014) studied fish swimming and schooling computationally, and noted the collective gains in efficiency that fish attain when swimming in schools. Treating the subject of fish swimming from a geometric perspective, and building on the previously mentioned work that involved coupled rigid bodies and fluid vortices, the authors in Kelly and Murray (1998) integrated Lagrangian reduction techniques into a theory of aquatic robotic locomotion. They used this theory to develop models and control strategies for a fish-like swimming robotic system. In Kelly et al. (2012), the authors built on this work and incorporated an oscillating Joukowski foil to represent the shape of a carangiform fish. They used this model in a series of simulations to evaluate open-loop and closed-loop control strategies for turning, propulsion, and wake vortex

energy harvesting.

Fish swimming is not just a topic that has been treated theoretically; it has been treated experimentally as well. Robotic versions of fish have been explored significantly in the literature. In Triantafyllou (1995), researchers developed one of the first such robots, RoboTuna. In Kelly (1998), the author worked on a set of experiments to complement his theoretical treatment of fish swimming. Other robotic incarnations of swimming fish have been documented in Kumph (1998), Morgansen (2007), and Hirata (2000). Robotic experiments involving an array of oscillating hydrofoils were carried out in Kelly and Xiong (2005) to study the effects of hydrodynamic coupling on schooling locomotion. Fish robots have recently seen applications in pollutant detection in Aron (2012), and with the Office of Naval Research for potential military uses in Ruffo (2010). Such successes motivate the continued study of these robotic systems.

To experimentally capture the effects of vortex wake on a swimming machine, one has to first generate fluid vorticies. The literature contains many studies on the experimental generation of such fluid vortex structures. These vortex structures are frequently analyzed with the aid of particle image velocimetry (PIV) techniques, as seen in Dazin et al. (2006), Richard et al. (2008), Cuypers et al. (2007). Experimental generation of standing fluid vortices has not been well documented though. However, in Forgoston et al. (2013), the authors developed an experimental test bed that could generate similar fluid flows, as seen in double-gyre wind-driven flows, to study the underlying manifold and Lagrangian coherent structure (LCS) one might observe in the ocean. These underlying structures coincided with minimum energy and time

optimal paths for autonomous underwater vehicles in the ocean. The fluid flow was characterized using PIV. The goal of their experimental work was similar to the simulation work of Kelly et al. (2012). Both studies address developing energy-optimal paths through fluid systems that exploit the underlying fluid structures for gains in energy efficiency.

1.2 Overview of Contributions

With its depth and richness, geometric mechanics can prove daunting for a new student to learn the tools of the field. Thus, a focused approach is used to provide a thorough introduction to Lagrangian reduction for unconstrained, dissipative, and nonholonomically constrained Lagrangian systems. Doing so provides the student with the essential tools necessary for analyzing these mechanical systems. Example problems are provided, with a detailed description of the calculations necessary to analyze the systems on a geometric level.

Often times in engineering problems, it is useful to model algebraic constraints as dissipation, and to model dissipation as algebraic constraints. When modeling systems with algebraic constraints, a common problem arises when constraints become extremely redundant. For example, in the case of a rigid door with three hinges, a natural temptation would be to place three rotational algebraic constraints on the door, one for each hinge. However, doing so creates a redundancy in constraints that does not make sense in the analysis of the system. In this simple example, one rotational constraint would be sufficient. However, in very complex mechanical systems, possibly with hundreds or thousands of components, identifying these redundancies

can be exhaustive if not nearly impossible for an analyst. In these cases, the MotionSolve 12.0 User's Guide (2013) mentions that it is common practice to replace the algebraic constraints with dissipative elements, then set the dissipation very high (MotionSolve is a software package for simulating multi-body, dynamic systems). Doing so mimics the behavior of the constraints, possibly saving enormous amounts of time for an engineer while yielding nearly identical results. The inverse of this technique is common as well. Constraints are often used to model dissipation. For example, in Georgiou et al. (2015), Arman et al. (2006), Yang et al. (2013), Tang et al. (2014), the authors carry out numerical simulations of common composite testing procedures. Often, the procedures require a composite panel to be held in position by a set of clamps or vices. The clamps are assumed to be tight enough that frictional forces prevent sliding of the test panel. Given this assumption, the authors model a simple boundary condition that sets translation to zero along the sliding direction. This leads to sufficiently accurate results for their studies. The aforementioned techniques provide motivation to pursue a rigorous mathematical study to ascertain the validity of modeling algebraic constraints as dissipative entities and vice versa. The study is carried out with tools from geometric mechanics, and ultimately puts the assumptions of the techniques on a solid mathematical footing.

Another significant benefit of geometric mechanics is that Lagrangian reduction techniques can aid in the control design of systems. Given that many of the tools were discovered and formalized in the last four decades, the treatment of a variety of new problems can prove useful in expanding the applicability and understanding the limitations of the techniques, thus ultimately developing tools' maturity and building

confidence in them. It also allows new insights into the existing canon of control problems encountered in the literature. A class of original example problems are used to demonstrate these techniques. In addition to Lagrangian reduction, this study includes novel techniques necessary for analyzing each unique problem. Thus, the class of systems that can be analyzed with the tools is expanded.

In this work, a robotic hydrofoild is constructed and used to study the fluid mechanics underpinning the motion of a fish. The machine is unique in that it was developed in conjunction with a series of simulations developed in Kelly and Pujari (2010). The simulations were conducted to study the fluid vortex interactions observed in a Joukowski foil that closely resembles the vortex shedding seen in the caudal fin of swimming fish. The idealized fluid vortices observed in the simulation are replicated experimentally. A machine that can experimentally create nearly irrotational fluid vortices is designed and fabricated. These fluid vortices are analyzed with the aid of PIV to characterize their flow properties. The characterization of the vortices ensures they are similar to the simulated vortices.

Given the created vortices, a simple technique allows the robot to extract energy from fluid vortices to attain dramatic gains in efficiency. The observed phenomenon provides evidence of a hydromechanical purpose to aspects of the swimming behavior of schooling fish.

CHAPTER 2: MATHEMATICAL PRELIMINARIES

In this chapter, mathematical definitions and descriptions pertinent to the analysis performed in this thesis are introduced. For those uninitiated in many of the topics in topology and differential geometry, this chapter includes an overview.

2.1 Manifolds, Vector Fields, and Functions

Definition 2.1.1. Given a set M, a **coordinate** chart on M is a subset $U \subset M$ together with a bijection

$$\phi : U \to \phi(U) \subset \mathbb{R}^n. \tag{1}$$

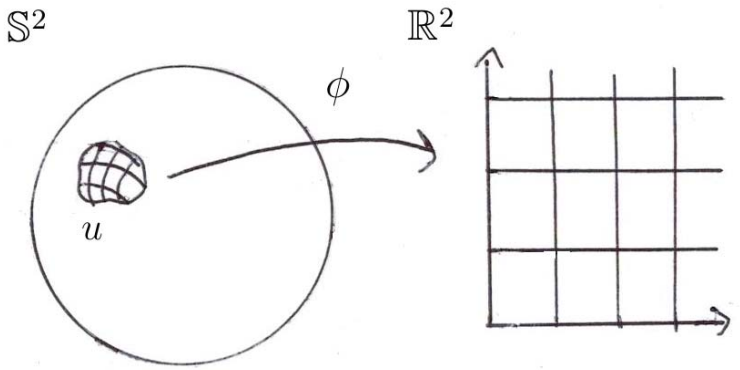

Figure 1: A chart on $\mathbb{S}^2$ that locally looks like $\mathbb{R}^2$.

Definition 2.1.2. A set M is a **differentiable manifold** that can be written as the union of a collection of compatible coordinate charts.

Examples of manifolds include the straight line in $\mathbb{R}^1$ or the surface of a sphere given in $\mathbb{S}^2$. For the sphere, the lines of latitude and longitude help define the points on the manifold.

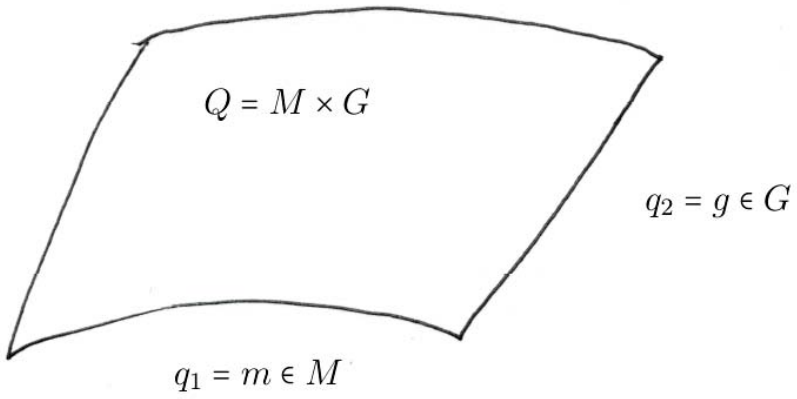

Figure 2: A configuration manifold formed by using the Cartesian product.

Definition 2.1.3. A **function** is a smooth mapping between manifolds M and N, $f : M \to N : x \to y$

Thus, the familiar notion of a function from calculus, $f(x)$, can be interpreted as a manifold comprised of all possible values of $f(x)$, mapped from a manifold comprised of all possible values of x. Both of these manifolds can be considered a single manifold using the Cartesian product of manifolds:

$$M \times M = (X, Y) : X, Y \in M. \tag{2}$$

Example 2.1.1.

An example is a $2D$ wheel rolling along the x axis. The angle of the wheel is

specified as ϕ. The angle ϕ is a coordinate in a particular choice of chart that covers some, but not all, of the $1D$ circular manifold M, such that $\phi \in M$. The set of all possible values of its position on the x axis can be considered a manifold G, such that $x \in G$. G is taken as the $1D$ real number line $\mathbb{R}$. As discussed in later sections, it can sometimes be helpful and informative to consider these two sets on the same topological space or manifold. Using the Cartesian product, such a manifold can be formed, such that $Q = M \times G$. This manifold consists of all possible configurations of the angle and position and is referred to as the *configuration manifold*. The angle and position can be considered coordinates, q on the configuration manifold, Q, as represented in Figure 2. Next, q is parameterized by time t, such that $q(t)$. Then a vector space is defined for $\dot{q}$, called the tangent space:

Definition 2.1.4. : Given a point on $x \in M$, the **tangent space** T_xM is defined as the set of mappings

$$V : C^{\text{inf}}(q) \to R \tag{3}$$

on M whose domain includes a neighborhood of x, satisfying

$$1. \quad v(\alpha f + \beta g) = \alpha(vf) + \beta(Vg),$$

$$\alpha, \beta \in R, \quad f, g \in C^{\inf}(x), \tag{4}$$

$$2. \quad v(fg)(x) = (vf)g(x) + f(x)(vg),$$

$$f, g \in C^{\inf}(x),$$

$$(v_1 + v_2)f = V_1 f + V_2 f,$$

$$(\alpha V)f = \alpha(Vf). \tag{5}$$

The set of all equivalence classes of curves passing through the point p of a manifold is said to be its tangent space there:

$$T_x(M) \equiv [c]_x, \forall c(t) \in, M \text{ with } c(0) = x. \tag{6}$$

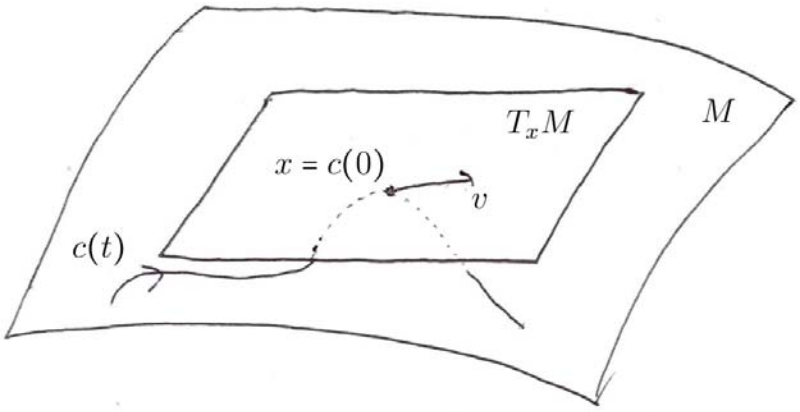

Figure 3: The tangent space.

Points in $q \in Q$ can be related to points in its tangent space by a vector field X.

Definition 2.1.5. Let Q be a manifold and $T(Q)$ its tangent space. A **vector field**,

X, is a manifold map from Q to $T(Q)$ such that, for every $p \in Q$, the vector field at the point q gives a point in the tangent space attached to the manifold there $X(q) \in T_q(Q)$.

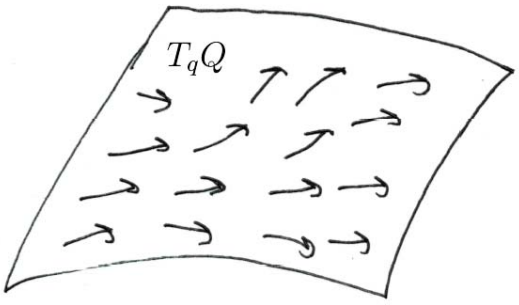

Figure 4: A vector field.

For the wheel, x and ϕ are related by $x = r\phi$. This is the function map, $f : M \to G$. Again, to learn more about how this system evolves through time, a tangent map for the system is constructed.

Definition 2.1.6. Given a function map $f : M \to N$, with $x \in M$ and $[c]_x \in T_xM$, such that $f \circ c$ is a curve at $f(x)$, then $Tf : TM \to TN$ is called the **tangent map** of f, where $Tf([c])_x) = [f \circ c]_{f(x)}$.

Thus, the tangent map for the wheel is $\dot{x} = r\dot{\phi}$.

In this work, directional derivatives help describe the motion of the systems. This motion has a geometric description as well, but first differential forms and natural pairings must be defined.

Definition 2.1.7. Given any linear vector space V, its **dual vector space** V^* consists of linear maps from V to $\mathbb{R}$ or covectors.

The differential of f at q is given as

$$df(q) : T_qM \to \mathbb{R}. \tag{7}$$

The differential df of a function f is known as a **differential form**.

Differential forms will play a key role in defining constrained momentum maps and constrained vector spaces in later chapters.

Definition 2.1.8. $X(M)$ represents smooth vector fields on M; then an element $\alpha \in X^*(M)$ is called a **one form** on M. To each point $q \in M$, it assigns a map $\alpha(q) : T_qM \to \mathbb{R}$. A **two form** Ω on M assigns a skew-symmetric bilinear map $\Omega(q) : T_qM \times T_qM \to \mathbb{R}$ to each point.

Definition 2.1.9. The **natural pairing** is the map

$$\langle \cdot, \cdot \rangle : T_q^*M \times T_qM \to \mathbb{R} \tag{8}$$

such that $\langle \alpha_1 dq^1 + \ldots + \alpha_n dq^n, V' \frac{\partial}{\partial q} + \ldots + V^n \frac{\partial}{\partial q^n} \rangle = \alpha_1 V^1 + \alpha_2 V^2 + \ldots \alpha_n V^n$.

The natural pairing $\langle df(q), V \rangle$ thus defines the directional derivative.

That T^*Q and TQ are duals has been established, but how is a particular element of TQ identified with T^*Q? The answer is the inner product.

Definition 2.1.10. The **inner product** is the map

$$\langle\!\langle \cdot, \cdot \rangle\!\rangle : T_qM \times T_qM \to \mathbb{R}, \tag{9}$$

and must be positive definite, symmetric, and bilinear.

Given $u, v, w \in TQ$ and $\alpha \in T^*Q$,

$$\langle \alpha, w \rangle = \langle\langle v, w \rangle\rangle. \tag{10}$$

The following example recaps the definitions used to describe this $2D$ wheel.

Example 2.1.2.

The constraint $x = r\phi$ defines a function $f : M \to \mathbb{R}$, with tangent map Tf. The differential of this system, $dx : TM \to \mathbb{R}$, defines the dual space T^*M and is also a one form. Thus, the following expression is defined: $\langle\langle v, w \rangle\rangle = \langle \alpha, w \rangle$, where $v = \frac{\partial}{\partial x} + \frac{\partial}{\partial \phi} \in TQ$, $w = \frac{\partial}{\partial x} + \frac{\partial}{\partial \phi} \in TQ$, and $\alpha = mdx + Jd\phi \in T^*Q$, with m and J as mass and moment of inertia.

2.2 Lie Groups and Lie Algebras

This section addresses ideas and concepts from abstract algebra and group theory that form the foundation for approaching dynamical systems in this work. The focus is on developments in the field by Sophus Lie in the late 1800s. Lie discovered that continuous transformation groups or Lie groups could be better understood by "linearizing" them and studying the corresponding generating vector fields, called *infinitesimal generators*. These generators are subject to a linearized version of the group law, the commutator bracket, and have the structure of a Lie algebra.

First, a group is simply an algebraic system with one operation. The operation considered for these groups is multiplication. It is necessary to understand how group multiplication can be abstracted to manifolds and aid in the analysis of systems like

the 2D wheel.

Definition 2.2.1. A **Lie group** is a manifold G on which a smooth group operation is defined, where $\forall f, g, h \in G$ satisfy the following four conditions:

1. Closure; $\forall\ a, b \in G$, the result of the operation $a \cdot b$, is also in G.
2. Associativity; $\forall\ a, b$, and $c \in G$, $(a \cdot b) \cdot c = a \cdot (b \cdot c)$.
3. Identity Element; $\exists\ e \in G$ such that $ea = ae = a$.
4. Inverse Element; $\exists\ g^{-1}$ such that $gg^{-1} = g^{-1}g = e$.

A broad classification of Lie groups describes different types of symmetries. Some simple Lie groups often encountered in dynamical systems include the $1D$ translation general linear group $GL(1)$ and the $2D$ rotation special orthogonal group $SO(2)$.

The above Lie group definition does not contain a commutative condition, thus there is a need to clarify the order by which the group operation occurs.

Definition 2.2.2. For $g, h \in G$, **left translation** by h corresponds to the map

$$L_h : g \mapsto hg.$$

Definition 2.2.3. For $g, h, \in G$, **right translation** by h corresponds to the map

$$R_h : g \mapsto gh.$$

The same maps apply in tangent spaces, with a slight change in notation.

With $v \in T_gG$,

$$hv = T_gL_hv \in T_{hg}G \quad \text{and} \quad vh = T_gR_hv \in T_{gh}G.$$

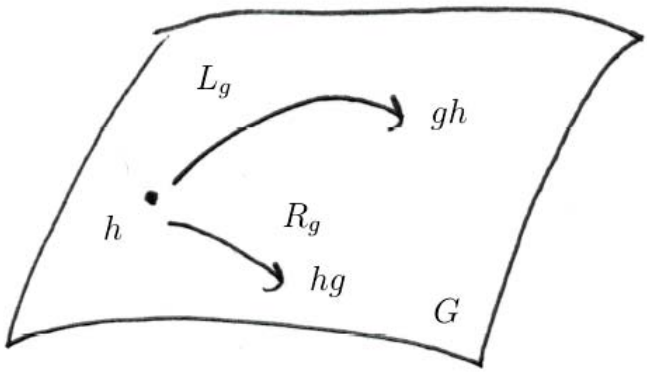

Figure 5: Group translation.

Again, back to the 2D wheel example:

Example 2.2.1. In this system, x can be identified as the set of nonzero real numbers with the multiplication operation. This corresponds to the matrix Lie group $GL(1)$, where the space of 1×1 matrices $M(1, \mathbb{R})$ is identified with $\mathbb{R}$. The group identity is 1.

Group translations map group elements onto group elements. The configuration manifold Q, thus far, has been comprised of Lie group elements and non group elements. The question is how group operations effect Q.

Definition 2.2.4. A (**smooth**) **left action** of a Lie group G on manifold M is a smooth mapping $\Phi : G \times M \to M$ such that

1. $\Phi(e, x) = x$ for all $x \in M$;

2. $\Phi(g, \Phi(h, x)) = \Phi(gh, x)$ for all $g, h \in G$ and $x \in M$;

3. For every $g \in G$, the map $\Phi_g : M \to M$, defined by $\Phi_g(x) := \Phi(g, x)$ is a diffeomorphism.

Definition 2.2.5. Properties of group actions The action $\Phi : G \times M \to M$ of a group G on a manifold is said to be

1. **transistive** if, for every $x, y \in M$, there exists a $g \in G$ such that $gx = y$;
2. **free** if it has no isotropic points; that is, $gx = x$ implies $g = e$;
3. **faithful** (or effective) if, for all $g \in G$ such that $g \neq e$, there exists $x \in M$ such that $gx \neq x$; and
4. **proper** if, whenever the sequences x_n and g_n, x_n converge in M, the sequence g_n has a convergent subsequence in G.

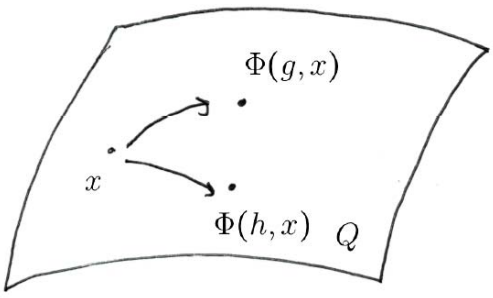

Figure 6: The group action.

Definition 2.2.6. The **lifted action** is the map $T\Phi_g : T_qQ \to T_{\Phi(q)}Q : (q, v) \mapsto (\Phi_g(q), T_q\Phi_g(v))$ for all $g \in G$ and $q \in Q$. For left translation on G, $T\Phi_g$ has the coordinate form:

$$T_q\Phi_h(\dot{q}) = \begin{pmatrix} T_gL_h\dot{g} \\ \\ \dot{s} \end{pmatrix} = \begin{pmatrix} h\dot{g} \\ \\ \dot{s} \end{pmatrix}. \tag{11}$$

Thus, for the wheel, the group action of $GL(1)$ on Q is such that

$$\Phi_g(q) = \begin{pmatrix} a_1 + x \\ \\ \phi \end{pmatrix}, \tag{12}$$

where $a_1 \in GL(1)$, with lifted action

$$T_q\Phi_g(\dot{q}) = \begin{pmatrix} \dot{x} \\ \\ \dot{\phi} \end{pmatrix}. \tag{13}$$

Given a Lie group action, one must understand how a point $x \in M$ can be moved by all possible elements in G.

Definition 2.2.7. (**Orbits**) G acts on M. For a given point $x \in M$, the subset

$$\mathrm{Orb}(x) := gx : g \in G \subseteq M \tag{14}$$

is called the **group orbit** through x.

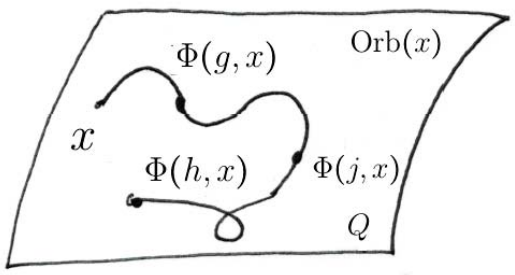

Figure 7: Group orbit.

As noted, the group operations are not necessarily commutative. Commonly, the vector fields of the systems will also not be commutative. To measure how non-commutative the vector fields are, the following definition applies:

Definition 2.2.8. A **Jacobi Lie bracket** is the operation $[\cdot,\cdot] : \mathfrak{X}(M) \times \mathfrak{X}(M) \to \mathfrak{X}(M)$ defined by

$$[X,Y]f = XYf - YXf, \qquad X,Y \in \mathfrak{X}(M). \tag{15}$$

In this work, the Jacobi Lie bracket $[X,Y]$ is often denoted by $\mathrm{ad}_X Y$.

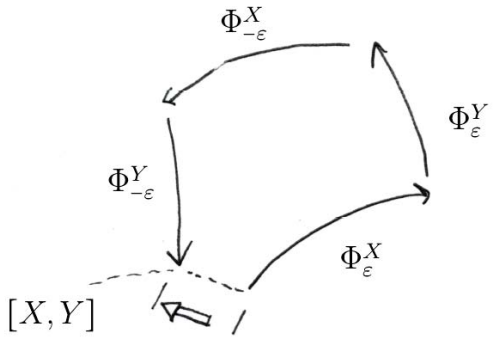

Figure 8: The flow interpretation of the Lie bracket.

Group operations are especially useful because they allow for a system treated on a body fixed coordinate frame to be translated to a global frame. Vector fields on the body fixed frame will always satisfy a few conditions regarding their commutative properties, understood through the (Jacobi) Lie bracket operation. In addition, vectors of this body fixed space can be understood as elements. These elements and the bracket operation comprise the necessary concepts to define an algebra.

Definition 2.2.9. A **Lie algebra** is a vector space V together with an operation $[\cdot,\cdot] : V \times V \to V$ such that

1. $[\cdot,\cdot]$ is bilinear;
2. $[v,v] = 0$ for every $v \in V$;
3. $[u,[v,w]] + [v,[w,u]] + [w,[u,v]] = 0$ for all $u,v,w \in V$ (*Jacobi identity*).

The elements of the Lie algebra are denoted by $\xi \in \mathfrak{g}$. Lie algebra elements are body fixed group tangent vectors or $\xi \in T_eG$.

Definition 2.2.10. The **left extension** of any $\xi \in T_eG$ is the vector field X^L_ξ given by

$$X^L_\xi(g) := T_eL_g(\xi). \tag{16}$$

Definition 2.2.11. A vector field $X : G \to TG$, $h \to X(h)$ is called **left invariant** if

$$L^*_g(X) = X \ \ , \forall g \in G. \tag{17}$$

Definition 2.2.12. With $\xi \in \mathfrak{g}$, the **one-parameter subgroup** corresponding to ξ, $g_\xi : \mathbb{R} \to G$ is the unique solution curve of the initial-value problem

$$\begin{aligned} \frac{dg}{dt} &= X_\xi(g), \\ g(0) &= e. \end{aligned} \tag{18}$$

Definition 2.2.13. G is a Lie group and $\mathfrak{g}$ is its Lie algebra. The **Lie exponential map** is a map

$$\exp : \mathfrak{g} \to G \tag{19}$$

given by $\exp(X) = \gamma(1)$, where $\gamma : \mathbb{R} \to G$ is the unique one-parameter subgroup of G, whose tangent vector at the identity is equal to X. It also coincides with the matrix exponential given by the series expansion

$$\exp(A) = \gamma_A(1) = e = I + \frac{A}{1!} + \frac{A^2}{2!} + \cdots. \tag{20}$$

Example 2.2.2.

For the 2D wheel, the Lie algebra is $\mathfrak{gl}(1) \simeq \mathbb{R}$. For any $x \in GL(1)$, the left translation map $L_x : GL(1) \to GL(1)$ is given by $L_x(y) = xy$. The left extension of a vector $\xi \in \mathfrak{gl}(1)$ is the vector field X_ξ given by $X_\xi(x) := T_e L_x(\xi) = x\xi$. Because the x velocity of the disc is the same no matter where the starting point of the x axis is defined, the vector field X is left invariant. The integral curve $t \to \gamma_\xi(t)$ is the solution of the corresponding ODE:

$$\frac{dx}{dt} = \xi x,$$
$$x(0) = 1.$$

Direct integration gives the one-parameter subgroup $\gamma_\xi(t) = e^{t\xi}$. The Lie exponential map is $\exp(\xi) = \gamma_\xi(1) = e^\xi$.

Definition 2.2.14. (**Infinitesimal Generator**) The **infinitesimal generator** associated with ξ at $x \in M$, denoted $\xi_M(x)$, is the tangent (or velocity) vector to this curve at x; that is,

$$\xi_M(x) = \frac{d}{dt}|_{t=0}(\exp(t\xi), x) \in T_xM. \tag{21}$$

The smooth vector field $\xi_M : M \to TM, x \to \xi_M(x)$, is called the **infinitesimal generator vector field associated to** ξ. The infinitesimal generator map $\mathfrak{g} \times M \to TM, (\xi, x) \to \xi_M(x)$ can be thought of as the "infinitesimal action" of $\mathfrak{g}$ on M. It is the expression at the tangent level of the action of G on M. For translating the disc example, with $\exp(t\xi) = e^{t\xi}$, the infinitesimal generator is given by

$$\begin{aligned} \xi_M(x) &= \frac{d}{dt}|_{t=0}(e^{t\xi}x) \\ &= (e^{t\xi}\xi x)|_{t=0} \\ &= \xi x. \end{aligned} \tag{22}$$

Definition 2.2.15. A function F is **invariant** with respect to an action Φ of a Lie group G if, for every $g \in G$, the map ϕ_g is a symmetry of F; that is, $F \circ \Phi_g = F$. The group G is called a Lie group symmetry or symmetry group of F.

For the rolling disc, the function $\dot{x} = r\dot{\phi}$ is invariant with respect to the group action

$$\Phi_{GL(1)}(q) = \begin{pmatrix} a_1 + x \\ \\ \phi \end{pmatrix}, \tag{23}$$

where $a_1 \in GL(1)$.

2.3 Unconstrained Reduction Without Dissipation

The concepts in this section are an introduction to the technique of Lagrangian reduction. This technique uses symmetries and Lie groups inherent in Lagrangian systems to simplify the systems, so they are expressed in terms of Lie algebra elements and momentum terms. It is often easier to work with a simplified set of equations because they are easier to manipulate and solve. This technique also yields significant insight into the system because it parses the non-drift terms from the drift terms and maps the motion of the actuation variables onto the body velocities of the system. First, some definitions are delineated.

For the *Lagrangian*, $L : TQ \to \mathbb{R}$ of a mechanical system,

Definition 2.3.1. The **fiber derivative** $\mathbb{F}L : TQ \to T^*Q$ of the Lagrangian $L : TQ \to \mathbb{R}$ is

$$\langle \mathbb{F}L(u), v \rangle = \frac{d}{dt}|_{t=0} L(u + tv) \text{ for } u, v \in T_qQ \tag{24}$$

at every $q \in Q$.

The fiber derivative simply gives the momenta of the system in the global frame. However, viewing the system on a body fixed frame will reduce the complexity of the system. To do so, the Lagrangian first must be G-invariant.

Definition 2.3.2. A Lagrangian function, $L : TQ \to \mathbb{R}$, is said to be G-invariant if it is invariant with respect to the lifted action, that is, if

$$L(q, v_q) = L(\Phi_h(q), T_q\Phi_h v_q) \tag{25}$$

for all $h \in G$ and all $v_q \in T_qQ$

Definition 2.3.3. A **kinetic energy metric** of a system can be expressed in terms of the fiber derivative of a G-invariant Lagrangian, such that

$$\langle\!\langle u, v \rangle\!\rangle_{\mathrm{KE}} = \langle \mathbb{F}L(u), v \rangle. \tag{26}$$

This relationship can then be used to express the global momentum in terms of body fixed momenta.

Definition 2.3.4. Given a G-invariant Lagrangian, the **momentum map** $J : TQ \to \mathfrak{g}^*$ is

$$\begin{aligned} \langle J(v_q), \eta \rangle &= \langle \mathbb{F}L(v_q), \eta_Q(q) \rangle \\ &= \langle\!\langle v_q, \eta_Q(q) \rangle\!\rangle_{\mathrm{KE}}, \end{aligned} \tag{27}$$

for $v_q \in T_qQ$ and $\eta \in \mathfrak{g}$.

If L is G invariant, then G is said to determine a symmetry of the system given by the Euler-Lagrange equations. The relationship between symmetries and conservation laws is formalized by the following.

Theorem 2.3.1. (**Noether**) *If $L : TQ \to$ is G invariant, then the momentum $J : TQ \to \mathfrak{g}^*$ is conserved along integral curves of the Euler-Lagrange equations corresponding to L.*

The kinetic energy metric can be used to define a second map for a Lagrangian system:

Definition 2.3.5. Given that G acts on Q to define a principal bundle over M. If $L : TQ \to \mathbb{R}$ is G invariant, the **locked inertia tensor** corresponds to the map $\mathbb{I} : \mathfrak{g} \to \mathfrak{g}^*$ at each $q \in Q$ such that

$$\langle \mathbb{I}(q)\xi, \eta \rangle = \langle\!\langle \xi_Q(q), \eta_Q(q) \rangle\!\rangle_{\mathrm{KE}}. \tag{28}$$

The locked inertia tensor gives the masses and moments of inertia of the system at an instant in time when the non-group elements of the system are considered locked.

The importance of the body fixed representation of the coordinate frame to the reduction process should be clear. To further clarify how to construct vector spaces considered in the different frames, the global and body frames are discussed.

Definition 2.3.6. The **Lagrangian or material velocity** is given by

$$v_{\mathrm{material}}(t) = \dot{g}(t) \in T_{g(t)}G, \tag{29}$$

where left and right translation in G both determine isomorphisms between T_eG and $T_{g(t)}G$. For the local, body fixed frame,

Definition 2.3.7. The **convective or body velocity** is given by

$$v_{\mathrm{body}}(t) = T_{g(t)}L_{g^{-1}}(t)\dot{g}(t) \in T_eG. \tag{30}$$

To help move between global and local vector spaces, the following is used:

Definition 2.3.8. The **adjoint action** of G on $\mathfrak{g}$, given by

$$G \times \mathfrak{g} \to \mathfrak{g}, \quad (g, \xi) \to \mathrm{Ad}_g \xi := T_e I_g(\xi) = T_e(L_g \circ R_{g^{-1}} \xi). \tag{31}$$

The adjoint action can be thought of as a map from G to $\mathfrak{g}$. One example of the usefulness of this action is its use to re-express the global representation of the locked inertia tensor in terms of a localized representation of the locked inertia tensor

$$\mathbb{I}(r, g) = \mathrm{Ad}^*_{g^{-1}} \mathbb{I}_{\mathrm{loc}}(r) \mathrm{Ad}_{g^{-1}}. \tag{32}$$

The next definition is possibly the most important in this chapter. For all problems in Parts I and II, the definition is central to constructing the reduced equations and understanding the system on a geometric level.

Definition 2.3.9. The **mechanical connection** corresponding to the one form $\Gamma_{\mathrm{mech}} : TQ \to \mathfrak{g}$ is given by

$$\Gamma_{\mathrm{mech}}(q, \dot{q}) = \mathbb{I}^{-1}(q) J(q, \dot{q}), \tag{33}$$

where $J : TQ \to \mathfrak{g}^*$ is the momentum map. The mechanical connection can also be expressed as

$$\Gamma_{\mathrm{mech}}(q, \dot{q}) = \mathrm{Ad}_g(g^{-1}\dot{g} + A_{\mathrm{mech}}\dot{r}). \tag{34}$$

The derivation can be found in Kelly (1998).

For example, a four-wheeled mobile robot has rear wheels that rotate at a given

angular velocity for forward motion of the robot and has front wheels that steer. Given the angular velocity of the rear wheels, the angle of the front wheels, and the body velocity of the system, all the motion of the system through space can be determined through the connection map.

To delve deeper into the abstract geometric description of mechanical systems, a few more concepts need to be defined. These concepts help to clarify the underlying structure of the configuration manifold $Q = M \times G$.

Definition 2.3.10. The **canonical projection** is a differentiable projection onto the second coordinate factor: $\pi(q) = \pi(g, s) = s$. The sets $\pi^{-1}(s) \subset Q$ for $r \in M$ are the *fibers*, and Q is the union over M of its fibers.

Definition 2.3.11. A (**left**) **principal fiber bundle** with base space M and structure group G comprises a manifold Q and a free (left) action Φ of G on Q such that

1. $M = Q/G$.
2. The canonical projection $\pi_M : Q \to M = Q/G$ is differentiable.
3. $Q = M \times G$ locally.

Thus, the fiber gives a way to relate coordinates in the base manifold M to coordinates anywhere in Q. Associating a free action to the fiber deepens the meaning behind the fiber. Because the action can be used to generate vector fields, the principal fiber bundle now carries information about how the system evolves over time.

For the configuration manifold Q, the tangent space at each point can be split into two vector spaces.

Definition 2.3.12. The **vertical space** is the space of all vectors $v_q \in T_qQ$ that are tangent to the fiber through Q.

Definition 2.3.13. The **horizontal space** is the kernel of the connection one form,

$$H_qQ = \{z|\Gamma(q)z = 0\}\,. \tag{35}$$

T_qQ can be decomposed into horizontal vectors in H_qQ and vertical vectors in V_qQ,

$$H_qQ \oplus V_qQ = T_qQ. \tag{36}$$

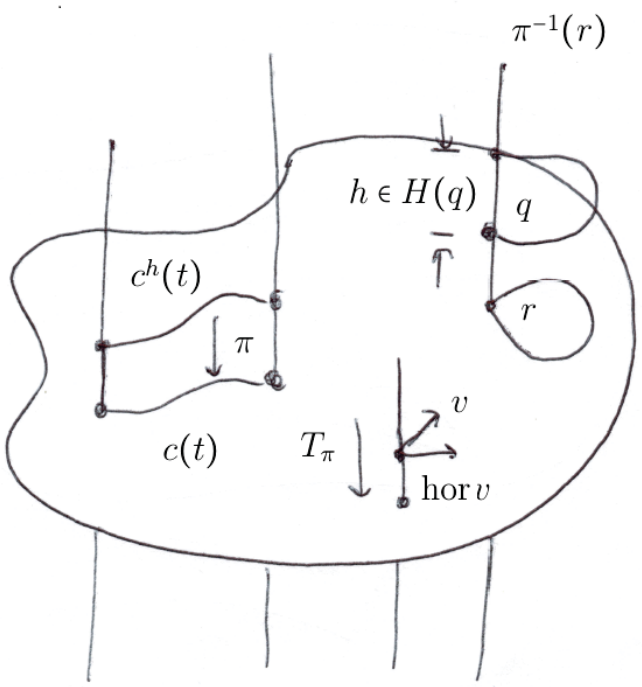

Figure 9: Operations on the fiber bundle.

Example 2.3.1.

To begin, the following system is constructed.

$$
\begin{aligned}
q_r &= (x, y), \\
q_f &= (x + l\cos\theta, y + l\sin\theta), \\
v_r &= \dot{q}_r, \\
v_f &= \dot{q}_f, \\
v_{r_{LB}} &= v_r \cdot (\cos\theta, \sin\theta), \\
v_{r_{SB}} &= v_r \cdot (-\sin\theta, \cos\theta), \\
v_{f_{LB}} &= v_f \cdot (\cos\theta, \sin(\theta)), \\
v_{f_{SB}} &= v_f \cdot (-\sin\theta, \cos\theta).
\end{aligned} \tag{37}
$$

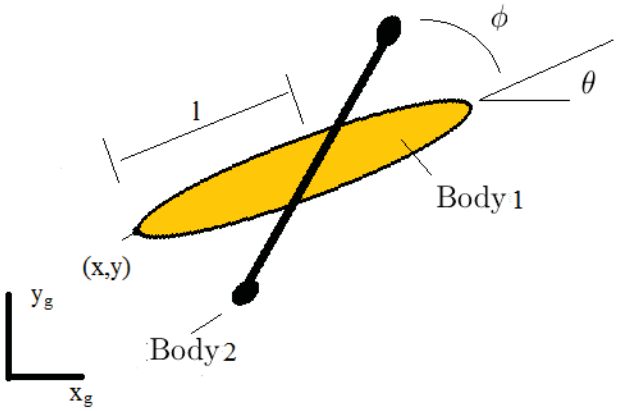

Figure 10: A beanie diagram.

This system consists of two planar rigid bodies attached at their centers of mass. The rigid bodies move freely in the plane, and the existence of control torques between the two bodies is assumed.

The Lagrangian corresponding to Figure 10 is as follows:

$$L = \frac{1}{2}m(v_{f_{LB}}^2 + v_{f_{SB}}^2) + \frac{1}{2}J_J\dot{\theta}^2 + \frac{1}{2}J_B(\dot{\theta} + \dot{\phi})^2, \tag{38}$$

or

$$L = \frac{1}{2}m(\dot{x}^2 + \dot{y}^2 + l^2m\dot{\theta}^2) + lm\dot{\theta}(\dot{y}\cos\theta - \dot{x}\sin\theta) + \frac{1}{2}J_J\dot{\theta}^2 + \frac{1}{2}J_B(\dot{\theta} + \dot{\phi})^2. \tag{39}$$

Remark 2.3.1. Before continuing further, a suitable Lie group for this particular system must be identified. With translation and rotation in the plane defined, the $SE(2)$ Lie group and its associated Lie algebra, $\mathfrak{se}(2)$, must be addressed. Elements of $SE(2)$ can be matrices of the form

$$g = \begin{bmatrix} \cos\theta & -\sin\theta & x \\ \sin\theta & \cos\theta & y \\ 0 & 0 & 1 \end{bmatrix}. \tag{40}$$

The group operation corresponds to matrix multiplication. The corresponding elements of $SE(2)$ will sometimes be denoted by triplets (x, y, θ). If $g_1 = (x_1, y_1, \theta_1), g_2 = (x_2, y_2, \theta_2) \in SE(2)$, then

$$g_1 \cdot g_2 = (x_1 + x_2\cos\theta_1 - y_2\sin\theta_1, y_1 + x_2\sin\theta_1 + y_2\cos\theta_1, \theta_1 + \theta_2). \tag{41}$$

Elements of $\mathfrak{se}(2)$ can be represented as matrices of the form

$$\begin{pmatrix} 0 & -\xi_\theta & \xi_x \\ \xi_\theta & 0 & \xi_y \\ 0 & 0 & 0 \end{pmatrix}. \tag{42}$$

The bracket operation corresponds to matrix commutation, and corresponding elements of $\mathfrak{se}(2)$ will sometimes be denoted by triplets $(\xi_x, \xi_y, \xi_\theta)$. If $\xi = (\xi_x, \xi_y, \xi_\theta), \eta = (\eta_x, \eta_y, \eta_\theta) \in \mathfrak{se}(2)$, then

$$[\xi, \eta] = (\xi_y\eta_\theta - \xi_\theta\eta_y, \xi_\theta\eta_x - \xi_x\eta_\theta, 0). \tag{43}$$

The exponential map $\exp : \mathfrak{se}(2) \to SE(2)$ is given by

$$\exp\xi = (\frac{1}{\xi_\theta}(-\xi_y + \xi_y\cos\xi_\theta + \xi_x\sin\xi_\theta, \frac{1}{\xi_\theta}(\xi_x - \xi_x\cos\xi_\theta + \xi_y\sin\xi_\theta), \xi_\theta) \tag{44}$$

if $\xi_\theta \neq 0$ and by the Abelian exponential map $(\xi_x, \xi_y, 0) \mapsto (\xi_x, \xi_y, 0)$ if $\xi_\theta = 0$. It follows that the infinitesimal generator of left translation corresponding to $\xi \in \mathfrak{se}(2)$ is given by

$$\xi_{SE(2)} = (\xi_x - y\xi_\theta, \xi_y + x\xi_\theta, \xi_\theta). \tag{45}$$

The adjoint action of $SE(2)$ on $\mathfrak{se}(2)$ is given by

$$\mathrm{Ad}_g\xi = (\xi_x\cos\theta - \xi_y\sin\theta + \xi_\theta y, \xi_x\sin\theta + \xi_y\cos\theta - \xi_\theta x, \xi_\theta). \tag{46}$$

If $g(t) = (x(t), y(t), \theta(t))$ is a curve in $SE(2)$, then

$$g^{-1}\dot{g} = (\dot{x}\cos\theta + \dot{y}\sin\theta, \dot{y}\cos\theta - \dot{x}\sin\theta, \dot{\theta}). \tag{47}$$

Example 2.3.1 continued.

First, the Lagrangian must be checked to determine whether it is invariant under left translation of the group. The fiber bundle for the system is given by $Q = SE(2) \times \mathbb{S} = G \times M$. With the element $h = (a^1, a^2, \alpha) \in G = SE(2)$ and $\phi \in M$, the corresponding group action is given by

$$\Phi_g(q) = \begin{pmatrix} a^1 + x\cos\alpha - y\sin\alpha \\ a^2 + x\sin\alpha + y\cos\alpha \\ \alpha + \theta \\ \phi \end{pmatrix},$$

and the lifted action by

$$T_q\Phi_g(\dot{q}) = \begin{pmatrix} \cos\alpha & -\sin\alpha & 0 & 0 \\ \sin\alpha & \cos\alpha & 0 & 0 \\ 0 & 0 & 1 & 0 \\ 0 & 0 & 0 & 1 \end{pmatrix} \begin{pmatrix} \dot{x} \\ \dot{y} \\ \dot{\theta} \\ \dot{\phi} \end{pmatrix} = \begin{pmatrix} \dot{x}\cos\alpha - \dot{y}\sin\alpha \\ \dot{x}\sin\alpha + \dot{y}\cos\alpha \\ \dot{\theta} \\ \dot{\phi} \end{pmatrix}.$$

Substituting these lifted velocities into the Lagrangian shows that

$$
\begin{aligned}
L(\Phi_g q, T_q\Phi_g \dot{g}) &= \frac{1}{2}m((\dot{x}\cos\alpha - \dot{y}\sin\alpha)^2 + (\dot{x}\sin\alpha + \dot{y}\cos\alpha)^2 + l^2 m\dot{\theta}^2) \\
&\quad + lm\dot{\theta}((\dot{x}\sin\alpha + \dot{y}\cos\alpha)\cos\theta \\
&\quad -(\dot{x}\cos\alpha - \dot{y}\sin\alpha)\sin\theta) + \frac{1}{2}J_J\dot{\theta}^2 + \frac{1}{2}J_B(\dot{\theta}+\dot{\phi})^2 \\
&= \frac{1}{2}m(\dot{x}^2 + \dot{y}^2 + l^2 m\dot{\theta}^2) + lm\dot{\theta}(\dot{y}\cos\theta - \dot{x}\sin\theta) + \frac{1}{2}J_J\dot{\theta}^2 + \frac{1}{2}J_B(\dot{\theta}+\dot{\phi})^2 \\
&= L(q,\dot{q}). \qquad (48)
\end{aligned}
$$

With group invariance demonstrated, the next step is to construct the fiber derivative $\mathbb{F}L(v_q)$ by taking the partial derivatives of the Lagrangian with respect to each group element x, y, θ.

$$
\mathbb{F}L(v_q) = \begin{pmatrix} \frac{\partial L}{\partial \dot{x}}, \\ \frac{\partial L}{\partial \dot{y}}, \\ \frac{\partial L}{\partial \dot{\theta}} \end{pmatrix} = \begin{pmatrix} m(\dot{x} - l\dot{\theta}\sin\theta) \\ m(\dot{y} + l\dot{\theta}\cos\theta) \\ -lm\dot{x}\sin\theta + lm\dot{y}\cos\theta + (J_B + J_J + l^2 m)\dot{\theta} + J_B\dot{\phi} \end{pmatrix}. \qquad (49)
$$

This can then be used to calculate the momentum map J.

$$\begin{aligned}
\langle J(v_q), \eta \rangle &= \langle\!\langle v_q, \eta_Q(q) \rangle\!\rangle_{\mathrm{KE}} \\
&= \langle \mathbb{F}L(v_q), \eta_Q(q) \rangle \\
&= \frac{\partial L}{\partial \dot{x}}(\xi_x - y\xi_\theta) + \frac{\partial L}{\partial \dot{y}}(\xi_y + x\xi_\theta) + \frac{\partial L}{\partial \dot{\theta}}\xi_\theta \\
J_x\xi_x + J_y\xi_y + J_\theta\xi_\theta &= m(\dot{x} - l\dot{\theta}\sin\theta)\xi_x + (m(\dot{y} + l\dot{\theta}\cos\theta)\xi_y \\
&\quad +(-m\dot{x}(l\sin\theta + y) + m\dot{y}(l\cos\theta - x) \\
&\quad +\dot{\theta}(J_B + J_J + l^2m + lmx\cos\theta + lmy\sin\theta) + J_B\dot{\phi})\xi_\theta. \quad (50)
\end{aligned}$$

Equating coefficients gives J momentum equations.

The fiber derivative can also be used to construct the locked inertia tensor $\mathbb{I}(q)$. Replacing vectors of TG in $L(v_q)$ with vectors of η_Q (same as ξ_Q) gives $\mathbb{F}L(\eta_Q)$. Starting with

$$\eta_{SE(2)} = (\eta_x - y\eta_\theta, \eta_y + x\eta_\theta, \eta_\theta), \quad (51)$$

and substituting into the Lagrangian gives

$$\begin{aligned}
L(q, \eta) &= \frac{1}{2}m((\eta_x - y\eta_\theta)^2 + (\eta_y + x\eta_\theta)^2 + l^2m\eta_\theta^2) + lm\eta_\theta((\eta_y + x\eta_\theta)\cos\theta \\
&\quad -((\eta_x - y\eta_\theta)\sin\theta) + \frac{1}{2}J_J\eta_\theta^2 + \frac{1}{2}J_B(\eta_\theta + \dot{\phi})^2, \quad (52)
\end{aligned}$$

$$\mathbb{F}L(\eta_q) = \begin{pmatrix} \frac{\partial L}{\partial \eta_x} \\ \frac{\partial L}{\partial \eta_y} \\ \frac{\partial L}{\partial \eta_\theta} \end{pmatrix} = \begin{pmatrix} m(\eta_x - l\eta_\theta\theta) \\ m(\eta_y + l\eta_\theta\theta) \\ -lm\eta_x \sin\theta + lm\eta_y \cos\theta + (J_B + J_J + l^2 m)\eta_\theta + J_B\dot{\phi} \end{pmatrix}, \quad (53)$$

$$\begin{aligned}
\langle \mathbb{I}(q)\xi, \eta \rangle &= \langle\!\langle \xi_Q(q), \eta_Q(q) \rangle\!\rangle_{\mathrm{KE}} \\
&= \langle \mathbb{F}L(\eta_Q), \xi_Q(q) \rangle \\
&= \frac{\partial L}{\partial \eta_x}(\xi_x - y\xi_\theta) + \frac{\partial L}{\partial \eta_y}(\xi_y + x\xi_\theta) + \frac{\partial L}{\partial \eta_\theta}\xi_\theta \\
&= \mathbb{I}_{xx}\eta_x\xi_x + \mathbb{I}_{xy}\eta_x\xi_y + \mathbb{I}_{x\theta}\eta_x\xi_\theta + \mathbb{I}_{yx}\eta_y\xi_x + \mathbb{I}_{yy}\eta_y\xi_y \\
&\quad + \mathbb{I}_{y\theta}\eta_x\xi_\theta + \mathbb{I}_{\theta x}\eta_\theta\xi_x + \mathbb{I}_{\theta y}\eta_\theta\xi_y + \mathbb{I}_{\theta\theta}\eta_\theta\xi_\theta, \\
&= m\eta_x\xi_x + 0\cdot\eta_x\xi_y - m(l\sin\theta_y)\eta_x\xi_\theta + 0\cdot\eta_y\xi_x + m\eta_y\xi_y \\
&\quad + m(l\cos\theta + x)\eta_y\xi_\theta - m(l\sin\theta + y)\eta_\theta\xi_x + m(l\cos\theta + x)\eta_\theta\xi_y \\
&\quad + (J_B + J_J + l^2 m + m(2lx\cos\theta + x^2 + 2ly\sin\theta + y^2))\eta_\theta\xi_\theta. \qquad (54)
\end{aligned}$$

The adjoint action of $SE(2)$ can be used to localize the locked inertia tensor:

$$
\begin{aligned}
\mathbb{I}_{\text{loc}} &= \text{Ad}_g^* \mathbb{I}(q) \text{Ad}_g \\
&= \begin{pmatrix} \cos\theta & \sin\theta & 0 \\ -\sin\theta & \cos\theta & 0 \\ y & -x & 1 \end{pmatrix} \begin{pmatrix} \mathbb{I}_{xx} & \mathbb{I}_{xy} & \mathbb{I}_{xz} \\ \mathbb{I}_{yx} & \mathbb{I}_{yy} & \mathbb{I}_{yz} \\ \mathbb{I}_{zx} & \mathbb{I}_{zy} & \mathbb{I}_{zz} \end{pmatrix} \begin{pmatrix} \cos\theta & -\sin\theta & y \\ \sin\theta & \cos\theta & -x \\ 0 & 0 & 1 \end{pmatrix} \\
\mathbb{I}_{\text{loc}} &= \begin{pmatrix} m & 0 & 0 \\ 0 & m & lm \\ 0 & lm & J_B + J_J + ml^2 \end{pmatrix}.
\end{aligned}
$$

The definition of Γ_{mech} can be used to calculate A_{mech}. Starting with

$$\mathbb{I}_{\text{loc}}^{-1} \text{Ad}_g^* J - g^{-1}\dot{g} = A_{\text{mech}} \dot{r}, \tag{55}$$

then

$$
\begin{pmatrix} \frac{1}{m} & 0 & 0 \\ 0 & \frac{l^2}{J_B+J_J} + \frac{1}{m} & -\frac{l}{J_B+J_J} \\ 0 & -\frac{l}{J_B+J_J} & \frac{1}{J_B+J_J} \end{pmatrix} \begin{pmatrix} \cos\theta & \sin\theta & 0 \\ -\sin\theta & \cos\theta & 0 \\ y & -x & 1 \end{pmatrix}
$$

$$
* \begin{pmatrix} m(\dot{x} - l\dot{\theta}\sin\theta)\xi_x \\ \\ (m(\dot{y} + l\dot{\theta}\cos\theta)\xi_y \\ \\ (-m\dot{x}(l\sin\theta + y) + m\dot{y}(l\cos\theta - x) \\ +\dot{\theta}(J_B + J_J + l^2 m + lmx\cos\theta + lmy\sin\theta) + J_B\dot{\phi})\xi_\theta \end{pmatrix}
$$

$$
- \begin{pmatrix} \dot{x}\cos\theta + \dot{y}\sin\theta \\ \\ \dot{y}\cos\theta - \dot{x}\sin\theta \\ \\ \dot{\theta} \end{pmatrix}
$$

$$
= \begin{pmatrix} 0 \\ \\ \frac{J_B l}{J_B + J_J} \\ \\ -\frac{J_B}{J_B + J_J} \end{pmatrix} \dot{r}, \tag{56}
$$

so

$$
A_{\text{mech}} = \begin{pmatrix} 0 \\ \\ \frac{J_B l}{J_B + J_J} \\ \\ -\frac{J_B}{J_B + J_J} \end{pmatrix}. \tag{57}
$$

Using

$$
\begin{aligned}
g^{-1}\dot{g} &= -A_{\text{mech}}\dot{r} + \mathbb{I}_{\text{loc}}^{-1} p, \\
\dot{p} &= \text{ad}^*_{g^{-1}\dot{g}} p
\end{aligned}
$$

renders

$$
\begin{pmatrix} \dot{g} \\ \dot{p} \end{pmatrix} = \begin{pmatrix} \dot{x} \\ \dot{y} \\ \dot{\theta} \\ \dot{p}_x \\ \dot{p}_y \\ \dot{p}_\theta \end{pmatrix} = \begin{pmatrix} \frac{\cos\theta p_x}{m} - \frac{\sin\theta(J_B+J_J+l^2m)p_y}{m(J_B+J_J)} + \frac{lm(-p_\theta+J_B\dot{\phi})}{m(J_B+J_J)} \\ \frac{\sin\theta p_x}{m} + \frac{\cos\theta(J_B+J_J+l^2m)p_y}{m(J_B+J_J)} + \frac{lm(-p_\theta+J_B\dot{\phi})}{m(J_B+J_J)} \\ \frac{-lp_y+p_\theta-J_B\dot{\phi}}{J_B+J_J} \\ -\frac{lp_y^2}{J_B+J_J} + \frac{p_y p_\theta}{J_B+J_J} + \frac{J_B p_y \dot{\phi}}{J_B+J_J} \\ \frac{lp_x p_y}{J_B+J_J} - \frac{p_x p_\theta}{J_B+J_J} - \frac{J_B p_x \dot{\phi}}{J_B+J_J} \\ \frac{l^2 p_x p_y}{J_B+J_J} - \frac{lp_x p_\theta}{J_B+J_J} - \frac{J_B l p_x \dot{\phi}}{J_B+J_J} \end{pmatrix}. \tag{58}
$$

These reduced equations completely describe the evolution of the system.

2.4 Reduction for Purely Dissipative Systems

The introduction of dissipation to a system is an important part of capturing the accurate behavior of mechanical systems. Dissipation is usually present in the form of friction or drag. Given its prevalence in mechanical systems, it deserves a thorough description in terms of Lagrangian reduction. To being, a purely dissipative system is one in which there is no momentum.

Reduction for such a system is based on the following concepts. These concepts are simply the dissipative analogues of the concepts introduced in the previous section. The first concept is the familiar notion of force.

Definition 2.4.1. A **force field** is a fiber preserving map $F : TQ \to T^*Q$ over the

identity. The force field determines a one form $\tilde{F} : T(TQ) \to \mathbb{R}$ such that

$$\tilde{F}(v)W = \langle F(v), T_v\tau_Q W\rangle \tag{59}$$

for $v \in TQ$ and $W \in T_v(TQ)$.

Given a Rayleigh dissipation function R for a system, a dissipative force field can be generated by $F = \mathbb{F}(-R)$.

Definition 2.4.2. Given a G-invariant Rayleigh dissipation function such that $F = \mathbb{F}(-R)$, the **momentum map**, $K : TQ \to \mathfrak{g}^*$, is given by

$$\langle K(q,\dot{q}), \xi\rangle = \langle F(q,\dot{q}), \xi_Q(q)\rangle. \tag{60}$$

Definition 2.4.3. Given a G-invariant Rayleigh dissipation function such that $F = \mathbb{F}(-R)$, the **viscosity tensor** $\mathbb{V} : \mathfrak{g} \to \mathfrak{g}^*$ is given by

$$\langle \mathbb{V}(q)\xi, \eta\rangle = \langle F(\xi_Q(q)), \eta_Q(q)\rangle. \tag{61}$$

Definition 2.4.4. The **Stokes connection** corresponding to the one form $\Gamma_{\text{Stokes}} : TQ \to \mathfrak{g}$ is given by

$$\Gamma_{\text{Stokes}} : (q,\dot{q}) \mapsto \mathbb{V}^{-1}(q)K(q,\dot{q}). \tag{62}$$

It can also be expressed as

$$\Gamma_{\text{Stokes}} = \text{Ad}_g(g^{-1}\dot{g} + A_{\text{Stokes}}\dot{r}). \tag{63}$$

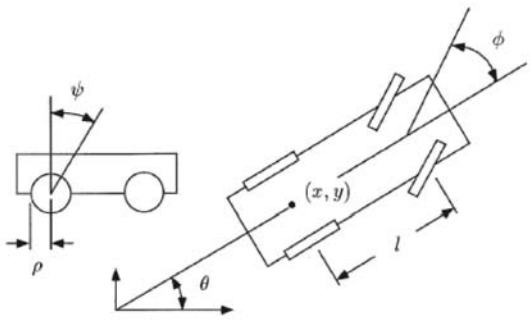

Figure 11: The Stokesian car model.

Comparing the Stokesian-based maps defined above to the Lagrangian-based maps defined in the previous section shows each Stokesian-based map is geometrically identical to a Lagrangian-based map. For instance,

$$\begin{aligned} R, L : TQ &\to \mathbb{R}, \\ \mathbb{F}(-R), \mathbb{F}(L) : TQ &\to T^*Q, \\ K, J : TQ &\to \mathfrak{g}^*, \\ \mathbb{V}, \mathbb{I} : \mathfrak{g} &\to \mathfrak{g}^*, \\ \Gamma_{\text{Stokes}}, \Gamma_{\text{mech}} : TQ &\to \mathfrak{g}. \end{aligned} \tag{64}$$

Given this relationship, the procedure for calculating each of the dissipative maps is identical to that for calculating the Lagrangian-based maps. Thus, detailed calculations are omitted in the following example.

Example 2.4.1.

Starting with a system defined by

$$\begin{aligned}
(x_r, y_r) &= (x, y), \\
(x_f, y_f) &= (x + l\cos\theta, y + l\sin\theta), \\
v_r &= \dot{x}_r, \dot{y}_r, \\
v_f &= \dot{x}_f, \dot{y}_f, \\
v_{r_{LB}} &= v_r \cdot (\cos\theta, \sin\theta), \\
v_{r_{SB}} &= v_r \cdot (-\sin\theta, \cos\theta), \\
v_{f_{LB}} &= v_f \cdot (\cos\theta, \sin(\theta)), \\
v_{f_{SB}} &= v_f \cdot (-\sin\theta, \cos\theta), \\
v_{fw_{LB}} &= v_f \cdot (\cos(\theta + \phi), \sin(\theta + \phi)), \\
\mathrm{v_{fw_{SB}}} &= v_f \cdot (-\sin(\theta + \phi), \cos(\theta + \phi)),
\end{aligned} \tag{65}$$

leads to the Rayleigh dissipation function:

$$\begin{aligned}
R = C_c(\dot{x}\sin\theta - \dot{y}\cos\theta)^2 + C_c(\dot{x}\sin(\theta + \phi + \pi) - \dot{y}\cos(\theta + \phi + \pi) \\
-l\dot{\theta}\cos(\phi + \pi))^2 + C_c(\dot{x}\cos\theta + \dot{y}\sin\theta - \dot{\nu})^2.
\end{aligned} \tag{66}$$

The same technique used for checking the Lagrangian for G-invariance shows that R is G-invariant. Starting with the G-invariant R, taking $\mathbb{F}(-R)$, pairing with ξ_Q, and using the definition for the momentum map K gives the following:

$$K = \begin{pmatrix} K_1 \\ \\ K_2 \\ \\ K_3 \end{pmatrix} = \begin{pmatrix} -3C_c\dot{x} + C_c\dot{x}\cos(2\theta+2\phi) + C_c\dot{y}\sin(2\theta+2\phi) \\ +2C_cl\dot{\theta}\cos\phi\sin(\theta+\phi) + 2C_c\dot{\nu}\cos\theta \\ C_c\dot{x}\sin(2\theta+2\phi) - 3C_c\dot{y} - C_c\dot{y}\cos(2\theta+2\phi) \\ -2C_cl\dot{\theta}\cos\phi\cos(\theta+\phi) + 2C_c\dot{\nu}\sin\theta \\ 2C_cl\dot{x}\cos\phi\sin(\theta+\phi) + C_cx\dot{x}\sin(2\theta+2\phi) + 3C_cy\dot{x} \\ -C_cy\dot{x}\cos(2\theta+2\phi) - 2C_cl\dot{y}\cos\phi\cos(\theta+\phi) - 3C_cx\dot{y} \\ -C_cx\dot{y}\cos(2\theta+2\phi) - 2C_cy\dot{y}\cos(\theta+\phi)\sin(\theta+\phi) \\ -2C_cl^2\dot{\theta}\cos^2\phi - 2C_clx\dot{\theta}\cos\phi\cos(\theta+\phi) \\ -2C_cly\dot{\theta}\cos\phi\sin(\theta+\phi) + 2C_cx\dot{\nu}\sin\theta - 2C_cy\dot{\nu}\cos\theta \end{pmatrix}. \tag{67}$$

Substituting the group element velocities $(\dot{x}, \dot{y}, \dot{\theta})$ with the infinitesimal generator elements of left translation corresponding to $\eta \in \mathfrak{se}(2)$ $(\eta_x - y\eta_\theta, \eta_y + x\eta_\theta, \eta_\theta)$ in $\mathbb{F}(-R)$, pairing with ξ_Q, and using the definition of $\mathbb{V}_{\text{loc}}$ gives the following:

$$V_{\text{loc}} = \begin{pmatrix} C_c(-3+\cos 2\phi) & C_c\sin 2\phi & C_cl\sin 2\phi \\ C_c\sin 2\phi & -C_c(3+\cos 2\phi) & -2C_cl\cos^2\phi \\ C_cl\sin 2\phi & -2C_cl\cos^2\phi & -2C_cl^2\cos^2\phi \end{pmatrix}. \tag{68}$$

With the definition of the Stokesian connection Γ_{Stokes}, A_{Stokes} can be calculated:

$$A_{\text{Stokes}} = \begin{pmatrix} d\nu \\ \\ 0 \\ \\ \frac{\tan\phi}{l}d\nu \end{pmatrix}, \tag{69}$$

giving the equations

$$g^{-1}\dot{g} = -A_{\text{Stokes}}\dot{r} + \mathbb{V}_{\text{loc}}^{-1}k \tag{70}$$

$$= \begin{pmatrix} -\dot{\nu} - \frac{k_x l + k_\theta \tan\phi}{2C_c l}, \\ \frac{k_\theta - k_y l}{2C_c l} \\ \frac{\dot{\nu}\tan\phi}{l} + \frac{-k_\theta \sec^2\phi + l(k_y - k_1\tan\phi)}{2C_c l^2} \end{pmatrix}. \tag{71}$$

2.5 Unconstrained Reduction with Dissipation

Reduction techniques for a mechanical system with dissipation can be synthesized from the techniques introduced in the last two sections. Starting with

$$g^{-1}\dot{g} + A_{\text{mech}}\dot{r} = \mathbb{I}_{\text{loc}}^{-1}p \tag{72}$$

where the body momentum is

$$p = \text{Ad}_g^* J. \tag{73}$$

Then considering

$$g^{-1}\dot{g} + A_{\text{Stokes}}\dot{r} = \mathbb{V}_{\text{loc}}^{-1}\text{Ad}_g^* K. \tag{74}$$

A function $\phi(t,s)$, such that $\phi(a,s) = \phi(b,s) = \phi(t,0) = 0$, can be selected and the variation considered:

$$q(t,s) = \exp(\phi(t,s)\xi)q(t), \tag{75}$$

where $\xi \in \mathfrak{g}$. Substituting the corresponding infinitesimal variation

$$\partial q(t) = \frac{\partial \phi}{\partial s} \mid_{s=0} \xi_Q(q(t)), \tag{76}$$

into

$$\partial \int_a^b L(q(t), \dot{q}(t))dt + \int_a^b F(q(t), \dot{q}) \cdot \partial q dt = 0, \tag{77}$$

gives

$$\begin{aligned} \langle F(q, \dot{q}, \xi_Q(q)) \rangle &= \frac{d}{dt} \langle \mathbb{F}L(q, \dot{q}), \xi_Q(q) \rangle & (78) \\ &= \frac{d}{dt} \langle J(q, \dot{q}), \xi \rangle & (79) \\ &= \left\langle \frac{d}{dt} J(q, \dot{q}), \xi \right\rangle. & (80) \end{aligned}$$

Thus, $K(q, \dot{q}) = \dot{J}(q, \dot{q})$ under the natural identification of $\mathfrak{g}^*$ with $T_J\mathfrak{g}^*$, and

$$g^{-1}\dot{g} + A_{\text{Stokes}}\dot{r} = \mathbb{V}_{\text{loc}}^{-1} \text{Ad}_g^* \dot{J}. \tag{81}$$

The expression $\text{Ad}_g^* \dot{J}$ can be re-expressed in terms of body momenta as

$$\text{Ad}_g^* \dot{J} = \dot{p} - \text{ad}_{g^{-1}\dot{g}}^* p. \tag{82}$$

See Kelly (1998) for the derivation. Substituting (82) back into (81) gives

$$\begin{aligned}
\dot{p} - \mathrm{ad}^*_{g^{-1}\dot{g}} p &= \mathrm{Ad}^*_g \dot{J} \\
\dot{p} - \mathrm{ad}^*_{g^{-1}\dot{g}} p &= \mathbb{V}_{\mathrm{loc}}(g^{-1}\dot{g} + A_{\mathrm{Stokes}}\dot{r}) \\
\dot{p} &= \mathbb{V}_{\mathrm{loc}}(g^{-1}\dot{g} + A_{\mathrm{Stokes}}\dot{r} + \mathrm{ad}^*_{g^{-1}\dot{g}} p. \qquad (83)
\end{aligned}$$

Substituting

$$g^{-1}\dot{g} = -A_{\mathrm{mech}}\dot{r} + \mathbb{I}^{-1}_{\mathrm{loc}} p \qquad (84)$$

into (83) gives

$$\dot{p} = \mathbb{V}_{\mathrm{loc}}(A_{\mathrm{Stokes}} - A_{\mathrm{mech}})\dot{r} + \mathbb{V}_{\mathrm{loc}}\mathbb{I}^{-1}_{\mathrm{loc}} p + \mathrm{ad}^*_{g^{-1}\dot{g}} p. \qquad (85)$$

Thus, (84) and (85) completely define the motion of an unconstrained inertial system with dissipation.

The classical *Reynolds number* can be applied to the present situation by constructing the Reynolds tensor $\mathbb{I}_{\mathrm{loc}}\mathbb{V}^{-1}_{\mathrm{loc}}$ and premultiplying (85) by $\mathbb{I}_{\mathrm{loc}}\mathbb{V}^{-1}_{\mathrm{loc}}$. In the low Reynolds number limit, as with $\mathbb{I}_{\mathrm{loc}}\mathbb{V}^{-1}_{\mathrm{loc}} \to 0$, (85) and (84) become

$$\begin{aligned}
g^{-1}\dot{g} &= -A_{\mathrm{mech}}\dot{r} + \mathbb{I}_{\mathrm{loc}} p, \\
0 &= \mathbb{I}_{\mathrm{loc}}(A_{\mathrm{Stokes}} - A_{\mathrm{mech}})\dot{r} + p; \qquad (86)
\end{aligned}$$

and rearranging gives

$$g^{-1}\dot{g} = -A_{\text{Stokes}}\dot{r}. \tag{87}$$

In the inviscid limit as $\mathbb{V} \to 0$, and (85) and (84) reduce to the familiar equations

$$\begin{aligned} g^{-1}\dot{g} &= -A_{\text{mech}}\dot{r} + \mathbb{I}_{\text{loc}}^{-1}p, \\ \dot{p} &= \text{ad}^*_{g^{-1}\dot{g}}p. \end{aligned}$$

The following example demonstrates all of these techniques.

Example 2.5.1.

In the unconstrained system from Section 3, A_{mech} and $\mathbb{I}_{\text{loc}}$ were already calculated. Now, the following dissipation function is added.

$$R = \frac{1}{2}C_d(\dot{x}\cos\theta + \dot{y}\sin\theta)^2 + \frac{1}{2}C_b(-\dot{x}\sin\theta + \dot{y}\cos\theta)^2. \tag{88}$$

This function defines a dissipative force that occurs whenever the (x, y) coordinate moves. Next, the following maps are calculated:

$$\mathbb{V}_{\text{loc}} = \begin{pmatrix} -C_d & 0 & 0 \\ 0 & -C_b & 0 \\ 0 & 0 & 0 \end{pmatrix}; \tag{89}$$

and

$$A_{\text{Stokes}} = \begin{pmatrix} 0 \\ 0 \\ 0 \end{pmatrix}. \tag{90}$$

These maps, along with the previously calculated maps, give all the information needed to realize the reduced equations of motion for the system.

$$\begin{aligned} g^{-1}\dot{g} &= -A_{\text{mech}}\dot{r} + \mathbb{I}_{loc}^{-1}p, \\ \dot{p} &= \mathbb{V}_{\text{loc}}(A_{\text{Stokes}} - A_{\text{mech}})\dot{r} + \mathbb{V}_{\text{loc}}\mathbb{I}_{\text{loc}}^{-1}p + \text{ad}^*_{g^{-1}\dot{g}}p, \end{aligned}$$

$$\begin{pmatrix} \dot{g} \\ \dot{p} \end{pmatrix} = \begin{pmatrix} \dot{x} \\ \dot{y} \\ \dot{\theta} \\ \dot{p}_x \\ \dot{p}_y \\ \\ \dot{p}_\theta \end{pmatrix} = \begin{pmatrix} \frac{\cos\theta p_x}{m} - \frac{\sin\theta(J_B+J_J+l^2m)p_y}{m(J_B+J_J)} + \frac{lm(-p_\theta+J_B\dot{\phi})}{m(J_B+J_J)} \\ \frac{\sin\theta p_x}{m} + \frac{\cos\theta(J_B+J_J+l^2m)p_y}{m(J_B+J_J)} + \frac{lm(-p_\theta+J_B\dot{\phi})}{m(J_B+J_J)} \\ \frac{-lp_y+p_\theta-J_B\dot{\phi}}{J_B+J_J} \\ -\frac{C_d p_x}{m} - \frac{lp_y^2}{J_B+J_J} + \frac{p_y p_\theta}{J_B+J_J} + \frac{J_B p_y\dot{\phi}}{J_B+J_J} \\ -\frac{C_b l^2 p_y}{J_B+J_J} - \frac{C_b J_B p_y}{(J_B+J_J)m} - \frac{C_b J_J p_y}{(J_B+J_J)m} + \frac{lp_x p_y}{J_B+J_J} \\ +\frac{C_b l p_\theta}{J_B+J_J} - \frac{p_x p_\theta}{J_B+J_J} + \frac{C_b J_B l\dot{\phi}}{J_B+J_J} - \frac{J_B p_x\dot{\phi}}{J_B+J_J} \\ \frac{l^2 p_x p_y}{J_B+J_J} - \frac{lp_x p_\theta}{J_B+J_J} - \frac{J_B l p_x\dot{\phi}}{J_B+J_J} \end{pmatrix}. \tag{91}$$

2.6 Nonholonomically Constrained Systems

A nonholonomic constraint is simply a constraint that is non-integrable. Deriving reduced equations of motion for such a system requires more consideration than deriving equations of motion for unconstrained systems.

Definition 2.6.1. Given a G-invariant local basis, $X_1, ..., X_{n-k}$, for D, there exist

G-invariant one forms, $\omega^1, ..., \omega^k$ such that the **constraint distribution** is given by

$$\mathcal{D} = v \in TQ | \langle \omega^i; v \rangle = 0, i = 1, ..., k. \tag{92}$$

Definition 2.6.2. The intersection of the constraints with the fiber distribution $S = \mathcal{D} \cap VQ$ is called the **constrained fiber distribution**. The subspace of $\mathfrak{g}$ that generates S is denoted as $\mathfrak{g}^q$, with elements ξ^q.

Definition 2.6.3. The **constrained Lie algebra** $\mathfrak{g}^S$ is the fiber bundle over Q with fibers $\mathfrak{g}^S$, such that $\mathfrak{g}^S \simeq S/G$.

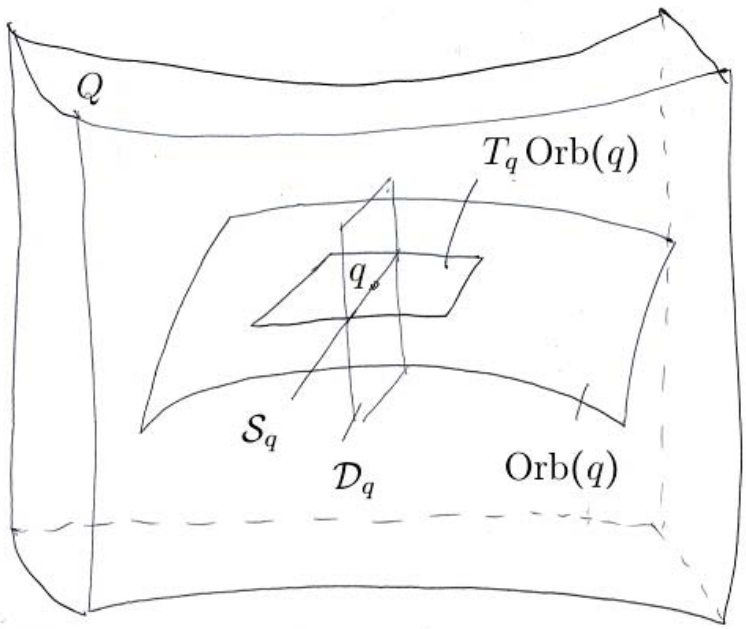

Figure 12: The manifold intersections forming $\mathcal{S}_q$.

Next, a fiber distribution $\mathcal{U}_q \subset T_q(\text{Orb}(q))$ is selected, such that $T_q(\text{Orb}(q)) = \mathcal{S}_q \oplus \mathcal{U}_q$. These concepts are clarified in the following example.

Example 2.6.1. Starting with a nonholonomically constrained system with one actuated degree of freedom, so that $Q = G \times M$, where TM consists of vectors in $\frac{\partial}{\partial \phi}$. The constraint is given by

$$\dot{x}\sin\theta - \dot{y}\cos\theta = 0. \tag{93}$$

It allows for rotation and translation in one direction. The one form corresponding to this constraint is

$$\omega = \sin\theta dx - \cos\theta dy. \tag{94}$$

A constraint distribution $\mathcal{D}$ corresponding to this one form is

$$\mathcal{D} = v \in TQ = \text{span}\{\cos\theta\frac{\partial}{\partial x} + \sin\theta\frac{\partial}{\partial y}, \frac{\partial}{\partial \theta}, \frac{\partial}{\partial \phi}\}, \tag{95}$$

where

$$\begin{aligned} \langle \omega, v \rangle &= \langle \sin\theta dx - \cos\theta dy, \cos\theta\frac{\partial}{\partial x} + \sin\theta\frac{\partial}{\partial y}\rangle \\ 0 &= \sin\theta\cos\theta - \cos\theta\sin\theta. \end{aligned} \tag{96}$$

This distribution is not necessarily unique. However, this particular choice is simple and lends itself well to the present discussion. With

$$VQ = \text{span}\{\frac{\partial}{\partial x}, \frac{\partial}{\partial y}, \frac{\partial}{\partial \theta}\}, \tag{97}$$

the constrained fiber distribution is

$$\begin{aligned}\mathcal{S} &= \mathcal{D} \cap VQ \\ &= \operatorname{span}\{\cos\theta\frac{\partial}{\partial x} + \sin\theta\frac{\partial}{\partial y}, \frac{\partial}{\partial \theta}\}. \end{aligned} \tag{98}$$

The constrained Lie algebra $\mathfrak{g}^S$ lies in the quotient group S/G. Its basis can be determined by taking S as the identity so that elements in $\mathfrak{g}^S$ lie in the vector space defined by

$$\operatorname{span}\{\frac{\partial}{\partial x}, \frac{\partial}{\partial \theta}\}. \tag{99}$$

Momentum maps and inertia/viscosity tensors can be defined for this system, much as they are for unconstrained and dissipative systems.

Definition 2.6.4. The **nonholonomic momentum map** is the map, $J_{\text{nhc}} : TQ \to (\mathfrak{g}^S)^*$, defined by

$$\langle J_{\text{nhc}}, \xi^q \rangle = \langle\!\langle v_q, \xi^q_Q \rangle\!\rangle, \tag{100}$$

where $\xi^q \in \mathfrak{g}^q$.

Definition 2.6.5. The **dissipative nonholonomic momentum map** is the map, $K_{\text{nhc}} : TQ \to (\mathfrak{g}^S)^*$, defined by

$$\langle K_{\text{nhc}}, \xi^q \rangle = \langle\!\langle v_q, \xi^q_Q \rangle\!\rangle, = \langle F, \xi^q_Q \rangle, \tag{101}$$

where $\xi^q \in \mathfrak{g}^q$.

To embed the constrained Lie algebra elements $\mathfrak{g}^S$ into the unconstrained Lie algebra elements, $f_1, ..., f_s$ is taken as a basis for $\mathfrak{g}^S$, along with the local form of the unconstrained locked inertia tensor for the system in $\mathfrak{g}$. Then,

Definition 2.6.6.

$$(\mathbb{I}^c_{\text{loc}})_{\alpha,\beta} = (\mathbb{I}_{\text{loc}})_{ab} f^a_\alpha f^b_\beta, \tag{102}$$

where $(\mathbb{I}^c_{\text{loc}})^{-1} : (\mathfrak{g}^S)^* \to \mathfrak{g}^S$.

As shown in Ostrowski (1996), elements in $\mathfrak{g}$ for a nonholonomically constrained system are given as

$$\xi = g^{-1}\dot{g} = -A_{\text{mech}}\dot{r} + \tilde{\mathbb{I}}^{-1}_{\text{loc}} p, \tag{103}$$

where

$$(\tilde{\mathbb{I}}^{-1}_{\text{loc}})^{a\alpha} = ((\mathbb{I}^c_{\text{loc}})^{-1})^{\alpha\beta} f^a_\beta. \tag{104}$$

Similarly,

Definition 2.6.7.

$$(\mathbb{V}^c_{\text{loc}})_{\alpha\beta} = (\mathbb{V}_{\text{loc}})_{ab} f^a_\alpha f^b_\beta, \tag{105}$$

where $\mathbb{V}_{\text{loc}}$ is the local form of the unconstrained locked viscosity tensor and $(\mathbb{V}^c_{\text{loc}})^{-1} : (\mathfrak{g}^S)^* \to \mathfrak{g}^S$. Elements in $\mathfrak{g}$ are given as

$$\xi = g^{-1}\dot{g} = -A_{\text{Stokes}}\dot{r} + \tilde{\mathbb{V}}_{\text{loc}}^{-1}\text{Ad}_g^* K, \tag{106}$$

where

$$(\tilde{\mathbb{V}}_{\text{loc}}^{-1})^{a\alpha}((\mathbb{V}_{\text{loc}}^c)^{-1})^{\alpha\beta}f_\beta^a. \tag{107}$$

Definition 2.6.8. The **nonholonomic connection** is the map $\Gamma^{\text{sym}} : TQ \to \mathfrak{g}^S$ given by

$$\Gamma^{\text{sym}} = (\mathbb{I}_{\text{loc}}^c)^{-1} J_{\text{nhc}}, \tag{108}$$

where $\Gamma_Q^{\text{sym}} : T_qQ \to T_qQ$ is the identity on all vectors in S.

Definition 2.6.9. The **dissipative nonholonomic connection** is the map $\Gamma_{\text{Stokes}}^{\text{sym}} : TQ \to \mathfrak{g}^S$ given by

$$\Gamma_{\text{Stokes}}^{\text{sym}} = (\mathbb{V}_{\text{loc}}^c)^{-1} K_{\text{nhc}}, \tag{109}$$

where $\Gamma_{\text{Stokes}Q}^{\text{sym}} : T_qQ \to T_qQ$ is the identity on all vectors in S.

The connections were constructed using $\mathcal{S}_q$. Using $\mathcal{U}_q$ gives Γ^{kin}. Because the constraints indicate that vectors in $\mathcal{U}_q$ are 0, the corresponding principal connection should be $\Gamma^{\text{kin}} = 0$. Both principal connections together forming a single principal connection for the entire system gives

$$\Gamma = \Gamma^{\text{sym}} + \Gamma^{\text{kin}}, \tag{110}$$

with

$$\Gamma^{\text{kin}}(\dot{q}) = 0, \tag{111}$$

$$\Gamma^{\text{sym}}(\dot{q}) = (\mathbb{I}^c_{\text{loc}})^{-1} J_{\text{nhc}}. \tag{112}$$

Example 2.6.2. In this example, equations for the Lie algebra elements of the system defined in Example 2.3.1 are derived, subject to the nonholonomic constraints in Example 2.6.1. This system corresponds to the following figure. However, for this example, the constraint does not allow the coordinate (x, y) to move normal to the length of body l. The basis elements of the constraint are used to define the nonholonomic momentum map, J_{nhc}. The map

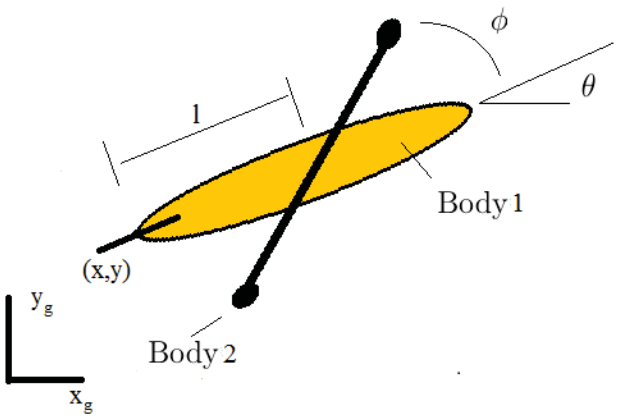

Figure 13: The beanie diagram with a nonholonomic constraint.

$$\begin{aligned}\langle J_{\text{nhc}};\xi^q\rangle &= \langle\!\langle v_q, \xi_Q^q\rangle\!\rangle \\ &= \langle \mathbb{F}L, \xi_Q^q\rangle,\end{aligned}$$

can be used to calculate the mechanical connection

$$A_{\text{mech}} = \begin{pmatrix} 0 \\ \frac{J_B l}{J_B+J_J} \\ -\frac{J_B}{J_B+J_J} \end{pmatrix}, \tag{113}$$

and the constrained locked inertia tensor

$$\tilde{\mathbb{I}}_{\text{loc}}^{-1} = \begin{pmatrix} 0 & 0 \\ \frac{J_B+J_J+ml^2}{m(J_B+J_J)} & -\frac{l}{J_B+J_J} \\ -\frac{l}{J_J+J_B} & \frac{1}{J_B+J_J} \end{pmatrix}, \tag{114}$$

which can then be used to calculate

$$g^{-1}\dot{g} = -A_{\text{mech}}(r)\dot{r} + \tilde{\mathbb{I}}_{\text{loc}}^{-1}p,$$

and

$$\begin{pmatrix} \dot{g} \end{pmatrix} = \begin{pmatrix} \dot{x} \\ \dot{y} \\ \dot{\theta} \end{pmatrix} = \begin{pmatrix} \frac{\cos\theta p_1}{m} \\ \frac{\sin\theta p_2}{m} \\ \frac{p_2 - J_B\dot{\phi}}{J_B+J_J+l^2m} \end{pmatrix}. \tag{115}$$

The Lie algebra elements can be used to define equations for the body momentum of a nonholonomically constrained system.

The body momentum equations can be defined using the following definitions:

Definition 2.6.10. Given a set of constraint one forms, $\omega^1, ..., \omega^k$ and a forcing function τ and splitting them using the trivial bundle structure as

$$\omega = \omega_g dg + \omega_r dr, \tag{116}$$

and

$$\tau = \tau_g dg + \tau_r dr, \tag{117}$$

the **nonholonomic constrained variational principle** can be written as

$$\frac{d}{dt}\left(\frac{\partial L}{\partial \dot{q}} - \frac{\partial L}{\partial q}\right) = \lambda\omega_r + \tau_r. \tag{118}$$

Definition 2.6.11. The **reduced Lagrangian** is the function $l : TQ/G \to \mathbb{R}$ induced by a G-invariant Lagrangian function, given by

$$l(\xi, r, \dot{r}) = L(g^{-1}g, r, \dot{r}, g^{-1}\dot{g}). \tag{119}$$

The invariance of the Lagrangian and its corresponding reduced Lagrangian can be used to write the nonholonomically constrained variational principle equations on the partially reduced space of $\mathfrak{g} \times TM$.

Definition 2.6.12. The **reduced nonholonomic constrained variational principle** on $\mathfrak{g} \times TM$ is given by

$$\begin{aligned} \frac{d}{dt}(\frac{\partial l}{\partial \xi^a}) - \mathrm{ad}^*_\xi \frac{\partial l}{\partial \xi^a} &= \lambda\omega_g \mathbf{g} + \tau_g \mathbf{g}, \\ \frac{d}{dt}(\frac{\partial l}{\partial \dot{r}}) - \frac{\partial l}{\partial r} &= \lambda\omega_r + \tau_r, \end{aligned} \tag{120}$$

where $\mathbf{g}$ denotes the coordinate version of the lifted left action T_eL_g on $T_eG = \mathfrak{g}$ and ad^*_ξ is the dual of the adjoint action of $\mathfrak{g}$ on $\mathfrak{g}$ such that $\mathrm{ad}_\xi\eta = [\xi, \eta]$ and $\mathrm{ad}^*_\xi p = \langle p; [\xi, \cdot]\rangle$.

Definition 2.6.13. If (L, D) is a constrained system on $Q(M, G)$ and L is G-invariant, for all curves $c : [a, b] \to Q$ satisfying the nonholonomic constrained variational principle, the following **generalized momentum equation** holds for all elements, $\xi^q \in \mathfrak{g}^q$:

$$\frac{d}{dt} = \frac{\partial L}{\partial \dot{q}}(\frac{d}{dt}[\xi^q(c(t))])_Q + \tau_r(\xi^q(c(t)))_q, \tag{121}$$

where

$$p = \frac{\partial L}{\partial \dot{q}}(\xi^q(c(t))_Q) \tag{122}$$

is the generalized momentum.

Definition 2.6.14. Given the above basis for the constrained Lie algebra, $f \in \mathfrak{g}^S$, the generalized momentum equation is along trajectories

$$\frac{d}{dt}(p_\alpha) = \frac{\partial L}{\partial \dot{q}}(\frac{d}{dt} f_\alpha)_Q(t) + \tau(f_\alpha)_Q, \tag{123}$$

where

$$p_\alpha = \frac{\partial L}{\partial \dot{q}}(f_\alpha)_Q. \tag{124}$$

Thus, the equations of motion governing flow along the fiber can be written

$$\frac{d}{dt}(\frac{\partial l}{\partial \xi}) = \mathrm{ad}^*_\xi(\frac{\partial l}{\partial \xi}) + \lambda\omega(e,r) + \tau^e, \tag{125}$$

where $\omega(e,r)$ are the constraints evaluated at $g = e$ as above. As noted, the basis for the constrained fiber distribution is $f_1, ..., f_s$. Noting that any element of this distribution is in the kernel of ω gives the following.

Definition 2.6.15. The **body momentum equations** are

$$\begin{aligned}
\frac{d}{dt}(p_\alpha) &= \frac{d}{dt}(\frac{\partial l}{\partial \xi})f_\alpha + \frac{\partial l}{\partial \xi}\frac{d}{dt}(f_\alpha) \\
&= \mathrm{ad}^*_\xi(\frac{\partial l}{\partial \xi})f_\alpha + \frac{\partial l}{\partial \xi}\frac{d}{dt}(f_\alpha) + \tau^e f_\alpha \\
&= \langle \frac{\partial l}{\partial \xi}; [\xi, f_\alpha] + \frac{d}{dt}(f_\alpha)\rangle + \tau^e f_\alpha,
\end{aligned} \tag{126}$$

where the definition of the generalized momentum, $p_\alpha = \frac{\partial l}{\partial \xi} \cdot f_\alpha$, is used.

The system is now completely defined by the equations

$$\begin{aligned}
\xi = g^{-1}\dot{g} &= -A^{\mathrm{sym}}_{\mathrm{mech}}(r)\dot{r} + \tilde{\mathbb{I}}^{-1}p, \\
\dot{p} &= \langle \frac{\partial l}{\partial \xi}; [\xi, f_\alpha\rangle + \frac{d}{dt}(f_\alpha)\rangle + \tau^e f_\alpha.
\end{aligned} \tag{127}$$

Example 2.6.3. The final example for this section derives the body momentum equations for the system. Because the above Lagrangian is G-invariant, the reduced

Lagrangian, l, of the system is given by

$$l = \frac{1}{2}m(\xi_x^2 + \xi_y^2 + l^2 m\xi_\theta^2) + lm\xi_y\xi_\theta + \frac{1}{2}(J_J)\xi_\theta^2 + \frac{1}{2}J_B(\xi_\theta + \dot{\phi})^2. \tag{128}$$

The partial derivatives of l with respect to Lie algebra elements ξ are

$$\frac{\partial l}{\partial \xi} = \begin{pmatrix} m\xi_x \\ m(\xi_y + l\xi_\theta) \\ (J_B - J_J)\xi_\theta + lm(\xi_y + l\xi_\theta) + J_B\dot{\phi}. \end{pmatrix}. \tag{129}$$

Lie bracketing the Lie algebra elements with the constrained Lie algebra elements gives

$$\begin{aligned} [\xi, f_1] &= \begin{pmatrix} 0 & -\xi_\theta & \xi_x \\ \xi_\theta & 0 & \xi_y \\ 0 & 0 & 0 \end{pmatrix}\begin{pmatrix} 0 & 0 & 1 \\ 0 & 0 & 0 \\ 0 & 0 & 0 \end{pmatrix} - \begin{pmatrix} 0 & 0 & 1 \\ 0 & 0 & 0 \\ 0 & 0 & 0 \end{pmatrix}\begin{pmatrix} 0 & -\xi_\theta & \xi_x \\ \xi_\theta & 0 & \xi_y \\ 0 & 0 & 0 \end{pmatrix} \\ &= \begin{pmatrix} 0 & 0 & 0 \\ 0 & 0 & \xi_\theta \\ 0 & 0 & 0 \end{pmatrix}, \end{aligned} \tag{130}$$

and written as a triple gives

$$[\xi, f_1] = \begin{pmatrix} 0 & \xi_\theta & 0 \end{pmatrix}. \tag{131}$$

In addition,

$$
\begin{aligned}
[\xi, f_2] &= \begin{pmatrix} 0 & -\xi_\theta & \xi_x \\ \xi_\theta & 0 & \xi_y \\ 0 & 0 & 0 \end{pmatrix} \begin{pmatrix} 0 & -1 & 0 \\ 1 & 0 & 0 \\ 0 & 0 & 0 \end{pmatrix} - \begin{pmatrix} 0 & -1 & 0 \\ 1 & 0 & 0 \\ 0 & 0 & 0 \end{pmatrix} \begin{pmatrix} 0 & -\xi_\theta & \xi_x \\ \xi_\theta & 0 & \xi_y \\ 0 & 0 & 0 \end{pmatrix} \\
&= \begin{pmatrix} 0 & 0 & \xi_y \\ 0 & 0 & -\xi_x \\ 0 & 0 & 0 \end{pmatrix}, \qquad (132)
\end{aligned}
$$

written as a triple gives

$$
[\xi, f_2] = \begin{pmatrix} \xi_y & -\xi_x & 0 \end{pmatrix}. \qquad (133)
$$

The time derivatives of the constrained Lie algebra elements are simply

$$
\begin{aligned}
\frac{d}{dt}(f1) &= 0, \\
\frac{d}{dt}(f2) &= 0. \qquad (134)
\end{aligned}
$$

Taking the natural pairing of the first calculation with the sum of the last two calculations gives

$$\begin{aligned}\dot{p_1} &= \langle \frac{\partial l}{\partial \xi}, [\xi, f_1] + \frac{d}{dt}(f_1) \rangle \\ &= \begin{pmatrix} m\xi_x \\ m(\xi_y + l\xi_\theta) \\ (J_B - J_J)\xi_\theta + lm(\xi_y + l\xi_\theta) + J_B\dot{\phi} \end{pmatrix}^T \begin{pmatrix} 0 \\ \xi_\theta \\ 0 \end{pmatrix}. \end{aligned} \tag{135}$$

Using (127), the Lie algebra elements are calculated as

$$\begin{pmatrix} \xi_x \\ \xi_y \\ \xi_\theta \end{pmatrix} = \begin{pmatrix} \frac{p_y}{m} \\ \frac{p_x}{m} \\ 0 \end{pmatrix}, \tag{136}$$

then

$$\dot{p_1} = \frac{lm(p_2 - J_B\dot{\phi})^2}{(J_B + J_J + l^2m)^2}. \tag{137}$$

Further,

$$\begin{aligned}\dot{p_2} &= \langle \frac{\partial l}{\partial \xi}, [\xi, f_2] + \frac{d}{dt}(f_2) \rangle \\ &= \begin{pmatrix} m\xi_x \\ m(\xi_y + l\xi_\theta) \\ (J_B - J_J)\xi_\theta + lm(\xi_y + l\xi_\theta) + J_B\dot{\phi} \end{pmatrix}^T \begin{pmatrix} \xi_y \\ -\xi_x \\ 0 \end{pmatrix} \\ &= -\frac{lp_1(p_1 - J_B\dot{\phi})}{J_B + J_J + l^2m}. \end{aligned} \tag{138}$$

Recognizing the system has no dissipation, that is, $\tau = 0$, the body momentum equations have been solved for.

CHAPTER 3: DISSIPATION AS A CONSTRAINT

Dissipative forces can be useful in modeling Lagrangian systems with friction and energy loss. They often have many applications, from modeling bushings in automotive models to modeling friction in systems with slippage. Understanding how these forces behave in the limiting cases can be useful for establishing and verifying the bounds of their applicability.

In this chapter, a theorem is proposed and proved, indicating in the limit, as a dissipative system becomes infinitely dissipative, it acts as though constrained. Then, analytical models for constrained and dissipative systems are constructed and compared to demonstrate the validity and applicability of the theorem. Last, simulations numerically support the validity of the theorem.

3.1 Theory

Before the theorem is proved, a few concepts must be defined.

Definition 3.1.1. In a vector space T_qQ corresponding to a Rayleigh interpolated system, the principal connection for this space is given by

$$\Gamma = \Gamma^0_{\text{Stokes+mech}}. \tag{139}$$

Definition 3.1.2. Given a G-invariant local basis, $X_1, ..., X_{n-k}$, there exist G-invariant one forms, $\omega^1_R, ..., \omega^k_R$, denoted as the restricted one forms.

Definition 3.1.3. Restricted one forms can be used to define the **Rayleigh restricted distribution**, given by

$$\mathcal{H} = v \in TQ | \langle \omega_R^i; v \rangle = 0, i = 1, ..., k. \tag{140}$$

Definition 3.1.4. The intersection of the restricted space with the fiber distribution,

$$\mathcal{N} = \mathcal{H} \cap VQ, \tag{141}$$

is called the **restricted fiber distribution**. The subspace of $\mathfrak{g}$ that generates N is denoted $\mathfrak{g}^N$, with elements ξ^N.

Thus, the following are defined:

Definition 3.1.5. The **complementary distribution** $\mathcal{F}_q$ such that

$$\mathcal{F}_q \oplus \mathcal{H}_q = T_q Q. \tag{142}$$

Definition 3.1.6. The **complementary one forms** define the distribution

$$\mathcal{F}_q = v \in TQ | \langle \omega_F^i; v \rangle = 0, i = 1, ..., k. \tag{143}$$

Definition 3.1.7. The **complementary fiber distribution** is given by

$$\mathcal{R}_q = \mathcal{F}_q \cap T_q(\mathrm{Orb}(q)), \tag{144}$$

with Lie algebra elements $\mathfrak{g}^R$.

The superscript $\mathcal{N}$ or $\mathcal{R}$ will be added to the principal connection maps to denote

the corresponding fiber distribution. The same procedures presented in Chapter 2, Section 6, can be used to arrive at these maps, giving

$$\Gamma^0_{\text{Stokes+mech}} = \Gamma^{\mathcal{N}}_{\text{Stokes+mech}} + \Gamma^{\mathcal{R}}_{\text{Stokes+mech}}. \tag{145}$$

These procedures and the previous definitions allow for the following theorem.

Proposition 3.1.1. *Given a set of complementary one forms $\omega^1_F \ldots, \omega^k_F$ identical to a set of constraint one forms from a given nonholonomically or holonomically constrained system, $\omega^1 \ldots, \omega^k$, and using these to split the tangent spaces and connections for a nonholonomic system and dissipative system, respectively, then in the limit as $\mathbb{V}^{-1}_{loc}\mathbb{I}_{loc} \to 0$ for $\Gamma^{\mathcal{N}}_{\text{Stokes+mech}}$, and in the limit as $\mathbb{V}_{loc} \to 0$ for $\Gamma^{\mathcal{R}}_{\text{Stokes+mech}}$, the principal connections $\Gamma^{\mathcal{N}}_{\text{Stokes+mech}}$ and $\Gamma^{\mathcal{R}}_{\text{Stokes+mech}}$ converge to the principal connections Γ_{kin} and Γ_{sym} for a nonholonomically or holonomically constrained system.*

Proof. The principal connection for a system that has been split using the constraint one forms $\omega^1, \omega^2, \ldots \omega^k$ into two connections is

$$\Gamma = \Gamma_{\text{sym}} + \Gamma_{\text{kin}},$$

where

$$\begin{aligned} \Gamma_{\text{kin}} &= 0, \\ \Gamma_{\text{sym}} &= (\mathbb{I}^c)^{-1} J_{\text{nhc}}. \end{aligned}$$

(147)

Given complementary one forms $\omega_F^1, \omega_F^2, \ldots \omega_F^k$ that are identical to the constraint one forms, and given a Rayleigh interpolated system with connection $\Gamma^0_{\text{Stokes+mech}}$, ω_F can be used to split $\Gamma^0_{\text{Stokes+mech}}$ into two connections, such that $\Gamma^{\mathcal{N}}_{\text{Stokes+mech}} + \Gamma^{\mathcal{R}}_{\text{Stokes+mech}} = \Gamma^0_{\text{Stokes+mech}}$. The reduced equations corresponding to $\mathcal{N}_q$ are

$$\begin{aligned} g^{-1}\dot{g} &= -A_{\text{mech}}\dot{r} + \mathbb{I}_{\text{loc}}^{-1} p, \\ \dot{p} &= \mathbb{V}_{\text{loc}}(A_{\text{Stokes}} - A_{\text{mech}})\dot{r} + \mathbb{V}_{\text{loc}}\mathbb{I}_{\text{loc}}^{-1} p + \text{ad}^*_{g^{-1}\dot{g}} p. \end{aligned}$$

Letting $\mathbb{I}_{\text{loc}}\mathbb{V}_{\text{loc}}^{-1} \to 0$, the equations become

$$\begin{aligned} g^{-1}\dot{g} &= -A_{\text{mech}}\dot{r} + \mathbb{I}_{\text{loc}}^{-1} p, \\ 0 &= \mathbb{I}_{\text{loc}}(A_{\text{Stokes}} - A_{\text{mech}})\dot{r} + p, \end{aligned}$$

or

$$g^{-1}\dot{g} = -A_{\text{Stokes}}\dot{r}.$$

Rearranging this equation gives

$$
\begin{aligned}
0 &= g^{-1}\dot{g} + A_{\text{Stokes}}\dot{r} \\
0 &= \text{Ad}_g(g^{-1}\dot{g} + A_{\text{Stokes}}\dot{r}) \\
0 &= \text{Ad}_g \mathbb{V}_{\text{loc}}^{-1} \text{Ad}_g^* K \\
0 &= \mathbb{V}^{-1} K \\
0 &= \Gamma_{\text{Stokes}}^{\mathcal{N}} = \Gamma_{\text{kin}}.
\end{aligned} \tag{148}
$$

To show the convergence of the second principal connection, reduced equations for an interpolated Rayleigh system corresponding to $\mathcal{R}_q$ are used.

$$
\begin{aligned}
g^{-1}\dot{g} &= -A_{\text{mech}}\dot{r} + \mathbb{I}_{\text{loc}}^{-1} p, \\
\dot{p} &= \mathbb{V}_{\text{loc}}(A_{\text{Stokes}} - A_{\text{mech}})\dot{r} + \mathbb{V}_{\text{loc}}\mathbb{I}_{\text{loc}}^{-1} p + \text{ad}_{g^{-1}\dot{g}}^* p.
\end{aligned}
$$

Then allowing $\mathbb{V}_{\text{loc}} \to 0$, the reduced equations go to

$$
\begin{aligned}
g^{-1}\dot{g} &= -A_{\text{mech}}\dot{r} + \mathbb{I}_{\text{loc}}^{-1} p, \\
\dot{p} &= \text{ad}_{g^{-1}\dot{g}}^* p.
\end{aligned}
$$

Rearranging the first equation gives

$$
\begin{aligned}
-A_{\text{mech}}\dot{r} + \mathbb{I}_{\text{loc}}^{-1} p &= g^{-1}\dot{g} \\
\mathbb{I}_{\text{loc}}^{-1} p &= g^{-1}\dot{g} + A_{\text{mech}}\dot{r} \\
\text{Ad}_g(\mathbb{I}_{\text{loc}}^{-1}\text{Ad}_g^* J) &= \text{Ad}_g(g^{-1}\dot{g} + A_{\text{mech}}\dot{r}) \\
\mathbb{I}^{-1} J &= \Gamma_{\text{mech}}^{\mathcal{R}} = \Gamma_{\text{sym}}.
\end{aligned} \tag{149}
$$

Since the Rayleigh interpolated connections were split with identical one forms used to split the non-dissipative system, it is ensured that $\mathcal{R}_q \equiv \mathcal{S}_q$ and $\mathcal{N}_q \equiv \mathcal{U}_q$.

3.2 Modeling

The proposition is demonstrated by constructing and exploring example systems that correspond to special cases of the nonholonomic connection (excluding the purely kinematic case). These special cases are classified by the generic and extreme ways the subspaces ($\mathcal{F}_q, \mathcal{H}_q, \mathcal{D}, S_q$, and $T_q\text{Orb}(q)$) interact with each other. To begin, the following system is constructed.

Case	Conditions	Connection
Unconstrained	$\mathcal{D}_q = T_qQ$	$\Gamma_{\text{sym}}(\dot{q}) = \mathbb{I}^{-1}J(\dot{q})$
Purely Kinematic	$\mathcal{D}_q \bigcap T_q(\text{Orb}(q)) = 0$	$\Gamma_{\text{kin}}(\dot{q}) = 0$
Horizontal Symmetries	$\mathcal{D}_q \bigcap T_q(\text{Orb}_G(q)) = T_q(\text{Orb}_H(q))$	$\Gamma_{\text{sym}}(\dot{q}) + \Gamma_{\text{kin}}(\dot{q}) = \mathbb{I}^{-1}J_H(\dot{q})$
General Principal Bundle Case	$\mathcal{D}_q + T_q(\text{Orb}(q)) = T_qQ$	$\Gamma_{\text{sym}}(\dot{q}) + \Gamma_{\text{kin}}(\dot{q}) = \mathbb{I}^{-1}J_{\text{nhc}}(\dot{q})$

Table 1: The special cases of the nonholonomic connection (principal case).

Case	Conditions	Connection
non-dissipative	$\mathcal{F}_q = T_qQ$ $\mathcal{H}_q \bigcap T_q(\mathrm{Orb}(q)) = 0$	$\Gamma^{\mathcal{R}}_{\mathrm{mech}}(\dot{q}) = \mathbb{I}^{-1}J(\dot{q}))$
Purely Dissipative	$\mathcal{H}_q = T_qQ$ $\mathcal{H}_q \bigcap T_q(\mathrm{Orb}(q)) = 0$	$\Gamma^{\mathcal{N}}_{\mathrm{Stokes}}(\dot{q}) = \mathbb{V}^{-1}K(\dot{q}) = 0$
Horizontal Symmetries	$\mathcal{F}_q \bigcap T_q(\mathrm{Orb}_G(q))$ $= T_q(\mathrm{Orb}_H(q))$	$\Gamma^{\mathcal{N}}_{\mathrm{Stokes}}(\dot{q}) + \Gamma^{\mathcal{R}}_{\mathrm{mech}}(\dot{q}) = \mathbb{I}^{-1}J_H(\dot{q})$
General Principal Bundle Case	$\mathcal{F}_q + T_q(\mathrm{Orb}(q)) = T_qQ$	$\Gamma^{\mathcal{N}}_{\mathrm{Stokes}}(\dot{q}) + \Gamma^{\mathcal{R}}_{\mathrm{mech}}(\dot{q}) = \mathbb{I}^{-1}J(\dot{q})$

Table 2: The special cases of a dissipative system when $\mathbb{V}_{\mathrm{loc}} \to 0$ for $\mathcal{R}$ and $\mathbb{I}_{\mathrm{loc}}\mathbb{V}^{-1}_{\mathrm{loc}} \to 0$ for $\mathcal{N}$ (principal case).

$$
\begin{aligned}
q_r &= (x, y), \\
q_f &= (x + l\cos\theta, y + l\sin\theta), \\
v_r &= \dot{q}_r, \\
v_f &= \dot{q}_f, \\
v_{r_{LB}} &= v_r \cdot (\cos\theta, \sin\theta), \\
v_{r_{SB}} &= v_r \cdot (-\sin\theta, \cos\theta), \\
v_{f_{LB}} &= v_f \cdot (\cos\theta, \sin(\theta)), \\
v_{f_{SB}} &= v.(-\sin\theta, \cos\theta),
\end{aligned} \tag{150}
$$

This is the system explored in the previous chapter. However, to analyze this robotic system, it makes sense to re-envision the system as a small cart-like robot, with a rotating disk on the front and two wheels on the back (Figure 14). The wheels are

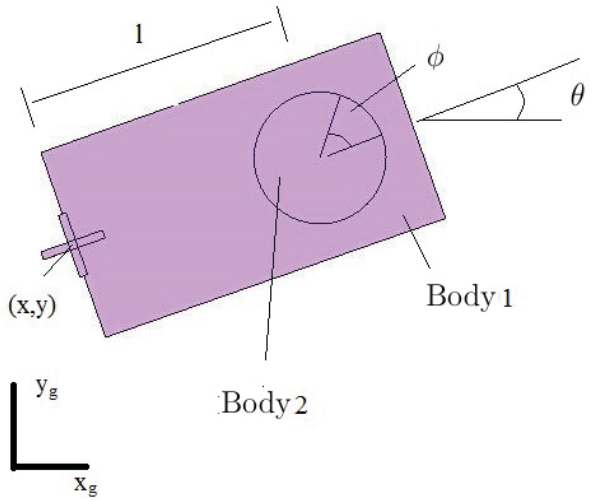

Figure 14: The beanie re-envisioned as a cart-like robot.

aligned perpendicular to one another.

3.2.1 Unconstrained, Non-Dissipative System

The unconstrained, non-dissipative case provides a way to explore the simplest form of the system. This can be thought of as the cart with both wheels removed. Throughout this chapter, constraints and dissipations will be added to this original system and results compared.

The position and orientation of the point at which the constraint is applied is $(x, y, \theta) \in SE(2)$, and $\phi \in \mathbb{S}$ is the relative angle between body one and body two. The total mass of the system is set at m, and the moments of inertias of body one and body two are J_B and J_J, respectively. Thus, the fiber bundle $Q = SE(2) \times \mathbb{S} = G \times M$ is the configuration space. The fiber coordinates are $g = (x, y, \theta)$, and base coordinate is $r = \phi$. This system has no potential energy. The Lagrangian corresponding to Figure 14 is

$$\mathcal{L} = \frac{1}{2}m(v_{f_{LB}}^2 + v_{f_{SB}}^2) + \frac{1}{2}J_J\dot{\theta}^2 + \frac{1}{2}J_B(\dot{\theta}+\dot{\phi})^2, \tag{151}$$

which is used to calculate

$$\mathbb{I}_{\text{loc}} = \begin{pmatrix} m & 0 & 0 \\ 0 & m & lm \\ 0 & lm & J_B + J_J + ml^2 \end{pmatrix}, \tag{152}$$

$$A_{\text{mech}} = \begin{pmatrix} 0 \\ \frac{J_B l}{J_B+J_J} \\ -\frac{J_B}{J_B+J_J} \end{pmatrix}. \tag{153}$$

Using

$$g^{-1}\dot{g} = -A_{\text{mech}}\dot{r} + \mathbb{I}_{\text{loc}}^{-1}p, \tag{154}$$

$$\dot{p} = \text{ad}^*_{g^{-1}\dot{g}}p, \tag{155}$$

give

$$\begin{pmatrix} \dot{g} \\ \dot{p} \end{pmatrix} = \begin{pmatrix} \dot{x} \\ \dot{y} \\ \dot{\theta} \\ \dot{p}_x \\ \dot{p}_y \\ \dot{p}_\theta \end{pmatrix} = \begin{pmatrix} \frac{\cos\theta p_x}{m} - \frac{\sin\theta(J_B+J_J+l^2m)p_y}{m(J_B+J_J)} + \frac{lm(-p_\theta+J_B\dot{\phi})}{m(J_B+J_J)} \\ \frac{\sin\theta p_x}{m} + \frac{\cos\theta(J_B+J_J+l^2m)p_y}{m(J_B+J_J)} + \frac{lm(-p_\theta+J_B\dot{\phi})}{m(J_B+J_J)} \\ \frac{-lp_y+p_\theta-J_B\dot{\phi}}{J_B+J_J} \\ -\frac{lp_y^2}{J_B+J_J} + \frac{p_y p_\theta}{J_B+J_J} + \frac{J_B p_y\dot{\phi}}{J_B+J_J} \\ \frac{lp_x p_y}{J_B+J_J} - \frac{p_x p_\theta}{J_B+J_J} - \frac{J_B p_x\dot{\phi}}{J_B+J_J} \\ \frac{l^2 p_x p_y}{J_B+J_J} - \frac{lp_x p_\theta}{J_B+J_J} - \frac{J_B l p_x\dot{\phi}}{J_B+J_J} \end{pmatrix}. \tag{156}$$

Equation (151) will serve as the Lagrangian for all systems in this chapter [1].

3.2.2 Nonholonomically Constrained Systems

In this section, three nonholonomic constraint cases, A, B, and C, are constructed for the system. Constraint A represents a system in which the constraint allows rotation only about the local origin. Constraint B [2] represents a system in which the constraint allows rotation about the local origin and translation along the direction that points to the center of masses of the rigid bodies (the local x direction). Constraint C represents a system in which the constraint disallows translation along the direction that points to the center of masses of the rigid bodies but allows it along the direction of the local y axis. The system is free to translate normal to this direction, as well as rotate. For each of the three systems,

$$\frac{\partial l}{\partial \xi} = \begin{pmatrix} m\xi_x \\ m(\xi_y + l\xi_\theta) \\ J + J\xi_\theta + lm(\xi_y + l\xi_\theta) + J_B(\xi_\theta + \dot{\phi}) \end{pmatrix}. \tag{157}$$

The constraint cases are shown in Table 3. The constraints, along with (152), (153), and (157), can be used to calculate the body momentum equations for the three cases. The only tensor unique to each constraint case is $\tilde{\mathbb{I}}^{-1}_{\text{loc}}$. Thus, it and the body momentum equations for each case will be calculated.

The resulting equations for the cases follow.

Case A

[1] When the system is not free to translate, the system is commonly referred to as Elroy's Beanie problem.

[2] Constraint Case B is referred to as the Chaplygin's Beanie problem in Kelly et al. (2012)

Case	A	B	C
constraint equation(s)	$\dot{x}\sin\theta - \dot{y}\cos\theta = 0$ $\dot{x}\cos\theta + \dot{y}\sin\theta = 0$	$\dot{x}\sin\theta - \dot{y}\cos\theta = 0$	$\dot{x}\cos\theta + \dot{y}\sin\theta = 0$
one form(s)	$\omega_{a_1} = \sin\theta dx - \cos\theta dy$ $\omega_{a_2} = \cos\theta dx + \sin\theta dy$	$\omega_{b_1} = \sin\theta dx - \cos\theta dy$	$\omega_{c_1} = \cos\theta dx + \sin\theta dy$
one form(s) at identity	$\omega_{a_{1_e}} = dy$ $\omega_{a_{2_e}} = dx$	$\omega_{b_{1_e}} = dy$	$\omega_{c_{1_e}} = dx$
subspace at identity	$f_{a_1}(r) = \frac{\partial}{\partial\theta}$	$f_{b_1}(r) = \frac{\partial}{\partial x}$ $f_{b_2}(r) = \frac{\partial}{\partial\theta}$	$f_{c_1}(r) = \frac{\partial}{\partial y}$ $f_{c_2}(r) = \frac{\partial}{\partial\theta}$

Table 3: The expressions, one forms, and subspaces (from the kernel of the one forms at the identity) for Cases A, B, and C.

$$\tilde{\mathbb{I}}^{-1}_{\text{loc}} = \begin{pmatrix} 0 \\ 0 \\ \frac{1}{J_J + J_B + ml^2} \end{pmatrix}, \tag{158}$$

$$\begin{pmatrix} \dot{g} \\ \dot{p} \end{pmatrix} = \begin{pmatrix} \dot{x} \\ \dot{y} \\ \dot{\theta} \\ \dot{p}_1 \end{pmatrix} = \begin{pmatrix} 0 \\ 0 \\ \frac{p_1 - J_B\dot{\phi}}{J_B + J_J + l^2 m} \\ 0 \end{pmatrix}. \tag{159}$$

Case B

$$\tilde{\mathbb{I}}_{\text{loc}}^{-1} = \begin{pmatrix} 0 & 0 \\ \frac{J_B+J_J+ml^2}{m(J_B+J_J)} & -\frac{l}{J_B+J_J} \\ -\frac{l}{J_J+J_B} & \frac{1}{J_B+J_J} \end{pmatrix}, \tag{160}$$

$$\begin{pmatrix} \dot{g} \\ \dot{p} \end{pmatrix} = \begin{pmatrix} \dot{x} \\ \dot{y} \\ \dot{\theta} \\ \dot{p}_1 \\ \dot{p}_2 \end{pmatrix} = \begin{pmatrix} \frac{\cos\theta p_1}{m} \\ \frac{\sin\theta p_2}{m} \\ \frac{p_2 - J_B\dot{\phi}}{J_B+J_J+l^2m} \\ \frac{ml(p_2-J_B\dot{\phi})^2}{(J_B+J_J+l^2m)^2} \\ \frac{-lp_1(p_2-J_B\dot{\phi})}{J_B+J_J+l^2m} \end{pmatrix}. \tag{161}$$

Case C

$$\tilde{\mathbb{I}}_{\text{loc}}^{-1} = \begin{pmatrix} \frac{1}{m} & 0 \\ 0 & 0 \\ 0 & \frac{1}{J_J+J_B+ml^2} \end{pmatrix}, \tag{162}$$

$$\begin{pmatrix} \dot{g} \\ \dot{p} \end{pmatrix} = \begin{pmatrix} \dot{x} \\ \dot{y} \\ \dot{\theta} \\ \dot{p}_1 \end{pmatrix} = \begin{pmatrix} -\frac{\sin\theta((J_B+J_J+l^2m)p_1+lm(-p_2+J_B\dot{\phi}))}{(J_B+J_J)m} \\ \frac{\cos\theta((J_B+J_J+l^2m)p_1+lm(-p_2+J_B\dot{\phi}))}{(J_B+J_J)m} \\ \frac{p_1-J_B\dot{\phi}}{(J_B+J_J+l^2)m} \\ \frac{-lp_1+p_2-J_B\dot{\phi}}{J_B+J_J} \end{pmatrix}. \tag{163}$$

3.2.3 Dissipative Systems

Next, three dissipative systems related to the nonholonomically constrained systems are constructed. Referring to Figure 14, each system will be generated by the

combination of wheels present at the body origin of the system. Again, the Lagrangian from (151), along with the Rayleigh dissipation function, are used.

Case A

Along with using (152) and (153), the first step is to construct a dissipation function by using the complementary one forms that are equal to the constraint one forms from Case A.

$$\begin{aligned} R &= \frac{1}{2}C_i\langle\omega_R^i, v\rangle^2 \\ &= \frac{1}{2}C_d\langle dy + d\theta + d\phi, \dot{x}\frac{\partial}{\partial x} + \dot{y}\frac{\partial}{\partial y} + \dot{\theta}\frac{\partial}{\partial \theta} + \dot{\phi}\frac{\partial}{\partial \phi}\rangle^2 \\ &\quad + \frac{1}{2}C_b\langle dx + d\theta + d\phi, \dot{x}\frac{\partial}{\partial x} + \dot{y}\frac{\partial}{\partial y} + \dot{\theta}\frac{\partial}{\partial \theta} + \dot{\phi}\frac{\partial}{\partial \phi}\rangle^2 \\ &= \frac{1}{2}C_d\dot{x}^2 + \frac{1}{2}C_b\dot{y}^2, \end{aligned} \tag{164}$$

then

$$\mathbb{V}_{\text{loc}} = \begin{pmatrix} -C_d & 0 & 0 \\ 0 & -C_b & 0 \\ 0 & 0 & 0 \end{pmatrix}, \tag{165}$$

$$A_{\text{Stokes}} = \begin{pmatrix} 0 \\ 0 \\ 0 \end{pmatrix}. \tag{166}$$

Equations (165),(166),(153) and (152), completely define the system as

$$
\begin{aligned}
g^{-1}\dot{g} &= -A_{\text{mech}}\dot{r} + \mathbb{I}_{\text{loc}}^{-1}p, \\
\dot{p} &= \mathbb{V}_{\text{loc}}(A_{\text{Stokes}} - A_{\text{mech}})\dot{r} + \mathbb{V}_{\text{loc}}\mathbb{I}_{\text{loc}}^{-1}p + \text{ad}^*_{g^{-1}\dot{g}}p,
\end{aligned}
$$

to arrive at

$$
\begin{pmatrix} \dot{g} \\ \\ \dot{p} \end{pmatrix} = \begin{pmatrix} \dot{x} \\ \dot{y} \\ \dot{\theta} \\ \dot{p}_x \\ \dot{p}_y \\ \\ \\ \dot{p}_\theta \end{pmatrix} = \begin{pmatrix} \frac{\cos\theta p_x}{m} - \frac{\sin\theta(J_B+J_J+l^2m)p_y}{m(J_B+J_J)} + \frac{lm(-p_\theta+J_B\dot{\phi})}{m(J_B+J_J)} \\ \frac{\sin\theta p_x}{m} + \frac{\cos\theta(J_B+J_J+l^2m)p_y}{m(J_B+J_J)} + \frac{lm(-p_\theta+J_B\dot{\phi})}{m(J_B+J_J)} \\ \frac{-lp_y+p_\theta-J_B\dot{\phi}}{J_B+J_J} \\ -\frac{C_d p_x}{m} - \frac{lp_y^2}{J_B+J_J} + \frac{p_y p_\theta}{J_B+J_J} + \frac{J_B p_y\dot{\phi}}{J_B+J_J} \\ -\frac{C_b l^2 p_y}{J_B+J_J} - \frac{C_b J_B p_y}{(J_B+J_J)m} - \frac{C_b J_J p_y}{(J_B+J_J)m} + \frac{lp_x p_y}{J_B+J_J} \\ +\frac{C_b l p_\theta}{J_B+J_J} - \frac{p_x p_\theta}{J_B+J_J} + \frac{C_b J_B l\dot{\phi}}{J_B+J_J} - \frac{J_B p_x\dot{\phi}}{J_B+J_J} \\ \frac{l^2 p_x p_y}{J_B+J_J} - \frac{lp_x p_\theta}{J_B+J_J} - \frac{J_B l p_x\dot{\phi}}{J_B+J_J} \end{pmatrix}. \tag{167}
$$

Next, the system is split using the restricted one forms, according to Proposition 3.1.1, giving

$$
\mathcal{N}_q = \text{span}\langle \frac{\partial}{\partial x}, \frac{\partial}{\partial y} \rangle, \tag{168}
$$

with $f_1 = (1,0,0)$, $f_2 = (0,1,0)$. Then

$$
(\mathbb{V}^c)_{\alpha,\beta} = \mathbb{V}_{ab} f^a_\alpha f^b_\beta = \begin{pmatrix} -C_d & 0 \\ \\ 0 & -C_b \end{pmatrix}, \tag{169}
$$

and

$$(\mathbb{I}^c)_{\alpha,\beta} = \mathbb{I}_{ab} f^a_\alpha f^b_\beta = \begin{pmatrix} m & 0 \\ 0 & m \end{pmatrix}. \tag{170}$$

This gives

$$\mathbb{V}^{-1}_{\rm loc}\mathbb{I}_{\rm loc} = \begin{pmatrix} -\frac{m}{C_b} & 0 \\ 0 & \frac{m}{C_d} \end{pmatrix}, \tag{171}$$

with eigenvalues

$$\lambda = \begin{pmatrix} -\frac{m}{C_b} \\ \frac{m}{C_d} \end{pmatrix}. \tag{172}$$

Allowing the eigenvalues to go to zero ensures that $\mathbb{V}^{-1}_{\rm loc}\mathbb{I}_{\rm loc}$ goes to zero.

Case B

Next, a dissipation function is constructed by using the restricted one forms corresponding to Case B. Starting with

$$\begin{aligned} R &= \frac{1}{2} C_i \langle \omega_R, \dot{q} \rangle^2 \\ &= \frac{1}{2} C_b \langle \cos\theta dx + \sin\theta dy + d\theta + d\phi, \dot{x}\frac{\partial}{\partial x} + \dot{y}\frac{\partial}{\partial y} + \dot{\theta}\frac{\partial}{\partial \theta} + \dot{\phi}\frac{\partial}{\partial \phi} \rangle^2 \\ &= \frac{1}{2} C_b (\dot{x}\sin\theta - \dot{y}\cos\theta)^2, \end{aligned} \tag{173}$$

gives

$$\mathbb{V}_{\rm loc} = \begin{pmatrix} 0 & 0 & 0 \\ 0 & -C_b & 0 \\ 0 & 0 & 0 \end{pmatrix}, \tag{174}$$

$$A_{\rm Stokes} = \begin{pmatrix} 0 \\ 0 \\ 0 \end{pmatrix}, \tag{175}$$

which then yields

$$g^{-1}\dot{g} = -A_{\rm mech}\dot{r} + \mathbb{I}_{\rm loc}^{-1} p, \tag{176}$$

$$\dot{p} = \mathbb{V}_{\rm loc}(A_{\rm Stokes} - A_{\rm mech})\dot{r} + \mathbb{V}_{\rm loc}\mathbb{I}_{\rm loc}^{-1} p + {\rm ad}^*_{g^{-1}\dot{g}} p, \tag{177}$$

$$\begin{pmatrix} \dot{g} \\ \dot{p} \end{pmatrix} = \begin{pmatrix} \dot{x} \\ \dot{y} \\ \dot{\theta} \\ \dot{p}_x \\ \dot{p}_y \\ \\ \dot{p}_\theta \end{pmatrix} = \begin{pmatrix} \frac{\cos\theta p_x}{m} - \frac{\sin\theta(J_B+J_J+l^2m)p_y}{m(J_B+J_J)} + \frac{lm(-p_\theta+J_B\dot{\phi})}{m(J_B+J_J)} \\ \frac{\sin\theta p_x}{m} + \frac{\cos\theta(J_B+J_J+l^2m)p_y}{m(J_B+J_J)} + \frac{lm(-p_\theta+J_B\dot{\phi})}{m(J_B+J_J)} \\ \frac{-lp_y+p_\theta-J_B\dot{\phi}}{J_B+J_J} \\ -\frac{lp_y^2}{J_B+J_J} + \frac{p_y p_\theta}{J_B+J_J} + \frac{J_B p_y\dot{\phi}}{J_B+J_J} \\ -\frac{C_b l^2 p_y}{J_B+J_J} - \frac{C_b J_B p_y}{(J_B+J_J)m} - \frac{C_b J_J p_y}{(J_B+J_J)m} \\ +\frac{lp_x p_y}{J_B+J_J} + \frac{C_b l p_\theta}{J_B+J_J} - \frac{p_x p_\theta}{J_B+J_J} + \frac{C_b J_B l\dot{\phi}}{J_B+J_J} - \frac{J_B p_x\dot{\phi}}{J_B+J_J} \\ \frac{l^2 p_x p_y}{J_B+J_J} - \frac{l p_x p_\theta}{J_B+J_J} - \frac{J_B l p_x\dot{\phi}}{J_B+J_J} \end{pmatrix}. \tag{178}$$

Again, the original system corresponding to Γ_0 is split using the restricted one forms, giving

$$\mathcal{N}_q = \text{span}\langle \sin\theta \frac{\partial}{\partial x} - \cos\theta \frac{\partial}{\partial y} \rangle, \tag{179}$$

with $f_1 = (0, 1, 0)$.

The constrained locked viscosity and inertia tensors are calculated as

$$\mathbb{V}^c_{\text{loc}} = \begin{pmatrix} -C_b \end{pmatrix} \tag{180}$$

and

$$\mathbb{I}^c_{\text{loc}} = \begin{pmatrix} m \end{pmatrix}. \tag{181}$$

In addition,

$$\mathbb{V}^{-1}_{\text{loc}}\mathbb{I}_{\text{loc}} = \begin{pmatrix} -\frac{m}{C_b} \end{pmatrix}, \tag{182}$$

along with its eigenvalue

$$\lambda = \begin{pmatrix} -\frac{m}{C_b} \end{pmatrix}. \tag{183}$$

Case C

A dissipation function is constructed by using the complementary one forms corresponding to Case C. Beginning with

$$\begin{aligned} R &= \frac{1}{2}C_i\langle\omega_F, v\rangle^2 \\ &= \frac{1}{2}C_d\langle\sin\theta dx - \cos\theta dy + d\theta + d\phi, \dot{x}\frac{\partial}{\partial x} + \dot{y}\frac{\partial}{\partial y} + \dot{\theta}\frac{\partial}{\partial\theta} + \dot{\phi}\frac{\partial}{\partial\phi}\rangle^2 \\ &= \frac{1}{2}C_d(\dot{x}\cos\theta + \dot{y}\sin\theta)^2, \end{aligned} \tag{184}$$

then

$$\mathbb{V}_{\text{loc}} = \begin{pmatrix} -C_d & 0 & 0 \\ 0 & 0 & 0 \\ 0 & 0 & 0 \end{pmatrix}, \tag{185}$$

$$A_{\text{Stokes}} = \begin{pmatrix} 0 \\ 0 \\ 0 \end{pmatrix}, \tag{186}$$

$$g^{-1}\dot{g} = -A_{\text{mech}}\dot{r} + \mathbb{I}_{\text{loc}}^{-1}p, \tag{187}$$

$$\dot{p} = \mathbb{V}_{\text{loc}}(A_{\text{Stokes}} - A_{\text{mech}})\dot{r} + \mathbb{V}_{\text{loc}}\mathbb{I}_{\text{loc}}^{-1}p + \text{ad}^*_{g^{-1}\dot{g}}p, \tag{188}$$

$$\begin{pmatrix} \dot{g} \\ \dot{p} \end{pmatrix} = \begin{pmatrix} \dot{x} \\ \dot{y} \\ \dot{\theta} \\ \dot{p}_x \\ \dot{p}_y \\ \dot{p}_\theta \end{pmatrix} = \begin{pmatrix} \frac{\cos\theta p_x}{m} - \frac{\sin\theta(J_B+J_J+l^2m)p_y}{m(J_B+J_J)} + \frac{lm(-p_\theta+J_B\dot{\phi})}{m(J_B+J_J)} \\ \frac{\sin\theta p_x}{m} + \frac{\cos\theta(J_B+J_J+l^2m)p_y}{m(J_B+J_J)} + \frac{lm(-p_\theta+J_B\dot{\phi})}{m(J_B+J_J)} \\ \frac{-lp_y+p_\theta-J_B\dot{\phi}}{J_B+J_J} \\ -\frac{C_d p_x}{m} - \frac{lp_y^2}{J_B+J_J} + \frac{p_y p_\theta}{J_B+J_J} + \frac{J_B p_y\dot{\phi}}{J_B+J_J} \\ \frac{lp_x p_y}{J_B+J_J} - \frac{p_x p_\theta}{J_B+J_J} - \frac{J_B p_x\dot{\phi}}{J_B+J_J} \\ \frac{l^2 p_x p_y}{J_B+J_J} - \frac{lp_x p_\theta}{J_B+J_J} - \frac{J_B lp_x\dot{\phi}}{J_B+J_J} \end{pmatrix}. \tag{189}$$

Constructing the system corresponding to the restricted one forms gives

$$\mathcal{N}_q = \text{span}\langle \frac{\partial}{\partial x} \rangle, \tag{190}$$

with $f_1 = (1, 0, 0)$.

The constrained locked viscosity and inertia tensors are calculated as

$$\mathbb{V}^c = \begin{pmatrix} -C_d \end{pmatrix} \tag{191}$$

and

$$\mathbb{I}^c = \begin{pmatrix} m \end{pmatrix}. \tag{192}$$

This gives

$$\mathbb{V}_{\text{loc}}^{-1}\mathbb{I}_{\text{loc}} = \begin{pmatrix} -\frac{m}{C_d} \end{pmatrix}, \tag{193}$$

along with the eigenvalues

$$\lambda = \left(\begin{array}{c} -\frac{m}{C_d} \end{array} \right). \tag{194}$$

3.3 Convergence

In this section, the convergences of the dissipative systems with the constrained systems in the limiting cases are investigated. The first part shows the convergences analytically while the second part shows them numerically.

3.3.1 Analytical

The analytical solutions for the three different constraint cases appear below. First, the reduced equations for each constraint case are shown; then substitutions are made to eliminate the body momentum terms. Next, the reduced equations for the dissipative case are shown, substitutions are made to eliminate the momentum terms, and the limit of the Reynolds number quantity is taken. In the limit, the dissipative equations converge to the constrained equations.

3.3.1.1 Case A

This system is an example of the general principal bundle case of the nonholonomic connection. It is modeled with the nonholonomic constraints

$$\dot{x}\sin\theta - \dot{y}\cos\theta = 0, \tag{195}$$

$$\dot{x}\cos\theta + \dot{y}\sin\theta = 0. \tag{196}$$

Constrained

First, the reduced equations calculated in Section 3.2 for constraint Case A are used; these are

$$\begin{pmatrix} \dot{g} \\ \dot{p} \end{pmatrix} = \begin{pmatrix} \dot{x} \\ \dot{y} \\ \dot{\theta} \\ \dot{p}_1 \end{pmatrix} = \begin{pmatrix} 0 \\ 0 \\ \frac{p_1 - J_B\dot{\phi}}{J_B + J_J + l^2 m} \\ 0 \end{pmatrix}, \tag{197}$$

with

$$p_1 = -lm\sin\theta\dot{x} + lm\cos\theta\dot{y} + (J_B + J_J + l^2 m)\dot{\theta} + J_B\dot{\phi}, \tag{198}$$

$$\dot{x}\sin\theta - \dot{y}\cos\theta = 0. \tag{199}$$

Substituting p_1, along with the constraint equation, into (197) gives

$$\begin{pmatrix} \dot{g} \\ \dot{p} \end{pmatrix} = \begin{pmatrix} \dot{x} \\ \dot{y} \\ \dot{\theta} \\ \dot{p}_1 \end{pmatrix} = \begin{pmatrix} 0 \\ 0 \\ \dot{\theta} \\ 0 \end{pmatrix}. \tag{200}$$

Dissipative

The reduced equations for the dissipative system are

$$\begin{pmatrix} \dot{g} \\ \dot{p} \end{pmatrix} = \begin{pmatrix} \dot{x} \\ \dot{y} \\ \dot{\theta} \\ \dot{p}_x \\ \dot{p}_y \\ \\ \dot{p}_\theta \end{pmatrix} = \begin{pmatrix} \frac{\cos\theta p_x}{m} - \frac{\sin\theta(J_B+J_J+l^2m)p_y}{m(J_B+J_J)} + \frac{lm(-p_\theta+J_B\dot{\phi})}{m(J_B+J_J)} \\ \frac{\sin\theta p_x}{m} + \frac{\cos\theta(J_B+J_J+l^2m)p_y}{m(J_B+J_J)} + \frac{lm(-p_\theta+J_B\dot{\phi})}{m(J_B+J_J)} \\ \frac{-lp_y+p_\theta-J_B\dot{\phi}}{J_B+J_J} \\ -\frac{C_d p_x}{m} - \frac{lp_y^2}{J_B+J_J} + \frac{p_y p_\theta}{J_B+J_J} + \frac{J_B p_y \dot{\phi}}{J_B+J_J} \\ -\frac{C_b l^2 p_y}{J_B+J_J} - \frac{C_b J_B p_y}{(J_B+J_J)m} - \frac{C_b J_J p_y}{(J_B+J_J)m} \\ +\frac{lp_x p_y}{J_B+J_J} + \frac{C_b l p_\theta}{J_B+J_J} - \frac{p_x p_\theta}{J_B+J_J} + \frac{C_b J_B l\dot{\phi}}{J_B+J_J} - \frac{J_B p_x \dot{\phi}}{J_B+J_J} \\ \frac{l^2 p_x p_y}{J_B+J_J} - \frac{l p_x p_\theta}{J_B+J_J} - \frac{J_B l p_x \dot{\phi}}{J_B+J_J} \end{pmatrix}, \tag{201}$$

with p_x, p_y, and p_θ as

$$p_x = m\cos\theta\dot{x} + m\sin\theta\dot{y}, \tag{202}$$

$$p_y = -m\sin\theta\dot{x} + m\cos\theta\dot{y} + lm\dot{\theta}, \tag{203}$$

$$p_\theta = -lm\sin\theta\dot{x} + lm\cos\theta\dot{y} + J_B\dot{\theta} + J_J\dot{\theta} + l^2m\dot{\theta} + J_B\dot{\phi}. \tag{204}$$

In addition, taking derivatives of p_x and p_y with respect to t gives

$$\dot{p}_x = -m\sin\theta\dot{x}\dot{\theta} + m\cos\theta\dot{y}\dot{\theta} + m\cos\theta\ddot{x} + m\sin\theta\ddot{y}, \tag{205}$$

$$\dot{p}_y = -m\cos\theta\dot{x}\dot{\theta} - m\sin\theta\dot{y}\dot{\theta} - m\sin\theta\ddot{x} + m\cos\theta\ddot{y} + lm\ddot{\theta}. \tag{206}$$

Substituting $p_x, p_y, p_\theta, \dot{p}_x$, and $\dot{p}_y$ back into the equations give

$$\begin{pmatrix} \dot{x} \\ \dot{y} \\ \dot{\theta} \\ m\dot{\theta}(-\sin\theta\dot{x} + \cos\theta\dot{y}) + m(\cos\theta\ddot{x} + \sin\theta\ddot{y}) \\ m\dot{\theta}(-\cos\theta\dot{x} - \sin\theta\dot{y} - \sin\theta\ddot{x} + \cos\theta\ddot{y} + l\ddot{\theta}) \\ \dot{p}_\theta \end{pmatrix} \tag{207}$$

$$= \begin{pmatrix} \dot{x} \\ \dot{y} \\ \dot{\theta} \\ -C_d(\cos\theta\dot{x} + \sin\theta\dot{y}) + m\dot{\theta}(-\sin\theta\dot{x} + \cos\theta\dot{y} + l\dot{\theta}) \\ C_b(\sin\theta\dot{x} - \cos\theta\dot{y}) - m\dot{\theta}(\cos\theta\dot{x} + \sin\theta\dot{y}) \\ -lm\dot{\theta}(\cos\theta\dot{x} + \sin\theta\dot{y}) \end{pmatrix}. \tag{208}$$

As noted, the eigenvalues are $\lambda = (-\frac{m}{C_d}, -\frac{m}{C_b})$. The fourth row is divided by C_d, and $\frac{m}{C_d} \to 0$. $\dot{p}_x$ vanishes, and the first nonholonomic constraint

$$\dot{x}\cos\theta + \dot{y}\sin\theta = 0 \tag{209}$$

is recovered. The fifth row is divided by C_b, $\frac{m}{C_b} \to 0$, $\dot{p}_y$ vanishes, and the second nonholonomic constraint

$$\dot{x}\sin\theta - \dot{y}\cos\theta = 0 \tag{210}$$

is recovered. Substituting the constraint equations back into the equations leaves

$$\begin{pmatrix} \dot{g} \\ \dot{p} \end{pmatrix} = \begin{pmatrix} \dot{x} \\ \dot{y} \\ \dot{\theta} \\ \dot{p}_\theta \end{pmatrix} = \begin{pmatrix} 0 \\ 0 \\ \dot{\theta} \\ 0 \end{pmatrix}. \tag{211}$$

3.3.1.2 Case B

This system is another example of the general principal bundle case. The nonholonomic constraint for the system is

$$\dot{x}\sin\theta - \dot{y}\cos\theta = 0. \tag{212}$$

Constrained

The reduced equations from Section 3.2 for Constraint Case B are as follows.

$$\begin{pmatrix} \dot{g} \\ \dot{p} \end{pmatrix} = \begin{pmatrix} \dot{x} \\ \dot{y} \\ \dot{\theta} \\ \dot{p}_1 \\ \dot{p}_2 \end{pmatrix} = \begin{pmatrix} \frac{\cos\theta p_1}{m} \\ \frac{\sin\theta p_2}{m} \\ \frac{p_2 - J_B\dot{\phi}}{J_B + J_J + l^2 m} \\ \frac{ml(p_2 - J_B\dot{\phi})^2}{(J_B + J_J + l^2 m)^2} \\ \frac{-lp_1(p_2 - J_B\dot{\phi})}{J_B + J_J + l^2 m} \end{pmatrix}. \tag{213}$$

The momenta p_1 and p_2 are calculated to be

$$p_1 = m(\cos\theta\dot{x} + \sin\theta\dot{y}), \tag{214}$$

$$p_2 = -lm\sin\theta\dot{x} + lm\cos\theta\dot{y} + (J_B + J_J + l^2 m)\dot{\theta} + J_B\dot{\phi}. \tag{215}$$

Substituting these equations back into the reduced equations give

$$\begin{pmatrix} \dot{g} \\ \dot{p} \end{pmatrix} = \begin{pmatrix} \dot{x} \\ \dot{y} \\ \dot{\theta} \\ \dot{p}_1 \\ \dot{p}_2 \end{pmatrix} = \begin{pmatrix} \cos\theta(\cos\theta\dot{x} + \sin\theta\dot{y}) \\ \sin\theta(\cos\theta\dot{x} + \sin\theta\dot{y}) \\ \frac{lm(-\sin\theta\dot{x}+\cos\theta\dot{y})}{J_B+J_J+l^2m} + \dot{\theta} \\ \frac{lm(-lm\sin\theta\dot{x}+lm\cos\theta\dot{y}+(J_B+J_J+l^2m)\dot{\theta})^2}{(J_B+J_J+l^2m)^2} \\ -\frac{lm(\cos\theta\dot{x}+\sin\theta\dot{y})(-lm\sin\theta\dot{x}+lm\sin\theta\dot{y}+(J_B+J_J+l^2m)\dot{\theta})}{J_B+J_J+l^2m} \end{pmatrix}. \tag{216}$$

Because these equations were constructed on the constrained subspace defined by $-\dot{x}\sin\theta + \dot{y}\cos\theta = 0$, the equations go to

$$\begin{pmatrix} \dot{g} \\ \dot{p} \end{pmatrix} = \begin{pmatrix} \dot{x} \\ \dot{y} \\ \dot{\theta} \\ \dot{p}_1 \\ \dot{p}_2 \end{pmatrix} = \begin{pmatrix} \cos\theta(\cos\theta\dot{x} + \sin\theta\dot{y}) \\ \sin\theta(\cos\theta\dot{x} + \sin\theta\dot{y}) \\ \dot{\theta} \\ ml\dot{\theta}^2 \\ -lm(\cos\theta\dot{x} + \sin\theta\dot{y})\dot{\theta} \end{pmatrix}. \tag{217}$$

Dissipative

Starting with the reduced equations for the dissipative system from Section 3.3 and substituting the expressions for the momenta give

$$\begin{pmatrix} \dot{x} \\ \dot{y} \\ \dot{\theta} \\ \dot{p}_x \\ m\dot{\theta}(-\cos\theta\dot{x} - \sin\theta\dot{y} - \sin\theta\ddot{x} + \cos\theta\ddot{y} + l\ddot{\theta}) \\ \dot{p}_\theta \end{pmatrix} \tag{218}$$

$$= \begin{pmatrix} \dot{x} \\ \dot{y} \\ \dot{\theta} \\ m\dot{\theta}(-\sin\theta\dot{x} + \cos\theta\dot{y} + l\dot{\theta}) \\ C_b(\sin\theta\dot{x} - \cos\theta\dot{y}) - m\dot{\theta}(\cos\theta\dot{x} + \sin\theta\dot{y}) \\ -lm\dot{\theta}(\cos\theta\dot{x} + \sin\theta\dot{y}) \end{pmatrix}. \tag{219}$$

The eigenvalue for this system is $\lambda = -\frac{m}{C_b}$. The equation in the fifth row is divided by C_b, and $\frac{m}{C_b} \to 0$. $\dot{p}_y$ vanishes, and the nonholonomic constraint is recovered:

$$-\dot{x}\sin\theta + \dot{y}\cos\theta = 0. \tag{220}$$

Substituting the constraint equation back into the equations give

$$\begin{pmatrix} \dot{g} \\ \dot{p} \end{pmatrix} = \begin{pmatrix} \dot{x} \\ \dot{y} \\ \dot{\theta} \\ \dot{p}_x \\ \dot{p}_\theta \end{pmatrix} = \begin{pmatrix} \cos\theta(\cos\theta\dot{x} + \sin\theta\dot{y}) \\ \sin\theta(\cos\theta\dot{x} + \sin\theta\dot{y}) \\ \dot{\theta} \\ ml\dot{\theta}^2 \\ -lm(\cos\theta\dot{x} + \sin\theta\dot{y})\dot{\theta} \end{pmatrix}. \tag{221}$$

3.3.1.3 Case C

This system is an example of the horizontally symmetric case of the nonholonomic connection. It considers the constraint

$$\dot{x}\cos\theta + \dot{y}\sin\theta = 0. \tag{222}$$

Constrained

Starting with the reduced equations from Section 3.2 for Constraint Case C,

$$\begin{pmatrix} \dot{g} \\ \dot{p} \end{pmatrix} = \begin{pmatrix} \dot{x} \\ \dot{y} \\ \dot{\theta} \\ \dot{p}_1 \end{pmatrix} = \begin{pmatrix} -\frac{\sin\theta((J_B+J_J+l^2m)p_1+lm(-p_2+J_B\dot{\phi}))}{(J_B+J_J)m} \\ \frac{\cos\theta((J_B+J_J+l^2m)p_1+lm(-p_2+J_B\dot{\phi}))}{(J_B+J_J)m} \\ \frac{p_1-J_B\dot{\phi}}{(J_B+J_J+l^2)m} \\ \frac{-lp_1+p_2-J_B\dot{\phi}}{J_B+J_J} \end{pmatrix}, \tag{223}$$

with

$$p_1 = m(-\sin\theta\dot{x} + \cos\theta\dot{y} + l\dot{\theta}), \tag{224}$$

$$p_2 = -lm\sin\theta\dot{x} + lm\cos\theta\dot{y} + (J_B + J_J + l^2m)\dot{\theta} + J_B\dot{\phi}, \tag{225}$$

give

$$\begin{pmatrix} \dot{g} \\ \dot{p} \end{pmatrix} = \begin{pmatrix} \dot{x} \\ \dot{y} \\ \dot{\theta} \\ \dot{p}_1 \\ \dot{p}_2 \end{pmatrix} = \begin{pmatrix} \sin\theta(\sin\theta\dot{x} - \cos\theta\dot{y}) \\ \cos\theta(-\sin\theta\dot{x} + \cos\theta\dot{y}) \\ \dot{\theta} \\ m\dot{\theta}(-\sin\dot{x} + \cos\theta\dot{y} + l\dot{\theta}) \\ 0 \end{pmatrix}. \tag{226}$$

Given that the constraint does not break the symmetry of the system, the center of mass remains stationary even when the group velocity is nonzero; thus,

$$m\dot{\theta}(-\dot{x}\sin\theta + \dot{y}\cos\theta + l\dot{\theta}) = 0, \tag{227}$$

giving the final equations for the system:

$$\begin{pmatrix} \dot{g} \\ \dot{p} \end{pmatrix} = \begin{pmatrix} \dot{x} \\ \dot{y} \\ \dot{\theta} \\ \dot{p}_1 \\ \dot{p}_2 \end{pmatrix} = \begin{pmatrix} \sin\theta(\sin\theta\dot{x} - \cos\theta\dot{y}) \\ \cos\theta(-\sin\theta\dot{x} + \cos\theta\dot{y}) \\ \dot{\theta} \\ 0 \\ 0 \end{pmatrix}. \tag{228}$$

Dissipative

Starting with the reduced equations for the dissipative system from Section 3.3 and substituting the expressions for the momenta give

$$\begin{pmatrix} \dot{x} \\ \dot{y} \\ \dot{\theta} \\ m\dot{\theta}(-\sin\theta\dot{x} + \cos\theta\dot{y}) + m(\cos\theta\ddot{x} + \sin\theta\ddot{y}) \\ \dot{p}_y \\ \dot{p}_\theta \end{pmatrix} \tag{229}$$

$$= \begin{pmatrix} \dot{x} \\ \dot{y} \\ \dot{\theta} \\ -C_d(\cos\theta\dot{x} + \sin\theta\dot{y}) + m\dot{\theta}(-\sin\theta\dot{x} + \cos\theta\dot{y} + l\dot{\theta}) \\ -m\dot{\theta}(\cos\theta\dot{x} + \sin\theta\dot{y}) \\ -lm\dot{\theta}(\cos\theta\dot{x} + \sin\theta\dot{y}) \end{pmatrix}. \tag{230}$$

The eigenvalue for this system is $\lambda = -\frac{m}{C_d}$. The equation in the fourth row is divided by C_d, $\frac{m}{C_d} \to 0$, $\dot{p}_x$ vanishes, and the nonholonomic constraint

$$\dot{x}\cos\theta + \dot{y}\sin\theta = 0 \tag{231}$$

is recovered. Substituting this back into the equations gives

$$\begin{pmatrix} \dot{g} \\ \dot{p} \end{pmatrix} = \begin{pmatrix} \dot{x} \\ \dot{y} \\ \dot{\theta} \\ \dot{p}_y \\ \dot{p}_\theta \end{pmatrix} = \begin{pmatrix} \cos\theta(\cos\theta\dot{x} + \sin\theta\dot{y}) \\ \sin\theta(\cos\theta\dot{x} + \sin\theta\dot{y}) \\ \dot{\theta} \\ 0 \\ 0 \end{pmatrix}. \tag{232}$$

3.3.2 Numerical

This section includes simulation results for each of the systems explored in the previous sections. Expressions for $\dot{J}$, $\dot{J}_{\text{nhc}}$, and K can be derived. The nonholonomic systems are simulated by solving the set of equations generated by solving for $\dot{J}_{\text{nhc}}$ for each constraint case. The Rayleigh system is simulated by solving the set of equations generated by setting

$$\dot{J} = K. \tag{233}$$

Case	Nonholonomic	Rayleigh
Unconstrained	none	$C_d, C_b \to 0$
Purely Kinematic (not explored in this section)	---	---
Horizontal Symmetries	C	$\frac{m}{C_d} \to 0$
General Principal Bundle Case	A and B	$\frac{m}{C_d}, \frac{m}{C_b} \to 0$

Table 4: The special cases of the connection and their corresponding constraint and dissipative cases.

Simulations for each of the cases in Table 3.4 were generated. Results appear below. The figures are organized so that each dissipative case is arranged beside its corresponding nonholonomic case. The system is driven by a sinusoidal forcing

function in $\ddot{\phi}$.

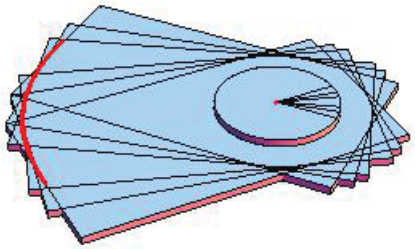

Figure 15: Time lapse of the unconstrained system, superimposed with the paths of p_r and p_f.

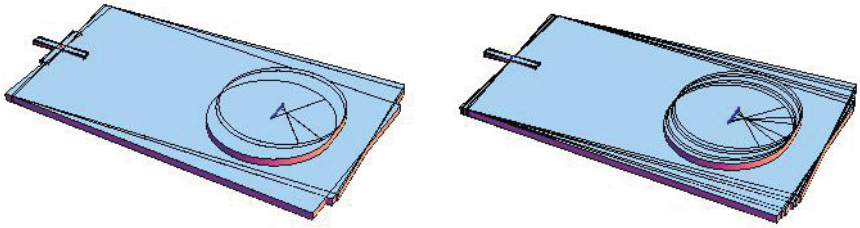

(a) Rayleigh System as $\frac{m}{C_d}, \frac{m}{C_b} \to 0$.

(b) Nonholonomic System A.

Figure 16: Case A.

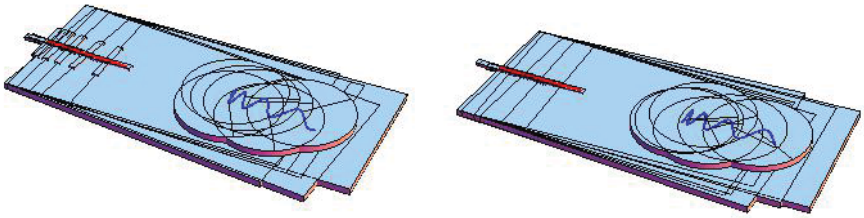

(a) The Rayleigh system as $C_d, \frac{m}{C_b} \to 0$.

(b) Nonholonomic System B.

Figure 17: Case B.

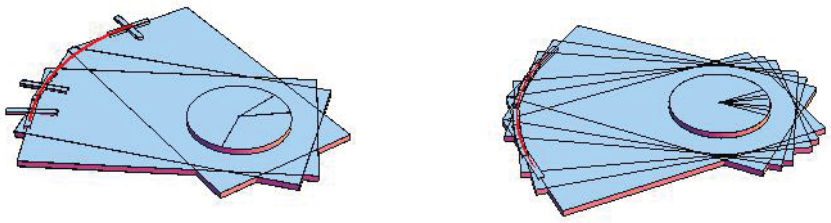

(a) The Rayleigh system as C_b, $\frac{m}{C_d} \to 0$.

(b) Nonholonomic System C.

Figure 18: Case C.

The paths of the center of mass and the center of the constraint for each figure are superimposed with a time-lapsed representation of each system. The path for each point is nearly identical in each of the corresponding dissipative and constrained cases, indicating the technique can indeed model constraints using dissipation. The unconstrained case looks identical to the horizontal symmetries case (Case C and $\frac{m}{C_d} \to 0$). It represents the two rigid bodies counter-rotating in space, where the constraint does not interfere with the motion because of the conservation of momentum (a horizontal symmetry). Constraint Case A shows, as the beanie is rotated, the center of mass of the system rotates around the constraint. The constraint is free to rotate, but not translate. Constraint Case B shows, as the beanie is rotated, the entire system begins to translate and rotate because of the constraint resisting the counter-rotation of rigid body two. Constraint Cases A and B represent the general principal bundle cases.

CHAPTER 4: CLOSED-LOOP REDUCED DISSIPATIVE SYSTEM

4.1 Introduction

Robotic systems with wheels are a frequent topic of interest in the dynamics and controls community. These frequently tend to be Lagrangian systems. For these systems, Lagrangian reduction techniques can be used to put the corresponding equations of motion in a form that is useful for control analysis.

In this chapter, a Lagrangian system with drift is modeled using geometric techniques of reduction from the previous chapters. Then, a test for accessibility is reviewed, stating that a controllable driftless system is accessible when drift is added. To use this test to show accessibility for the system with drift, $\mathbb{V}_{\text{loc}}^{-1}\mathbb{I}_{\text{loc}}$ is set to 0, thus removing the drift from the system. Controllability for this system is easily achieved via a simple control law. Drift is added back to the system by allowing $\mathbb{V}_{\text{loc}}^{-1}\mathbb{I}_{\text{loc}}$ to be nonzero. The test for accessibility shows this system is accessible. Finally, the control law for the driftless system is used to help construct a control law for the system with drift.

4.2 The Geometry of Accessiblity and Controllability

This section introduces geometric tools that can be used to make statements about controllability and accessibility of systems with drift that also have Lie group symmetries.

Definition 4.2.1. Given a finite-dimensional control system,

$$\dot{x} = f(x, u^1, \ldots, u^m), \;\; x \in M, \tag{234}$$

and a particular point, $x_0 \in M$, then $\mathbb{R}^V_T(x_0)$ is denoted as the set of points in M that are reachable from x_0 in time $t \leq T$ along trajectories that remain in the neighborhood $V \subset M$ of x_0.

Definition 4.2.2. Given all $x_0 \in M$ in the system defined by (234), if $\mathbb{R}^V_T(x_0)$ contains a non-empty open subset of M for every choice of $T > 0$ and V, the system is **locally accessible**.

Definition 4.2.3. For all $x_0 \in M$, if x_0 is interior to $\mathbb{R}^V_T(x_0)$ for every choice $T > 0$ and V, the system is **locally controllable**.

Definition 4.2.4. The **standard form** for a nonlinear control system with affine inputs

$$\dot{z} = f(z) + h_i(z)v^i. \tag{235}$$

Definition 4.2.5. Starting with

$$\triangle_0 = \text{span}\{f, h_1, \ldots, h_m\} \tag{236}$$

(the span taken over C^∞ functions on N), then

$$\triangle_k = \triangle_{k-1} + \text{span}[X, Y] | X, Y \in \triangle_{k-1} \tag{237}$$

is a nondecreasing sequence of distributions on N that terminates at some k_f under certain regularity conditions.

The **accessibility distribution** is given by C :

$$C = \triangle_{k_f} = \triangle_\infty \tag{238}$$

Theorem 4.2.1. ***Lie Algebra Rank Condition*** *(LARC) If* $\dim C(z) = \dim T_z N$ *for all* $z \in N$*, then the system is locally accessible.*

This condition is a result of Frobenius' theorem (see Nijmeijer and van der Schaft 1990).

If $f = 0$ in (234), the *driftless* system is:

$$\dot{x} = h_1(x)u^1 + \ldots + h_m(x)u^m. \tag{239}$$

Local controllability and local accessibility are equivalent notions in the absence of drift, in which case, Theorem 4.2.1 is equivalent to *Chow's theorem* (see Chow (1949)).

Definition 4.2.6. A system on $Q = M \times G$ is **totally controllable** if it is locally Q controllable and **fiber controllable** if it is locally G controllable.

Definition 4.2.7. Given a differential form $\alpha : (TQ)^n \to \mathfrak{g}$, its **covariant exterior**

derivative is defined $D\alpha : (TQ)^{n+1} \to \mathfrak{g}$ with respect to a connection, such that

$$D\alpha(X_1, \ldots, X_{n+1}) = d\alpha(\mathrm{hor}X_1, \ldots, \mathrm{hor}X_{n_1}). \tag{240}$$

Definition 4.2.8. The **curvature form** $D\Gamma : TQ \times TQ \to \mathfrak{g}$ corresponding to the connection form Γ is given by its covariant exterior derivative:

$$D\Gamma(X, Y) = d\Gamma(\mathrm{hor}X, \mathrm{hor}Y). \tag{241}$$

In practice, it is often easier to compute the curvature of a connection by using

Definition 4.2.9. Cartan's structure equation : if $\Gamma : TQ \to \mathfrak{g}$ is a connection form and $D\Gamma : TQ \times TQ \to \mathfrak{g}$ the corresponding curvature form, then

$$D\Gamma(X, Y) = d\Gamma(X, Y) - [\Gamma(X), \Gamma(Y)]. \tag{242}$$

Definition 4.2.10. The local curvature form is the map $DA : TM \times TM \to \mathfrak{g}$, which satisfies

$$D\Gamma(r, g)(X^h, Y^h) = \mathrm{Ad}_g(DA(r)(X, Y) \tag{243}$$

for $X, Y \in \mathcal{X}(M)$. The form can be calculated in terms of the Lie bracket on $\mathfrak{g}$ by

$$DA(X, Y) = dA(X, Y) - [A(X), A(Y)] \tag{244}$$

for $X, Y \in \mathcal{X}(M)$.

Definition 4.2.11. Subspaces of the Lie algebra can be defined as

$$
\begin{aligned}
\mathfrak{h}_1 &= \operatorname{span}\{A(X_i)\},\\
\mathfrak{h}_2 &= \operatorname{span}\{DA(X_i, X_j)\},\\
\mathfrak{h}_3 &= \operatorname{span}\{X_k DA(X_i, X_j) - [A(X_k) DA(X_i, X_j)]\},\\
&\vdots\\
\mathfrak{h}_k &= \operatorname{span}\{X_i\xi - [A(X_i), \xi], [\xi, \eta]\xi \in \mathfrak{h}_{k-1}, \eta \in \mathfrak{h}_2 + \cdots + \mathfrak{h}_{k-1}\}. \qquad (245)
\end{aligned}
$$

Theorem 4.2.2. *The driftless system is fiber controllable near $q = (r, g) \in Q$ if and only if*

$$\mathfrak{g} = \mathfrak{h}_1 + \mathfrak{h}_2 + \ldots$$

there and totally controllable near $q \in Q$ if and only if

$$\mathfrak{g} = \mathfrak{h}_2 + \mathfrak{h}_3 + \ldots$$

there.

Theorem 4.2.3. *If the system without dissipation on $M \times G$ is locally controllable, the system with dissipation on $TM \times G \times \mathfrak{g}^*$ is locally $TM \times G$ accessible or* ***accessible modulo momentum****.*

Lemma 4.2.1. *If a system with drift is accessible and $[h_i, [h_i, f]] = 0$, then this system is small-time locally controllable (STLC) from all equilibrium points, $z_0 \in N$.*

Lemma 4.2.1 is a result of techniques seen in Sussman (1987) and Ostrowski (1996).

In those papers it stated that, whenever a drift term appears an odd number of times and with the control vector fields appearing an even number of times (including zero times), the bracket can be defined as bad. The sufficient conditions for STLC can be restated as requiring that all "bad" brackets be expressible in terms of brackets of lower degree ("good" brackets). These conditions are met when $[h_i, [h_i, f]] = 0$.

4.3 The Four-Wheeled Robotic Car on Ice

The dissipative inertial system is constructed by simply adding a Lagrangian to the previous Stokes system in Example 2.4.1 (see Figure 11):

$$\mathcal{L} = \frac{1}{2}m(\dot{x}^2 + \dot{y}^2) + \frac{1}{2}J_J\dot{\theta}^2 + \frac{1}{2}J_w(\dot{\theta} + \dot{\phi})^2. \tag{246}$$

Performing reduction on the system gives

$$\begin{pmatrix} \dot{g} \\ \dot{p} \\ \dot{r} \end{pmatrix} = \begin{pmatrix} \dot{x} \\ \dot{y} \\ \dot{\theta} \\ \dot{p}_x \\ \dot{p}_y \\ \dot{p}_\theta \\ \dot{\nu} \end{pmatrix}$$

$$= \begin{pmatrix} \frac{p_x \cos\theta - p_y \sin\theta}{m} \\ \frac{p_y \cos\theta + p_x \sin\theta}{m} \\ \frac{p_\theta}{J_J} \\ -\frac{3C_c p_x}{m} + \frac{C_c p_x \cos 2\phi}{m} + \frac{p_y p_\theta}{JJ} + \frac{C_c p_y \sin 2\phi}{m} + \frac{C_c l p_\theta \sin 2\phi}{J_J} \\ -\frac{3C_c p_y}{m} - \frac{C_c p_y \cos 2\phi}{m} - \frac{2C_c p_\theta l \cos^2\phi}{JJ} - \frac{p_x p_\theta}{J_J} + \frac{C_c p_x \sin 2\phi}{m} \\ -\frac{2C_c p_y l \cos^2\phi}{m} - \frac{2C_c p_\theta l^2 \cos^2\phi}{J_J} + \frac{2C_c l p_x \sin\phi\cos\phi}{m} \\ 0 \end{pmatrix} + \begin{pmatrix} 0 \\ 0 \\ 0 \\ -2C_c \\ 0 \\ 0 \\ 1 \end{pmatrix} \dot{\nu}. \tag{248}$$

(249)

The eigenvalues of the reduced Reynolds tensor are calculated as

$$\lambda_R = \begin{pmatrix} -\frac{m}{2C_c} \\ -\frac{m}{4C_C} - \frac{J_J \sec^2\phi}{2C_c l^2} - \frac{\sqrt{16J_J^2 + l^4m^2 + l^4m^2\cos 2\phi(2+\cos 2\phi)}\sec^2\phi}{8C_c l^2} \\ -\frac{m}{4C_C} - \frac{J_J \sec^2\phi}{2C_c l^2} + \frac{\sqrt{64J_J^2 + 6l^4m^2 + 2l^4m^2(4\cos 2\phi + \cos 4\phi)}\sec^2\phi}{16C_c l^2} \end{pmatrix}. \tag{250}$$

Since the Rayleigh one forms span all of $T_q(\mathrm{Orb}(q))$ and $\mathbb{V}_{\mathrm{loc}}^{-1}\mathbb{I}_{\mathrm{loc}} \to 0$, (148) can be used. This describes a system with dissipation that, in the limiting case, converges to the fully constrained, kinematic car system, defined by

$$\dot{g} = -gA_{\mathrm{Stokes}}\dot{r}.$$

Thus, the system goes to

$$\begin{aligned} \begin{pmatrix} \dot{g} \\ \dot{r} \end{pmatrix} &= \begin{pmatrix} \dot{x} \\ \dot{y} \\ \dot{\theta} \\ \dot{\nu} \end{pmatrix} \\ &= \begin{pmatrix} \cos\theta \\ \sin\theta \\ \frac{\tan\phi}{l} \\ 1 \end{pmatrix} \dot{\nu}. \end{aligned} \tag{251}$$

Controllability for this driftless system is shown by, first, taking the bracket $[h_1, h_2]$, which gives

$$\mathfrak{h}_1 = \text{span}\left\{\begin{pmatrix} \cos\theta \\ \sin\theta \\ \frac{\tan\phi}{l} \\ 1 \end{pmatrix}\right\}, \tag{252}$$

$$\mathfrak{h}_2 = \text{span}\left\{[h_1, h_2]\right\} = \text{span}\left\{\begin{pmatrix} -\frac{\sin\theta\tan\phi}{l} \\ \frac{\cos\theta\tan\phi}{l} \\ -\sin\theta \\ 0 \end{pmatrix}\right\}. \tag{253}$$

Thus,

$$\mathfrak{g} = \mathfrak{h}_1 + \mathfrak{h}_2 + ...$$

and

$$\mathfrak{g} = \mathfrak{h}_2 + \mathfrak{h}_3 + ...$$

Therefore, by Theorem 4.2.2, the system without drift is fiber controllable and totally controllable. By Theorem 4.2.3, the system with drift is accessible.

4.4 Control

This section addresses construction of a control law for the driftless system. This control law is used as a starting point to develop a control law for the system with drift. Then, simulations and results for each controlled system are examined.

With the control law

$$\phi = k(\theta - \theta_d), \tag{254}$$

such that

$$\dot{\theta} = -\frac{\dot{\nu}\tan\phi}{l}, \tag{255}$$

the Lyapunov functions for the system are taken as

$$\begin{aligned} S &= \frac{1}{2}\dot{\nu}(k(\theta - \theta_d))^2, \\ \dot{S} &= \frac{k^2\dot{\nu}^2\tan\left(k(\theta - \theta_d)\right)(\theta - \theta_d)}{l}, \end{aligned} \tag{256}$$

for

$$-2\pi < \theta_d < 2\pi,$$

and

$$0 > k > -\frac{1}{4}.$$

Because S is positive definite and $\dot{S}$ is negative definite, S satisfies the conditions for a Lyapunov function.

For a full system with drift, a control law candidate could be

$$\phi = k_p(\theta - \theta_d) + k_d\dot{\theta}.$$

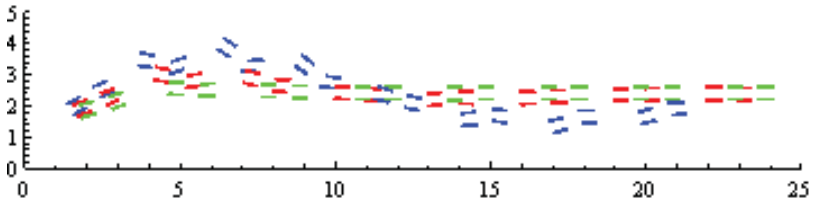

Figure 19: Time lapse of the cart over 9 s at 1 s intervals for three different C_c values of .5, 1, and 2.

This control law is the same as the previous control law, except that a derivative/drift term has been added to the end. This control law is valid as long as

$$\pi/2 \geq k_p(\theta_0 - \theta_d),$$

and

$$k_p > k_d.$$

Simulating the closed loop system with the control law, the navigational goal is achieved even in scenarios where the cart wheels have different levels of traction (governed by changing the constant values in the Rayleigh dissipation function). In Figure 19, the system easily attains the navigational goal. For the case in which the cart wheels have the least amount of traction, the system performs a fish tail maneuver, commonly seen in rear-wheel-drive vehicles when the driver takes a turn too fast and the back wheels lose traction [3].

[3]This move is a common phenomenon in car chase scenes of Hollywood action movies.

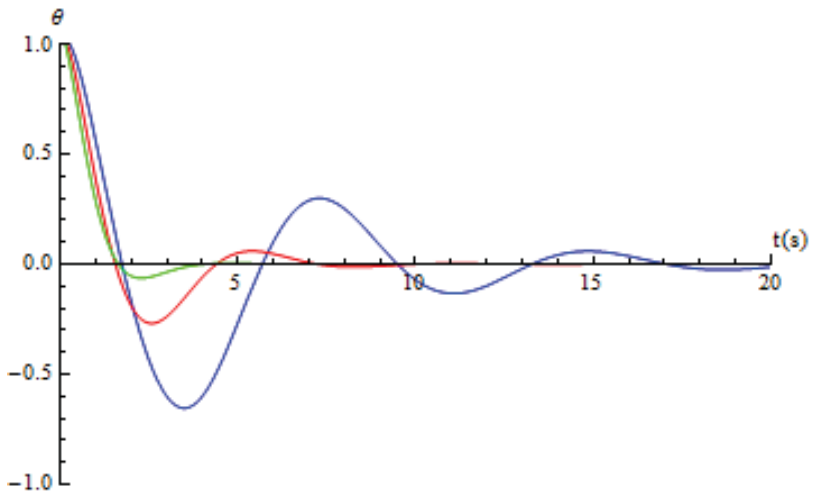

Figure 20: Heading (in radians) vs. time of the car over 20 s for three different C_c values of .5, 1, and 2.

CHAPTER 5: GEOMETRIC APPROACH TO UNDERACTUATED PLANAR NAVIGATION

Underactuated mechanical systems present unique problems in the field of control. These are systems in which there are fewer control inputs than degrees-of-freedom. In this chapter, an underactuated control system will be analyzed with the aid Lagrangian reduction techniques.

5.1 Underactuated Control

Starting with the beanie system from Chapter 2, Section 6, defined by (137) and (138), a proportional controller $\dot{\alpha} = k\theta$ is added, and the final equations for the closed loop system become

$$\begin{pmatrix} \dot{p}_1 \\ \dot{p}_2 \\ \dot{\theta} \\ \dot{\phi} \\ \dot{\alpha} \end{pmatrix} = \begin{pmatrix} \frac{ml(p_2 - J_B\dot{\phi})^2}{(J_B + J_J + l^2 m)^2} \\ \frac{-lp_1(p_2 - J_B\dot{\phi})}{J_B + J_J + l^2 m} \\ \frac{p_2 - J_B\dot{\phi}}{J_B + J_J + l^2 m} \\ \alpha \\ k\theta \end{pmatrix} \tag{257}$$

$$= \begin{pmatrix} ml\dot{\theta}^2 \\ -lp_1\dot{\theta} \\ \frac{p_2 - J_B\dot{\phi}}{J_B + J_J + l^2 m} \\ \alpha \\ k\theta \end{pmatrix}. \tag{258}$$

Defining the following variables as

$$r = \frac{-ap_1}{ml^2 + J_B + J_J}, \tag{259}$$

$$w = \frac{p_2}{ml^2 + J_B + J_J}, \tag{260}$$

$$p = \frac{J_J - J_B\alpha}{ml^2 + J_B + J_J}, \tag{261}$$

and constants as

$$\gamma = \frac{-ml^2}{ml^2 + J_B + J_J}, \tag{262}$$

$$\lambda = \frac{kJ_B}{ml^2 + J_B + J_J}, \tag{263}$$

the equations for the closed loop system are re-expressed as

$$\dot{r} = \gamma p^2, \tag{264}$$

$$\dot{w} = rp, \tag{265}$$

$$\dot{\theta} = p, \tag{266}$$

$$\dot{p} = rp - \lambda\theta. \tag{267}$$

Using these equations, a Lyapunov function for the system is defined as

$$S = \frac{1}{2}\lambda\theta^2 + \frac{1}{2}p^2, \tag{268}$$

with derivative

$$\dot{S} = \lambda\theta\dot{\theta} + p\dot{p} = \lambda\theta p + p(rp - \lambda\theta) = rp^2. \tag{269}$$

It is clear that S is always positive definite. It is also clear that $\dot{S}$ is always negative definite as long as $J_{LT} \geq 0$. Thus, conditions for a Lyapunov function are satisfied.

An energy-like quantity can be defined as

$$\Lambda = \frac{(p_2 - J_B\alpha)^2}{ml^2 + J_B + J_J} + kJ_B\theta^2 + \frac{p_1^2}{m}, \tag{270}$$

and it is straightforward to verify that it is conserved by the flow of the closed-loop system (258). The asymptotic value of the cart's forward momentum can thus be determined by

$$\lim_{t\to\infty} p_1^2 = m\Lambda(0) = D + kF, \tag{271}$$

where

$$D = m\frac{(p_2(0) - J_B\alpha(0)^2}{ml^2 + J_B + J_J} = m(ml^2 + J_B + J_J)\dot{\theta}(0)^2, \tag{272}$$

and

$$F = mJ_B(\theta(0))^2. \tag{273}$$

Simulation results are given in Figures 21 and 22 by solving the equations for the closed-loop system for different values of k.

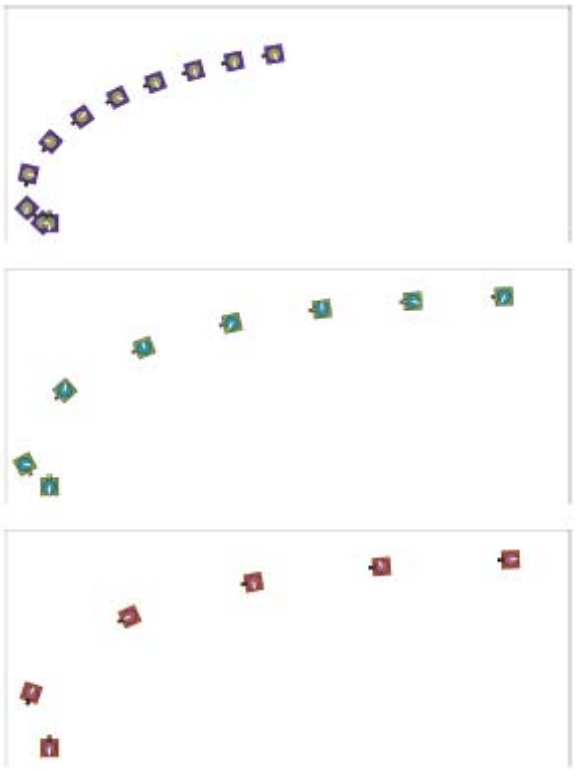

Figure 21: Still frame snapshots of three different gains at equal time intervals.

Larger values of k tend to cause the system to reach its navigational goal more

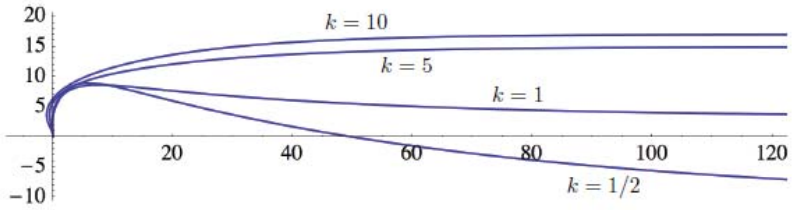

Figure 22: An extended duration plot of beanie trajectories for different gains.

quickly and in less distance than do smaller values. For different k values, the system does not always reach the goal monotonically. Sometimes it reaches it through a damped oscillation. If the same system in which actuation enters the system as control velocities instead of control torques is used, the control law $\dot{\phi} = \frac{p_2 + k\theta}{J_B}$ can be applied to achieve similar results as above.

CHAPTER 6: OPEN-LOOP REDUCED INERTIAL SYSTEM WITH GEOMETRIC PHASE

To initiate the exploration of fish-like swimming, in this chapter, geometric techniques are used to study a fish-like system with no drift. A three-link elliptical system that approximates the motion of a carangiform fish is constructed and its locomotion due to geometric phase studied. Given that this system is driftless, the evolution of the system is completely governed by the control variables and the local connection of the system.

6.1 Geometric Phase

First, more concepts must be defined.

Definition 6.1.1. A **gait** can be considered a time-parameterized cyclic shape change or a map $\gamma : I \to M : t \mapsto r(t)$ from some interval $I \subset \mathbb{R}$ into a shape manifold M.

The motion of the system through G can be calculated by introducing the area rule.

Definition 6.1.2. The **area rule** for Abelian bundles is shown by starting along a curve in Q that is everywhere horizontal,

$$\dot{g} = -gA(r)\dot{r}$$

in local coordinates. In general, the geometric phase associated with a closed curve $c : [0, T] \to M$ is given by

$$g(T) = g(0)\exp\xi(c),$$

where

$$\xi(c) = -\overline{A} + \frac{1}{2}\overline{[\overline{A}, A]} - \frac{1}{3}\overline{[[\overline{A}, A], A]} - \frac{1}{12}[\overline{A}, \overline{[\overline{A}, A]}] + \ldots \tag{274}$$

and

$$\begin{aligned}
\overline{A} &= \int_0^T A(c(t))\dot{c}(t)dt, \\
\overline{[\overline{A}, A]} &= \int_0^T \left[\int_0^t A(c(\tau))\dot{c}(\tau)d\tau, A(c(t))\dot{c}(t)\right]dt, \\
&\vdots
\end{aligned}$$

.

If G is Abelian, only the first term in this expansion is nonzero, so that

$$g(T) = g(0)\exp\left(-\int_0^T A(c(t))\dot{c}(t)dt\right).$$

By Stokes' theorem,

$$\begin{aligned}
g(T) &= g(0)\exp\left(-\int_S dA(r)\right) \\
&= \exp\left(-\int_S dA(r)\right)g(0),
\end{aligned}$$

where S is any oriented submanifold of M whose boundary is traced by $c(t)$ as t increases from 0 to T. If G is Abelian, then the local curvature form satisfies

$$DA(X,Y) = D\Gamma(X^h, Y^h)$$

for $X, Y \in \mathfrak{X}(M)$. However,

$$DA(X,Y) = dA(X,Y).$$

The area rule can be used to devise an open-loop control strategy.

Step 1: Given a driftless Lagrangian system with two control inputs, create a 3D plot for the values of the local curvature form.

Step 2: Identify regions in the plot that have the highest values of curvature.

Step 3: Generate gaits that encircle these regions.

The area rule indicates, whenever the areas of two different gaits are equal, the gait that encompasses a region with higher values of curvature will result in a larger net displacement or geometric phase. Thus, efficient gaits can easily be designed by encircling regions with high curvature values.

6.2 Open-Loop System

These ideas can be used to construct an optimal open-loop control gait for a fish-like system. This system consists of three elliptical linkages, moves only along the x-axis, and has two actuated joints. This gives a system with the product structure $Q = G \times M = GL(1) \times \mathbb{R}^2$.

The system is constructed with the following equations:

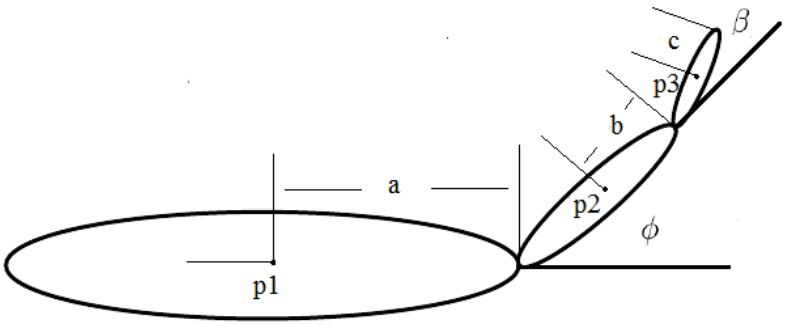

Figure 23: The three link system.

$$
\begin{aligned}
p_1 &= (x, 0), \qquad (275)\\
p_2 &= (x + a + b\cos\phi, b\sin\phi),\\
p_3 &= (x + a + 2b\cos\phi + c\cos(\phi+\beta), 2b\sin\phi + c\sin(\phi+\beta),\\
v_1 &= \dot{p}_1,\\
v_2 &= \dot{p}_2,\\
v_3 &= \dot{p}_3,\\
v_{1_L} &= v_1.(1, 0),\\
v_{1_S} &= v_1.(0, 1),\\
v_{2_L} &= v_2.(\cos\phi, \sin\phi),\\
v_{2_S} &= v_2.(-\sin\phi, \cos\phi),\\
v_{3_L} &= v_3.(\cos(\phi+\beta), \sin(\phi+\beta)),\\
v_{3_S} &= v_3.(-\sin(\phi+\beta), \cos(\phi+\beta)).
\end{aligned}
$$

The Lagrangian for the system is given by

$$L = \frac{1}{2}m_1 v_{1_L}^2 + \frac{1}{2}m_2 v_{2_L}^2 + \frac{1}{2}M_2 v_{2_S}^2 + \frac{1}{2}m_3 v_{3_L}^2 + \frac{1}{2}\dot{J}_2^2 + \frac{1}{2}(\dot{\phi} + \dot{\beta})^2 + \frac{1}{2}\dot{J}_3^2. \tag{276}$$

Applying this equation gives a local mechanical connection of the form

$$A_{\text{mech}} = \left(A_1 d\phi + A_2 d\beta\right), \tag{277}$$

with

$$A_1 = \frac{-(5b^3(5\rho_f + \rho_s) + 2bc^2(13\rho_f + 5\rho_s))\sin\phi}{(a^2(\rho_f + 5\rho_s) + (b^2 + c^2)(13\rho_f + 5\rho_s) - 12\rho_f(b^2\cos(2\phi) + c^2\cos(2(\beta + \phi))))} \\ -\frac{c^2(5c(5\rho_f + \rho_s)\sin(\beta + \phi) + 24b\rho_f\sin(2\beta + \phi))}{(a^2(\rho_f + 5\rho_s) + (b^2 + c^2)(13\rho_f + 5\rho_s) - 12\rho_f(b^2\cos(2\phi) + c^2\cos(2(\beta + \phi))))}, \tag{278}$$

and

$$A_2 = \frac{-(5c^3(5\rho_f + \rho_s)\sin(\beta + \phi))}{(a^2(\rho_f + 5\rho_s) + (b^2 + c^2)(13\rho_f + 5\rho_s) - 12\rho_f(b^2\cos(2\phi) + c^2\cos(2(\beta + \phi))))}. \tag{279}$$

Because the system is Abelian, the local curvature form is equal to the exterior derivative calculated by

$$DA = dA.$$

Plotting the DA values over the range of the actuation variables ϕ and β gives the following figures.

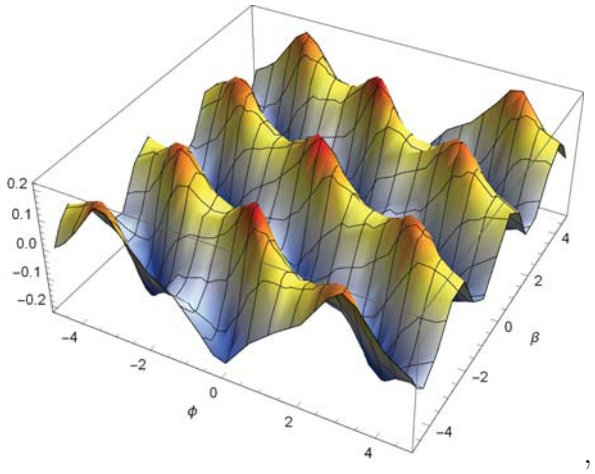

Figure 24: A 3D curvature plot of the system.

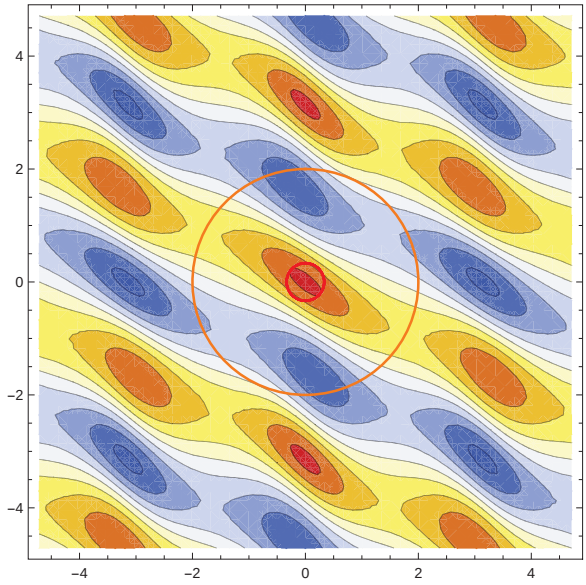

Figure 25: A curvature contour plot of the system with two different trajectories.

The second contour plot has two trajectories overlayed on it. The orange gait gives a likely (although uninformed) first choice for the system. Using the curvature plot, the smaller, red gait can be constructed around a section with larger values of DA. This smaller gait has a radius that is $\frac{1}{6}$ that of the larger trajectory. When the smaller trajectory is actuated at a frequency 6 times that of the larger gait, each trajectory moves through equal amounts of shape space over a given time period T.

Plotting the x values of the system over time t, the smaller gait achieves a net displacement in the negative x direction, the desirable direction. The larger gait achieves motion in the opposite direction with the same amount of distance through shape space. However, this net motion is still nearly 3 times less than the net motion of the smaller gait. Tracing out the larger gait in reverse would give a net motion in the negative x direction.

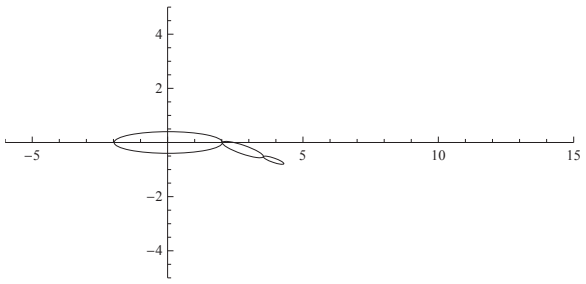

Figure 26: A snapshot of the smaller gait extended to its maximum range.

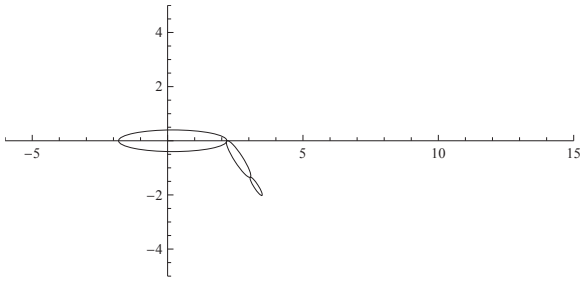

Figure 27: A snapshot of the larger gait extended to its maximum range.

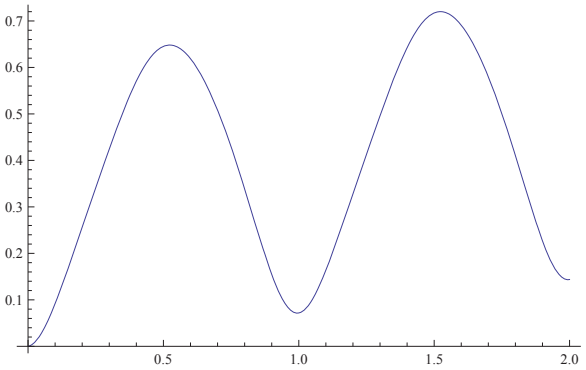

Figure 28: $\frac{1}{2}$ Hertz; net x distance .1437.

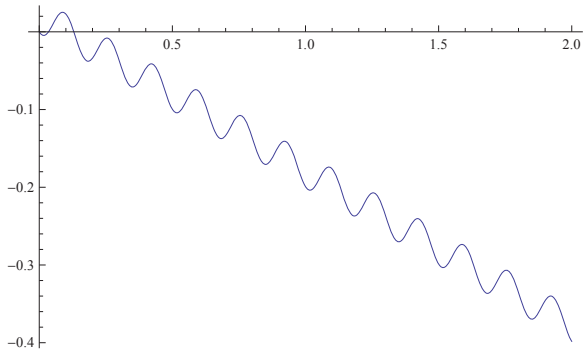

Figure 29: 3 Hertz; net x distance -.398.

CHAPTER 7: EXPERIMENTAL APPROACH TO UNDERACTUATED PLANAR NAVIGATION

In Kelly and Pujari (2010), a model was constructed for a fish-like swimmer that could vary its camber to shed discrete point vortices that induced forward motion. It was also shown that the swimmer could execute a turning maneuver along a specified heading and continue to oscillate and, therefore, swim in that direction. This movement was accomplished with the control law $\dot{\phi} = k\theta$. This chapter presents experimental data that complement the model seen in Figure 30.

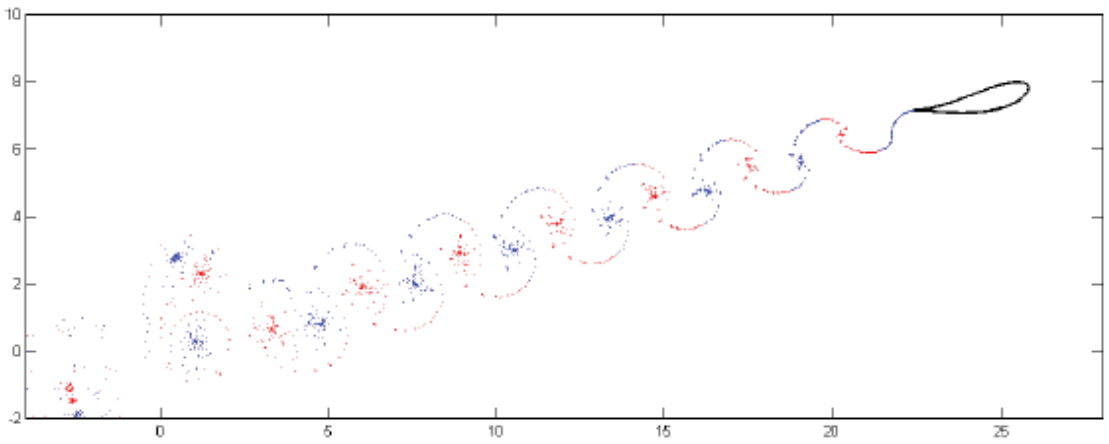

Figure 30: Simulation snapshots of the swimmer. Notice the blue CW and red CCW counter-rotating vortices in the trailing wake.

7.1 Experiment Construction

A robot was rapid prototyped from an initial CAD design. It was split into three sections, the front, mid, and tail sections. Each adjoining section was connected by a steel shaft. On the end of each shaft was a sprocket and chain, which connected

to the sprocket on the servomotor. The robot had two Hitec HSR-5990 high-torque servomotors controlled by an onboard Arduino microcontroller. This microcontroller communicated with a laptop through an onboard X-Bee bluetooth unit. The roof and floor of the robot were constructed of aluminum. Between the aluminum and the rapid prototyped sections was a rubber gasket that created a water-tight seal.

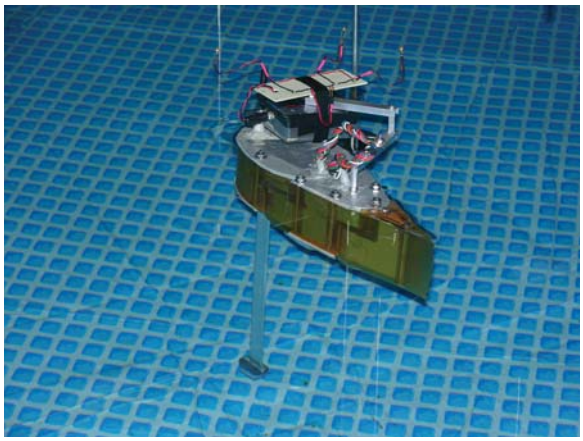

Figure 31: The robotic fish floating in the pool.

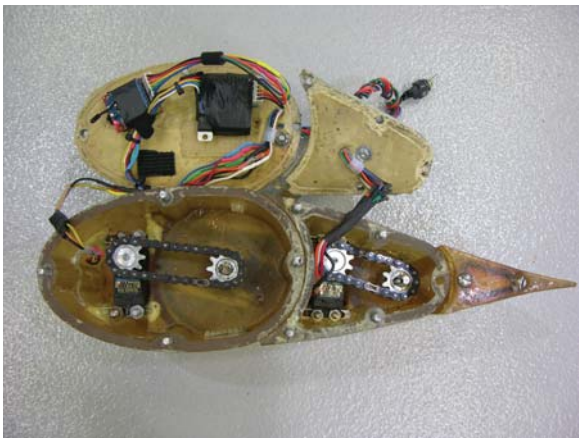

Figure 32: An inside view of the robotic fish.

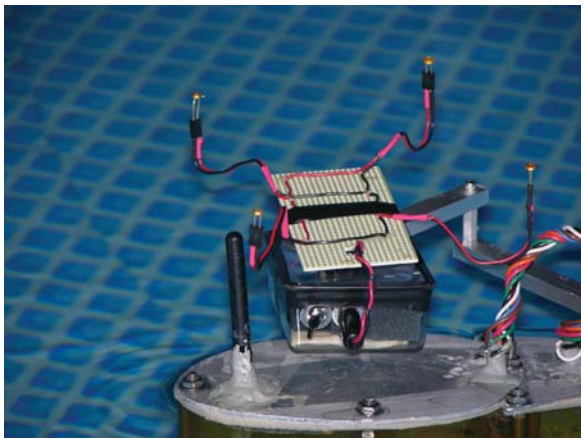

Figure 33: The IR tracking LEDs.

Figure 34: The experimental pool.

Figure 35: One of six cameras used in tracking the motion of the robot.

In the simulation, the mathematical model implicitly contained information about the position, orientation, and camber of the fish-like swimmer. This could be specified or solved for and analyzed as needed. However, to attain these data in the experiment, a sophisticated measurement and control system was implemented.

The measurement system was an OptiTrack camera system (Figure 35) running NaturalPoint motion tracking software. It could record position and orientation information for any object in the pool. Six cameras were mounted along the perimeter of the pool (as seen in Figure 34), a few feet above the surface of the water. The system tracked infrared points in the viewing area of the cameras. When three cameras had a point in view, the software was capable of tracking its location. Given multiple points mounted on a rigid object, the software would recognize it as a rigid object and return not only its position but also its orientation. Because the system tracked infrared points of light, care was taken to ensure that extraneous sources of infrared light(the sun, ceiling lights) were blocked. To make sure that the robot would be tracked by the system, a circuit of four infrared light-emitting diodes was constructed and mounted on top of the robot (Figure 33).

The control system for the robot was a laptop running LabVIEW 8.5. The LabVIEW program would read in the position and orientation data from the NaturalPoint motion-tracking software and use this information in a proportional feedback control loop based on maintaining a desired heading. The output of this control loop was tail position. The program recorded time, robot position, robot orientation, and tail position data for the duration of the experiment.

7.2 Results

In the simulation, the swimmer would experience stable oscillations of its tail to provide forward propulsion. The gain could be directly tuned to achieve a specific speed. The experimental swimmer could swim in a similar way; a higher gain meant a higher speed. However, there was a slight difference in their swimming styles. When the robotic swimmer would swim using stable tail oscillations, the oscillations would damp out over time, and the robot would come to a stop. However, by tuning the gain beyond a certain threshold value, the controller could induce unstable oscillations. These unstable oscillations were bounded by the mechanical range of the tail. The speed at which these unstable oscillations occurred could be influenced by adjusting the gain of the controller. Thus, speed and heading could be specified for the underactuated system. Figure 36 shows the oscillation values for a typical swimming experimental run. Figure 37 plots the moving average velocities for different values of k. Higher values of k lead to higher final velocities.

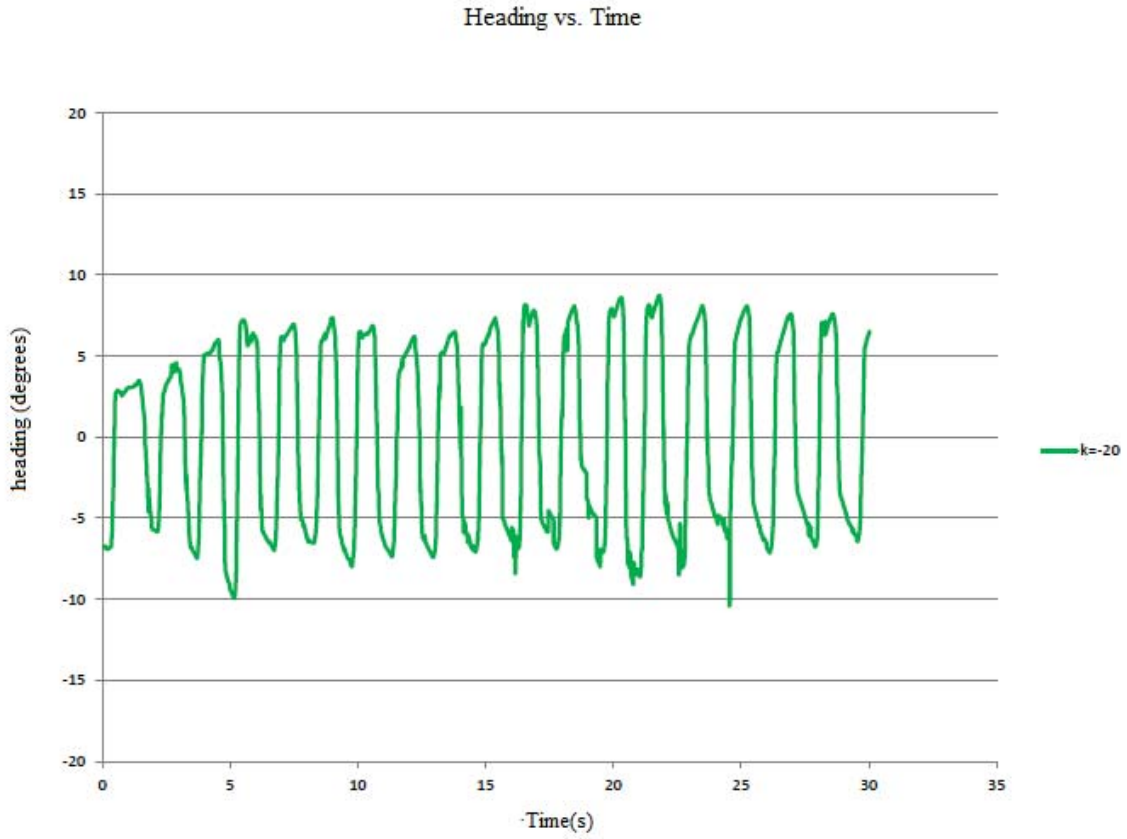

Figure 36: Heading of the robot vs. time.

Figure 37: Moving average velocities for different values of k.

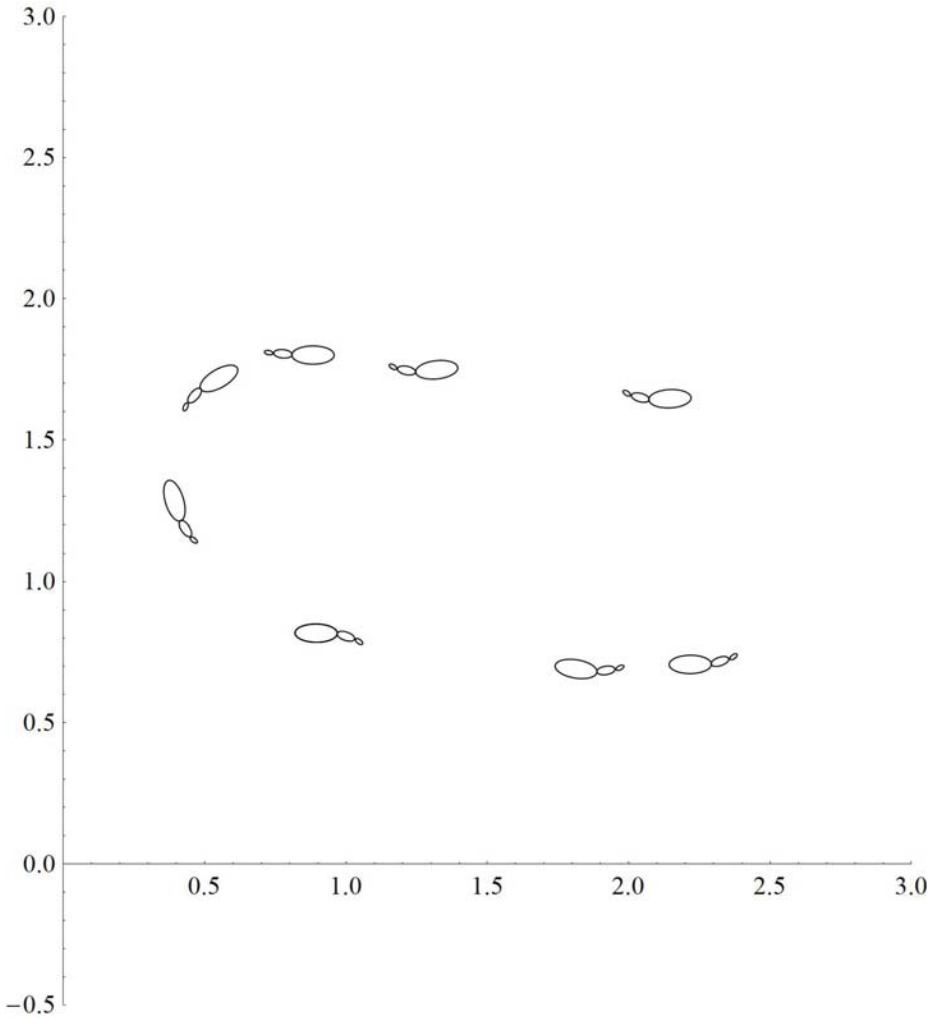

Figure 38: Still-frame pictures showing a 180-degree turn.

Figure 38 shows images generated from experimental data. A run was conducted initially specifying a heading for the swimmer, which was then re-specified in the opposite direction. Data from the experiment included heading data, x and y position and velocity data, and joint angle (camber) data. Importing these data into Mathematica and representing the swimmer as a three-ellipse system, the data were used to construct the still frame image in Figure 38. The data show the robot swimming along a given heading, turning 180 degrees, and then swimming along its new heading.

CHAPTER 8: VORTEX CHARACTERIZATION

In this chapter and the next, an experiment is constructed to complement a simulation conducted in Kelly and Pujari (2010). The simulation demonstrated, with a simple control law, a swimmer could navigate a staggered array of idealized fluid vortices (see Figure 39). Not only did the swimmer navigate the array, but it used the vortices to propel itself along its desired heading, resulting in a higher swimming efficiency than was observed in the absence of vortices. The first step in constructing the experiment was to develop a machine that could generate standing fluid vortices. These fluid vortices needed characteristics similar to those of the fluid vortices of the simulations.

This chapter begins with a brief review of the theory behind planar, irrotational fluid flow. Then, a machine for generating experimental vortices is described. Finally, the experimental vortices are characterized to determine their fitness for comparison with the simulations.

8.1 Modeling of 2D Flow Regions

The continuity equation for steady, planar, incompressible, and irrotational regions of flow in polar coordinates is

$$r\frac{\partial}{\partial r}\left(\frac{1}{r}\frac{\partial \phi}{\partial r}\right)+\frac{\partial^2 \phi}{\partial \theta^2}=0. \tag{280}$$

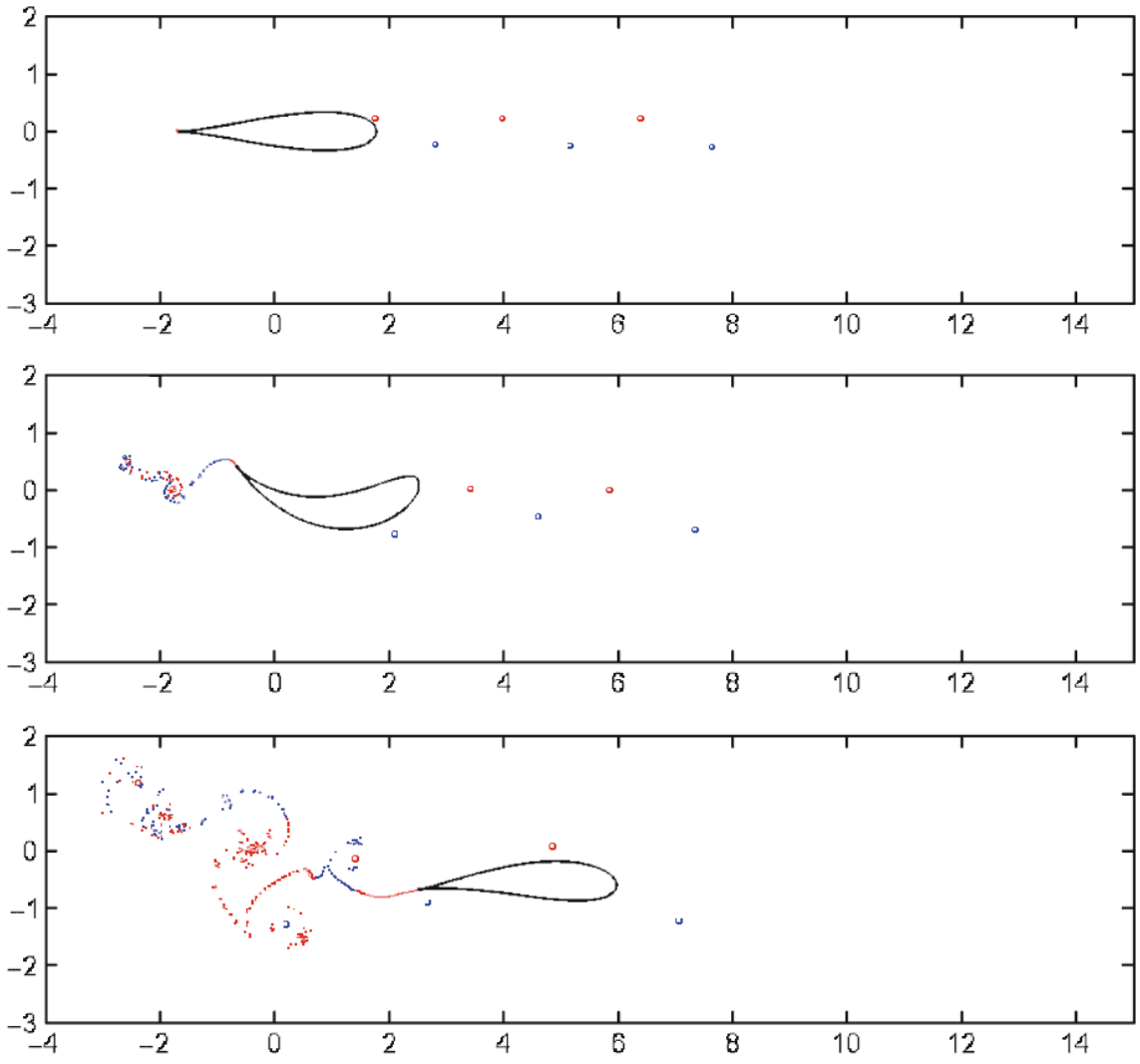

Figure 39: Drafting through the array of fluid vortices via PID control.

The stream function ψ is defined as

$$v_r = \frac{1}{r}\frac{\partial \psi}{\partial \theta} \quad \text{and} \quad v_\theta = -\frac{\partial \psi}{\partial r}. \tag{281}$$

The vorticity is given by

$$\omega = \frac{1}{r}\frac{\partial}{\partial r}(r v_\theta) - \frac{1}{r}\frac{\partial v_r}{\partial \theta}, \tag{282}$$

and the divergence by

$$\nabla \cdot \mathbf{v} = \frac{\partial v_r}{\partial r} + \frac{1}{r}\left(\frac{\partial v_\theta}{\partial \theta} + v_r\right). \tag{283}$$

For an ideal point source,

$$\begin{aligned} v_r &= \frac{q_o}{2\pi r}, \\ v_\theta &= 0. \end{aligned} \tag{284}$$

For an ideal vortex,

$$\begin{aligned} v_r &= 0, \\ v_\theta &= \frac{\Gamma_o}{2\pi r}, \\ \omega &= 0, \\ \nabla \cdot \mathbf{v} &= 0. \end{aligned} \tag{285}$$

Because the Laplace equation is a linear homogeneous differential equation, the linear combination of two or more solutions of the equation must also be a solution. Thus, the stream functions of the source and vortex can be superimposed and differentiated to arrive at the equations for a source and vortex:

$$\begin{aligned} v_r &= \frac{q_o}{2\pi r}, \\ v_\theta &= \frac{\Gamma_o}{2\pi r}. \end{aligned} \tag{286}$$

8.2 Experimental Setup

The experiment consisted of three basic components: a single vortex generator, a pool of water, and a PIV measurement system. The vortex generator consisted of an 18-inch long, quarter-inch diameter metal shaft, with two 8 by 2 by 16 inch metal plates welded onto the diameter. These created a paddle-like structure. To prevent water from being pumped into the paddle during operation, a flat disc was welded onto the bottom.

Figure 40: The vortex generator.

The pool of water for this experiment was a small section of a water channel. A motor drive system was mounted onto the structure and connected to the vortex generator. The top of the vortex generator was flush with the surface of the water.

The measurement system for this experiment was a Dantec Dynamics Particle

Image Velocimetry (PIV) system. This system consists of seed particles, a laser, a high-speed camera, and a laptop running post-processing software. The laser component formed a planar sheet of laser light, oriented normal to the axial direction of the vortex generator shaft, about 3 inches from the bottom of the shaft. The seed particles consisted of tiny reflective particles of silver that float in the water. The high-speed camera was positioned a couple of feet away, pointed normal to the laser sheet so that the laser sheet was in the camera's field of view. When the laser was turned on, the camera captured the laser's reflections off the seed particles at 1600 frames per second. The post-processing software then monitored the change in position of each particle from frame to frame to create a velocity vector field plot for the system.

8.3 Experimental Results

The PIV system was used to characterize the fluid vortices.

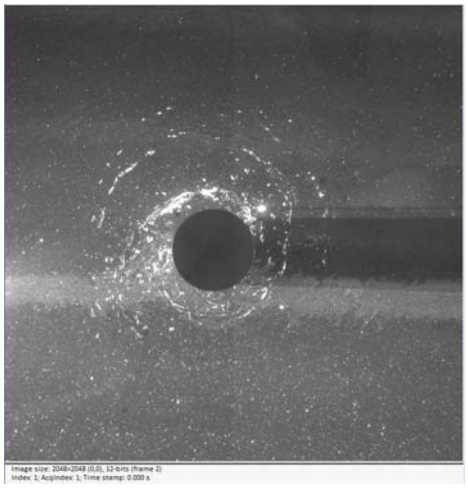

Figure 41: A view of the vortex paddle from below.

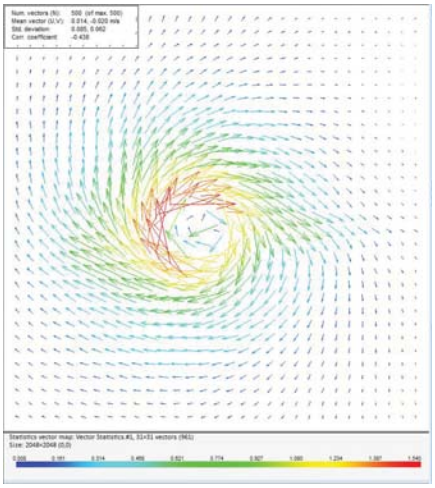

Figure 42: A snapshot of the PIV velocity vectors of the paddle.

Figure 41 shows the view of the vortex generator from below. It is a snapshot of the

camera footage used in the PIV calculations. Figure 42 shows the raw vector field data calculated from the camera footage. The following figures were generated using the velocity vector field in Figure 42.

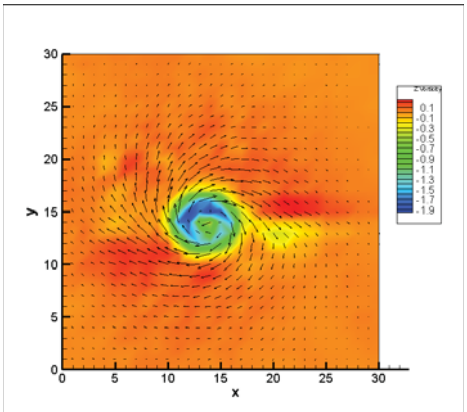

Figure 43: Vorticity.

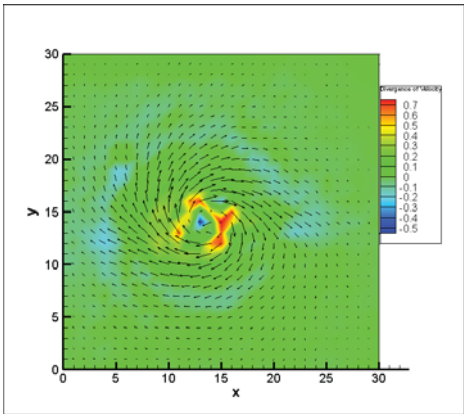

Figure 44: Divergence.

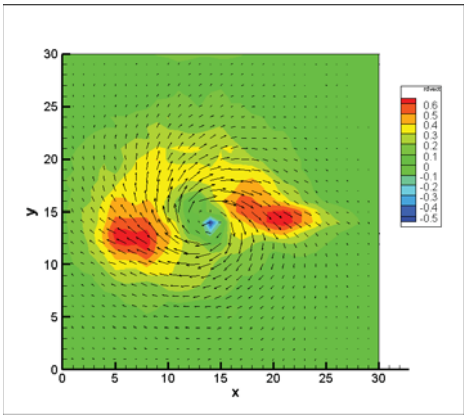

Figure 45: Radial velocity from vortex center.

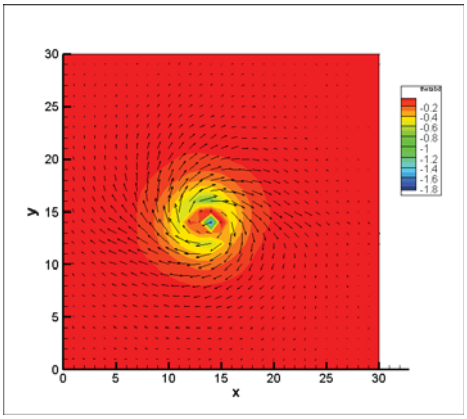

Figure 46: Angular velocity about vortex center.

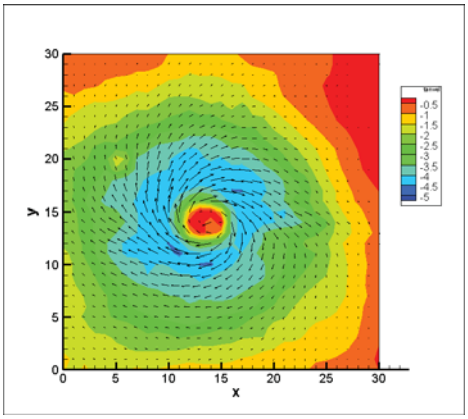

Figure 47: Tangential velocity about vortex center.

The figures suggest a few characteristics of the system. Figure 43 shows ω for the system. Because $\omega \neq 0$, the test indicates the system is not irrotational. Figure 44 shows $\nabla \cdot \mathbf{v}$ for the system. Because $\nabla \cdot \mathbf{v} \neq 0$, it indicates the presence of a point source/sink. The positive values indicate a point source, which can be interpreted as water entering the viewing plane from the z direction. Figures 45 and 46 decompose the velocity field into radial and angular velocity components. Figure 45 shows regions of outward fluid velocity. The lack of symmetry in the system might have been caused by the lack of symmetry in the boundary locations of the fluid. The max and min y locations were locations of the walls, whereas the locations of the other two walls were much further out of the measurement window in the positive and negative x directions. Figure 45 clearly shows regions of decreasing angular fluid velocity about the generator. The angular velocity decreases steadily as radial distance increases, consistent with irrotational behavior. Figure 47 shows the tangential velocity of the fluid about the center point. It indicates that the tangential velocity of the fluid decreases with radial distance from the center. This is inconsistent with irrotational vortex behavior.

Because there are inconsistencies between the experimental vortex and an ideal vortex, a measurement was needed to determine how much the experimental values deviated from the ideal case. First, a vector plot was constructed from the equations for an ideal vortex. Then, (287) was used to sum the differences in each vector in the field, normalizing by the maximum possible sum for the combined vector field magnitude. The idea was, given two vectors, a third vector could be constructed from vector subtraction of the initial two vectors. Doing so would give an indication of the

deviation of one vector from another. The max value for this vector would be the magnitudes of the two vectors combined, meaning both vectors were placed tail-to-tail, pointed in exactly opposite directions. Summing all the deviations and dividing that sum by the sum of all of the maximum values gives a normalized coefficient indicating how nonideal a vector field is from an ideal case. Thus, for identical vector fields, the value of this coefficient was zero. For exactly opposite vector fields or the zero case, the value was one.

$$id_{coeff} = \frac{\sum_N^{i_{max}} |v_2^i - v_1^i|}{\sum_N^{i_{max}} |v_2^i| + |v_1^i|} \tag{287}$$

Different coefficients for different ideal vortices were compared to a baseline ideal vortex. Doing so helped in determining what an acceptable coefficient value would be for the experimental data. These coefficients are shown in Table 5. Values are also given for an ideal vortex as opposed to an ideal vortex of constant strength, plus an ideal point source of varying strength.

The experimental vector field was compared to seven different ideal cases: the zero, the rotational, the reverse rotational, the irrotational, the point source, the irrotational plus point source, and the modified Rankine vortex plus point source. Figures 48 through 53 show the different numerically generated vector fields for each case. Table 6 shows the different cases, along with the equations for each case, the values of the variables for each case, and the calculated coefficient values for each case. The worst cases were the zero and reverse rotational cases, and the best case was the modified Rankine vortex plus source.

Γ_1	Γ_2	q_1	q_2	coefficient
1	0	0	0	1
1	.5	0	0	$\frac{1}{3}$
1	1	0	0	0
1	2	0	0	$\frac{1}{3}$
1	3	0	0	$\frac{1}{2}$
1	4	0	0	$\frac{3}{5}$
1	5	0	0	$\frac{2}{3}$
1	6	0	0	$\frac{5}{7}$
1	7	0	0	$\frac{3}{4}$
1	1	0	0	0
1	1	0	$\frac{1}{4}$	.068545
1	1	0	$\frac{1}{3}$	.090943
1	1	0	$\frac{1}{2}$	.13458
1	1	0	1	.25298
1	1	0	$\frac{3}{2}$	.35057
1	1	0	2	.429549
1	1	0	3	.545993
1	1	0	4	.625747
1	1	0	6	.725631
1	1	0	9	.805823
1	1	0	15	.878595

Table 5: The coefficient values for the different ideal vortices.

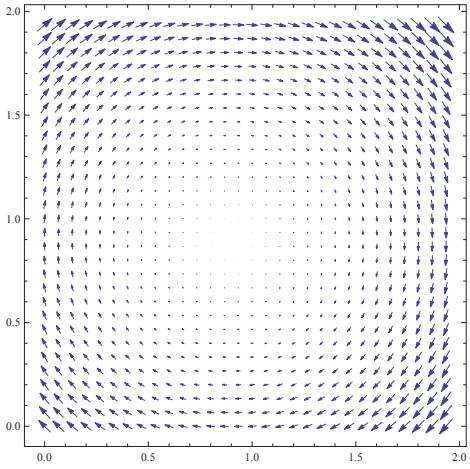

Figure 48: Reverse rotational.

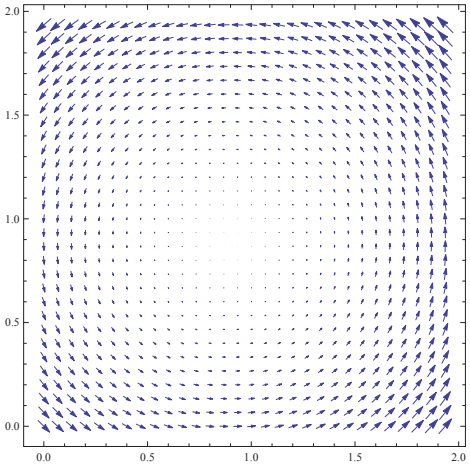

Figure 49: Rotational.

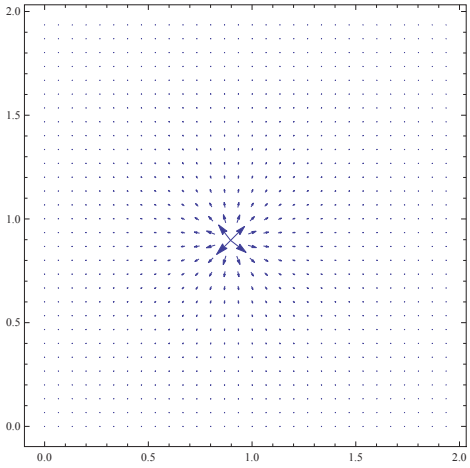

Figure 50: Point source.

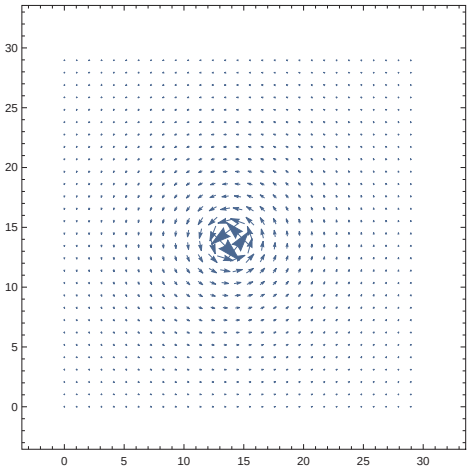

Figure 51: Irrotational.

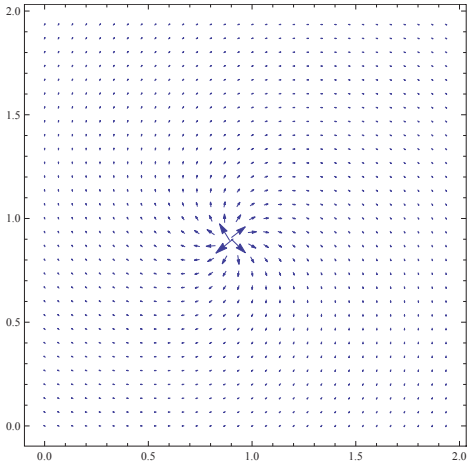

Figure 52: Source plus irrotational.

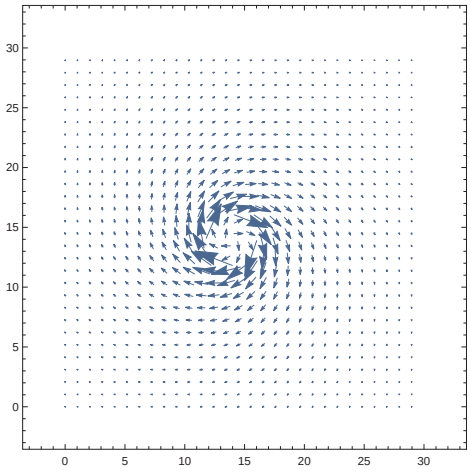

Figure 53: Modified vortex plus source.

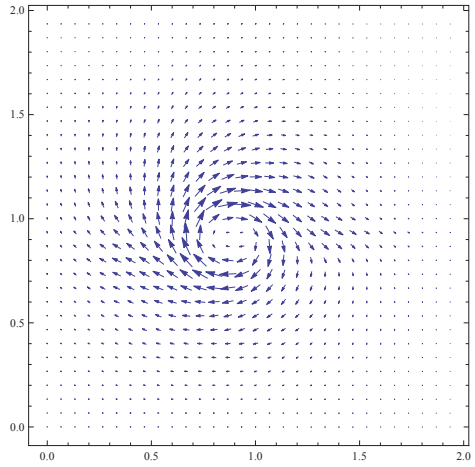

Figure 54: Experimental vector plot.

Vector Field	equation	constants	coefficient
Zero Velocity	$v_\theta = 0$ $v_r = 0$	$\Gamma = 0$ $(\frac{m^2}{s})$ $q = 0$	1
Reverse Rotational	$v_\theta = r\dot{\theta}$ $v_r = 0$	$\dot{\theta} = .000112$ $(\frac{rad}{s})$	.974
Rotational	$v_\theta = -r\dot{\theta}$ $v_r = 0$	$\dot{\theta} = -.000112$	.566224
Point Source	$v_\theta = 0$ $v_r = \frac{q}{r}$	$q = .023913$	0.584776
Irrotational	$v_\theta = \frac{\Gamma}{r}$ $v_r = 0$	$\Gamma = -.023913$	0.396671
Irrot. + Source	$v_\theta = \frac{\Gamma}{r}$ $v_r = \frac{q}{r}$	$\Gamma = -.016909$ q=.016909	.346372
Modified Rankine +Source	$\begin{cases} v_\theta = -0.004913 & R \geq r \\ v_r = .004913 & \\ v_\theta = \frac{\Gamma}{r^\nu} & R < r \\ v_r = \frac{q}{r^\nu} & \end{cases}$	$\Gamma = -.083207$ q=.036981 R=.125(m) $\nu = 1.5$	.251533

Table 6: Coefficient values for the different runs

The best case indicates that, although the experimental vortex had characteristics of both an ideal point source and a modified ideal vortex, the vortex behavior dominated the point source behavior. This result also indicates the experimental vortex is a satisfactory representation of a vortex from the simulations.

CHAPTER 9: VORTEX ENERGY HARVESTING

9.1 Experimental Setup

Figure 55 shows the setup of the experiment. The vortex generating machine rests above the pool and spins the fluid below. The robot is placed within the vortices at the beginning of the experiment. The tracking system setup and control programs are identical to the setup in Chapter 7.

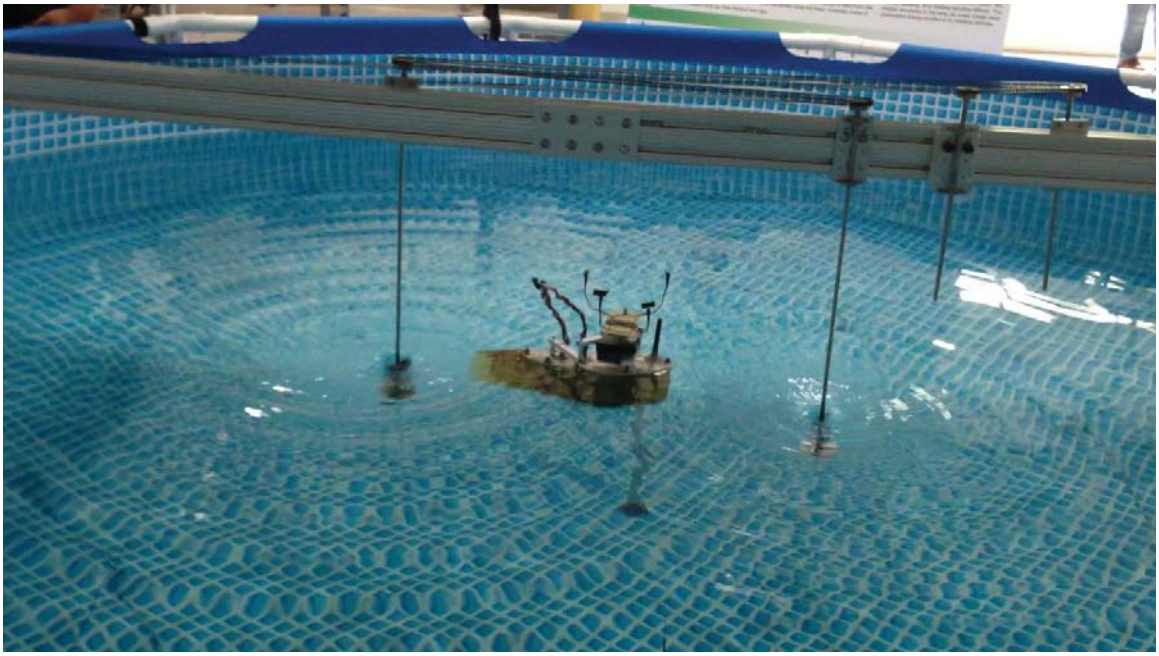

Figure 55: The robot steering through the vortex array.

9.2 Experimental Results

Three types of experiments were performed that paralleled the three simulations discussed previously.

1. Vortices were present. The robot was guided by a closed-loop control system using $\phi = k\theta$ as the control law.

2. Vortices were present. The robot was unguided by any control and did not actuate/swim. It was essentially dead in the water.

3. Vortices were not present. The robot was again guided by $\phi = k\theta$. This experiment was identical to the swimming demonstrated in Chapter 7.

Multiple runs for each type of experiment were performed, and the data were recorded. The data were loaded into Mathematica and used to generate still frame pictures depicting the motion of the robot throughout the duration of the experiment.

The three experimental runs had distinct behaviors. Experiment 1, Figure 56, showed that the robot steered in a way that always pointed along the given heading. With the aid of the fluid vortices, the robot was propelled along the entire width of the pool. It followed the path in Figure 56. It was observed in Experiment 2, Figure 57, that the robot was propelled around the vortex, then was ejected out the side of the vortex pair. In Experiment 3, Figure 58, as expected, the robot swam the width of the pool.

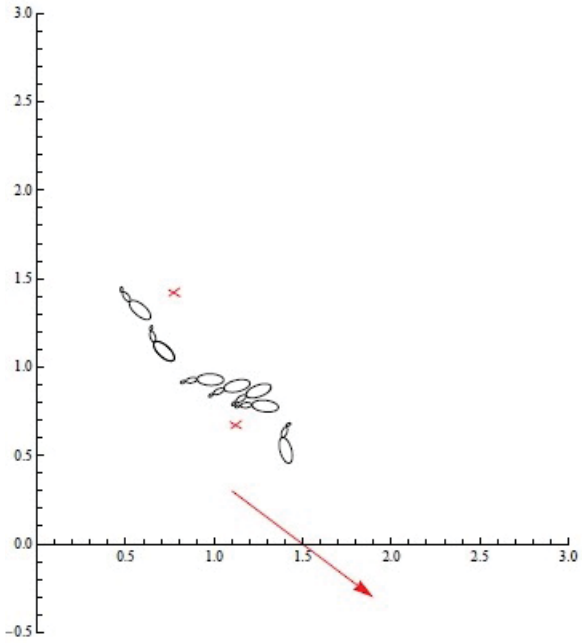

Figure 56: Still frames showing vortex energy harvesting.

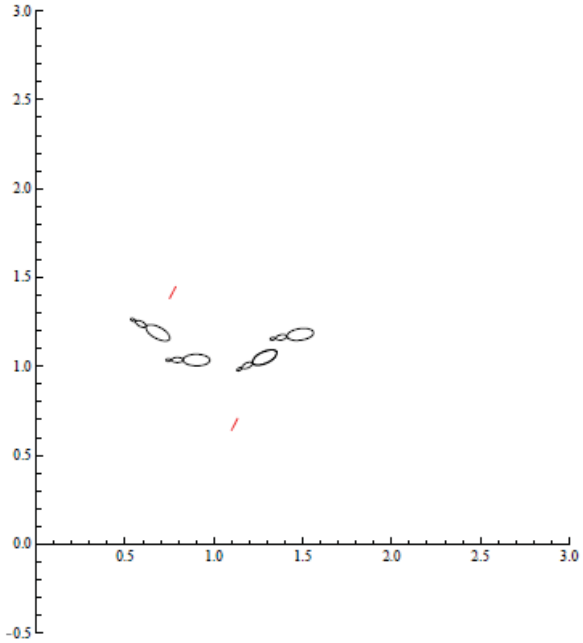

Figure 57: Still frames showing the robot dead in the water.

Each of the experimental runs displayed similar behavior to the simulation runs in Kelly and Pujari (2010).

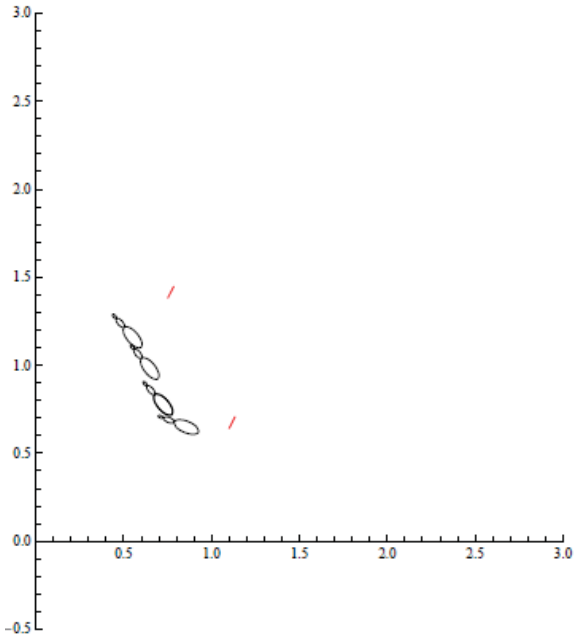

Figure 58: Still frames showing free swimming.

9.2.1 Tail Data

The angular position of the tail was recorded for each experimental run. Curves were fitted to the position data for the runs. Doing so helped characterize the actuation effort required from the robot for each run. Figures 59 through 64 show all the measured tail data over the duration of the closed-loop and open-loop runs. Because the actuation was turned off, no data were recorded for Experiment 2.

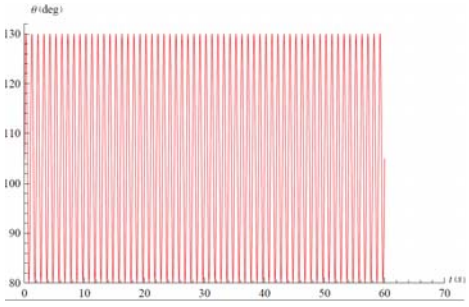

Figure 59: Open-loop tail position data, f = 60Hz, A = 30 deg.

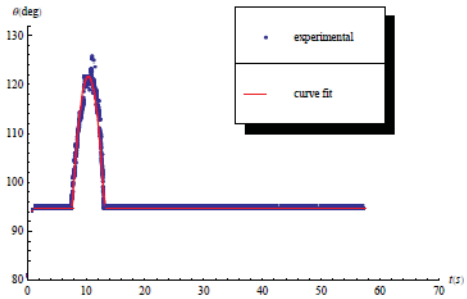

Figure 60: Closed-loop run 1.

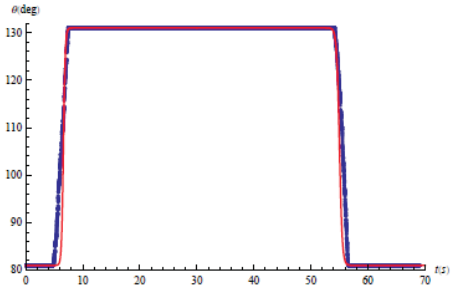

Figure 61: Run 2.

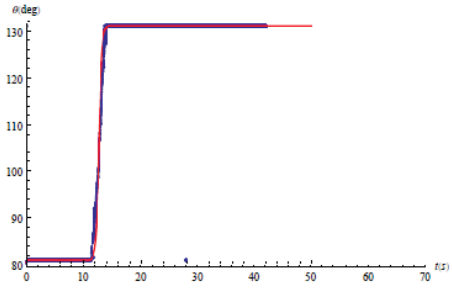

Figure 62: Run 3.

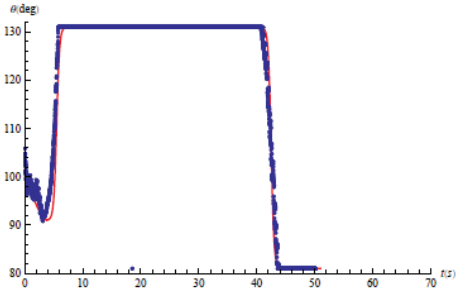

Figure 63: Run 4.

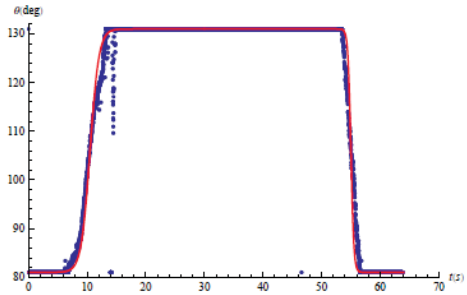

Figure 64: Run 5.

For Experiment 3, a periodic gait was needed to propel the robot across the same distance of the pool as the vortex runs in a roughly equal interval of time. The average time needed for the vortex run to traverse the pool was about 60 seconds. A sinusoidal gait was chosen because it approximates the motion of a fish tail. After experimenting with different frequencies and amplitudes of the sinusoidal gait, a gait with a 60 Hz frequency and a range of ± 30 degrees was chosen because it was able to traverse the distance of the pool in about 60 seconds.

9.2.2 Calculating Efficiency

The curve fits for each run in the following equations were used to calculate the economy of motion (total angle swept by the tail) for each run and to measure a total energy-like quantity expended by the tail over each run.

$$\dot{\theta}_{net} = \int_0^t |\ddot{\theta}(\tau)| d\tau \tag{288}$$

$$\theta_{net} = \int_0^t |\dot{\theta}(\tau)| d\tau \tag{289}$$

Run	$\theta_{net}(deg)$	$\dot{\theta}_{net}(\frac{deg}{s})$	$\frac{\theta_{net}}{\theta_{free}}\%$	$\frac{\dot{\theta}^2_{net}}{\dot{\theta}^2_{free}}\%$	final velocity (m/s)
free	860.36	5403.70	100	100	.014
1	27.7	73.8	3.2	.019	.026
2	47.1	56.2	5.5	.011	.011
3	40.8	73.0	4.7	.018	.030
4	44.4	63.9	5.1	.014	.021
5	47.1	74.4	5.5	.019	.029

Table 7: Efficiency values for the different runs

The table above shows the calculated values of (288) and (289), the ratio of the closed-loop over the open-loop values for the economy of motion and for the rotational energy, and the final velocity for each run. The net angular distances of the runs for Experiment 1 are about two orders of magnitude less than the angular distance of those for Experiment 3. The net angular distance of each run for Experiment 1 is less than the distance traveled by one oscillation for Experiment 3. The ratios of the rotational energy for Experiment 1 over Experiment 3 differ by four orders

of magnitude. The final velocities for Experiment 1 runs were usually nearly twice those for Experiment 3, with one exception, when it was less. All these results are consistent with the results of the simulations.

CHAPTER 10: CONCLUSIONS

This work has included a thorough introduction to techniques of Lagrangian reduction, including concepts, definitions, and detailed examples. The reader will obtain a sufficient foundation for performing reduction of problems. In addition, it showed theoretically, analytically, and numerically that dissipation can be used to model nonholonomic, holonomic, and kinematic constraints. Thus, a technique commonly used by practicing engineers was placed on firm theoretical footing.

Lagrangian reduction was used to develop control laws for three different novel robotic systems. For the first system, dissipation was used to model the constraints. Controllability was demonstrated. When the dissipation was reduced, accessibility was shown. For the second system, a strategy for underactuated control was demonstrated. For the third system, the geometric phase was used to generate an optimal open-loop control strategy.

Experiments were conducted to complement a previous set of simulations. The first experiment explored underactuated planar navigation for a fish-like robot. That experiment showed that navigational and velocity goals could be achieved with a control law using unstable oscillations to generate propulsion. The results were consistent with the simulations.

The next experiment characterized standing fluid vortices generated by custom-built vortex generators. These vortex generators were the experimental analogs to

the ideal vortices in the simulations. The generated vortices were analyzed with a PIV system, and their behavior was compared to the behavior of ideal vortices. A coefficient was defined to specify the degree to which the experimental vortices deviated from the ideal. As expected, the experimental vortices were not perfectly ideal. However, they were dominated by circulatory behavior seen in the ideal case. This result indicated the vortices could sufficiently replicate ideal vortices.

The last set of experiments showed the robot could extract energy from fluid vortices to assist in propulsion. This technique was shown to be vastly more efficient than swimming in the absence of vortices. These experiments provided evidence that schooling fish could harvest the vortex energy created within the school to achieve net gains in efficiency and that engineers can unlock these efficiency gains for aquatic robots as well.

CHAPTER 11: FUTURE WORK

Extensions of this work could be made in theoretical, computational, and experimental directions. A few such possibilities are presented.

Possibilities for theoretical developments include exploring when the viscosity tensor and other reduced structures built on the Rayleigh dissipation function can be used for various systems. Since the dissipation momentum map K was derived in Kelly (1998), it has yet to make its way into the geometric mechanics canon. Thus, it can be applied to many problems involving dissipation, including structural dissipation in elastic continua (see Marsden and Hughes (1983)) and dissipation in variational integrators (see Leok (2004) and West (2004)). Thus far, dissipation in these problems has not been considered within the context of a momentum map.

The proof presented in this work only considers constraints where the velocities enter linearly into the constraint equation. This is sufficient for most mechanical systems. A possible direction for study would be to extend this proof to systems with nonintegrable constraints where the velocities do not enter linearly into the constraint equations. These types of constraints are much more common in optimization problems (see Arora (2004)).

Future simulations could involve continued development of reduced models for land-based fish-like systems that lend themselves well to geometric control and analysis. Recently in Choset et al. (2013), such a system has been modeled. This system,

as well as systems in this thesis, have been analyzed assuming that they translate through a flat, 2D surface. Interesting mechanics could be observed by mapping such surfaces to non-flat, 2D surfaces. Such candidates would be conic or spherical surfaces, that could be used as approximations of mountains or asteroids.

Future experiments could include building an experimental analogue to a simulated closed-loop hydrofoil swimmer with a source-seeking controller developed by Cochran et al. (2009). A sensor has already been designed and constructed to output a voltage level proportional to the magnitude of a sound source. This sensor could serve as a control input to the system source-seeking control law. Other possible experiments include designing and fabricating land-based robots that complement the Chaplygin beanie and the robotic swimmer, such as the one explored in Choset et al. (2013).

REFERENCES

[1] C.F. Gauss *Disquisitiones Generales Circa Superficies Curvas* Collected Papers, vol 4, pp. 217-58 1827

[2] C.F. Gauss *Untersuchungen Uber Gegenstadne Der Hohern Geodaesie* Collected Papers, vol 4, pp. 259-334 1844

[3] C.F. Gauss *Die Theile Einger Gegebnen Flache Auf Einer Andern Gegebnen Flache So Abzubilden, Daβ Die Abbildung Dem Abgebildeten In Den Kleinsten Theilen Ahnlich Wird* Collected Papers, vol 4, pp. 189-216 1822

[4] G. Monge *Memoire Sur Les Developpees Et Les Points Singuliers Des Courbes A Double Courbure* Mem. Des Savants Etrangers, 10 1785

[5] G. Monge *Memoire Sur Les Developpees, Les Rayons De Courbure Et Lese Differents Genres D'inflexion De Courbes A Double Courbure* Mem. Des Savants Etrangers, 10 1785

[6] S. Lie *Die Grundlagen Fur Die Theorie Der Unendlichen Kontinuierlichen Transformationsgruppen. I. Treatise* Leipz. Ber. 1891, issue III, p 316 1891

[7] E. Noether *Invariante Variationsprobleme* Nachr. D. Knoig. Gesellsch. D. Wiss. Zu Gottingen, Math-phys. Klasse, p 235-257 1918

[8] D.J. Struik *Outline of a History of Differential Geometry* Saint Catherine Press Limited 1933

[9] E.J. Routh *Advanced Rigid Dynamics* London, MacMillian, and Co 1884

[10] E. Cartan *Sur Certaines Expressions Diffrentielles Et Le Problme De Pfaff* Annales Scientifiques De L'cole Normale Suprieure, p. 239332 1899

[11] J. Kepler *Astronomia Nova* 1609

[12] I. Newton *Philosophiae Naturalis Principia Mathematica* 1687

[13] G. Galilei *Dialogues Concerning Two New Sciences* 1638

[14] R. W. Brockett *Feedback Invariants for Nonlinear Systems* Proc. IFAC Congress 1978

[15] R. W. Brockett *Control Theory and Singular Riemannian Geometry* New Direction in Applied Mathematics Spring-Verlag 1981

[16] R. W. Brockett *Differential Geometric Control Theory* Birkhauser 1983

[17] R. W. Brockett *Nonlinear Control Theory and Differential Geometry* Proceedings of the International Congress of Mathematicians 1983

[18] R. W. Brockett *The Early Days of Geometric Nonlinear Control* Elsevier-Automatica, 50, p 2203-2224 2014

[19] R. Murray, Z Li, S Sastry *Mathematical Introduction to Robotic Manipulation* CRC Press 1994

[20] F. Bullo and A. Lewis *Geometric Control of Mechanical Systems* Springer 2005

[21] S. Kelly and R. Murray *Geometric Phases and Robotic Locomotion* CDS Technical Report 1994

[22] S. Kelly and R. Murray *The Geometry and Control of Dissipative Systems* Proceedings of the IEEE Control and Decision Conference 1996

[23] S. Kelly and R. Murray *Lagrangian Mechanics and Carangiform Locomotion* IFAC Symposium on Nonlinear Control Systems Design (NOLCOS) 1998

[24] J. Marsden, R. Montgomery, T. Ratiu *Reduction, Symmetry and Phases in Mechanics* Memoirs of the American Mathematical Society, 436 1990

[25] S. Morita *Geometry of Differential Forms* Translations of Mathematical Monographs, 201 1996

[26] S. Kelly, P. Pujari, H. Xiong *Geometric Mechanics, Dynamics, and Control of Fishlike Swimming in a Planar Ideal Fluid* The IMA Volumes in Mathematics and it Applications Volume 155, p 101-116 2012

[27] H. J. Sussman *A General Theorem on Local Controllability* SIAM Journal on Control and Optimization, 25, p 158-194 1987

[28] Y. Aharonov and J. Anandan *Phase Change During Acyclic Quantum Evolution* Phys Rev. Lett. p. 1598-1596 1987

[29] H. Nijmeijer, A.J. van der Schaft *Nonlinear Dynamical Control Systems* Springer-Verlag 1990

[30] H.J. Sussman *A General Theorem on Local Controllability.* SIAM Journal on Control and Optimization 25(1):158-194 January 1987

[31] W.L. Chow *On Compact Complex Analytic Varieties* Amer. J. Math, 71, p. 893-914 1949

[32] J. Marsden, J. Scheurle *Lagrangian Reduction and the Double Spherical Pendulum* Zeitschrift fur angewandt Mathematik und Physik, 44:17-43, 1993

[33] J. Marsden, J. Scheurle. The Reduced Euler-Lagrange Equations. Fields Institute Communications, 1:139-164,1993

[34] Marsden, J.E., and A. Weinstein [1974] Reduction of Symplectic Manifolds With Symmetry Rep. Math. Phys. 5, p 121-130 1974

[35] E. Cartan *Sur La Representation Geometrique Des Systemes Materiels Non Holonomes.* Atti. Cong. Int Matem. 4, p. 253-261 1928

[36] S. Chaplygin *On the Theory of the Motion of Nonholonomic Systems. Theorem on the Reducting factor.* Mat. Sbornik 28, p 303-314 1911

[37] S. Chaplygin *Analysis of the Dynamics of Nonholonomic Systems* Classical Natural Sciences 1949

[38] S. Kelly *The Mechanics and Control of Robotic Locomotion with Applications to Aquatic Vehicles*. PhD thesis, California Institute of Technology 1998

[39] J. Ostrowski *The Mechanics and Control of Undulatory Robotic Motion* 1996

[40] J. Ostrowski *Reduced Equations for Nonholonomic Mechanical Systems with Dissipative Forces* 1998

[41] S. Crandall, D. Karnopp, E. Kurtz, D Pridmore-Brown *Dynamics of Mechanical and Electromechanical Systems 1968 115*, New York, McGraw-Hill, 1982.

[42] J. Marsden and T. Ratiu *Introduction to Mechanics and Symmetry* Springer 1998

[43] R. Ortega, J.A. Loria Perez, P.J. Nicklasson, H.J. Sira-Ramirez *Passivity-Based Control of Euler-Lagrange Systems* 1st Edition, 1998

[44] A. Bloch *Nonholonomic Mechanics and Control* Springer 2003

[45] A. Bloch, P. Krishnaprasad, J. Marsden, R. Murray *Nonholonomic Mechanical Systems and Symmetry* Archive for Rational Mechanics and Analysis, 136:21-99 1996

[46] M.J. Fairchild, P.M. Hassing, S.D. Kelly, P. Pujari and P. Tallapragada *Single-Input Planar Navigation Via Proportional Heading Control Exploiting Nonholonomic Mechanics and Vortex Shedding* Proceedings of ASME Dynamic Systems and Controls Conference 2011

[47] S.D. Kelly, M.J. Fairchild, P.M. Hassing, and P. Tallapragada *Proportional Heading Angle Control for Planar Navigation: The Chaplygin Beanie and Fish-like Robotic Swimming* Proceedings of the American Control Conference 2012

[48] B. Doolin and C. Martin *Introduction to Differential Geometry for Engineers* Marcel Dekker 1990

[49] J. Ostrowski *Reduced Equations for Nonholonomic Mechanical Systems with Dissipative Forces* 1998

[50] H. Xiong *Geometric Mechanics, Ideal Hydrodynamics, and the Locomotion of Planar Shape-Changing Aquatic Vehicles* 2007

[51] V. Belyayev, V. Zuyev *Hydrodynamic Hypothesis of School Formation in Fishes* Problems of Ichthyology, vol 9, pp. 578-584 1969

[52] B.L. Partridge, T.J. Pitcher *Evidence Against a Hydrodynamic Function of Fish Schools* Nature, vol 279, pp. 418-419 1979

[53] S.D. Kelly, H. Xiong *Controlled Hydrodynamic Interactions in Schooling Aquatic Locomotion* Proceedings of the 44th IEEE Conference on Decision and Control, pp. 3904-3910 2005

[54] L.J. Zhang and J. Eldredge *Hydrodynamics of Undulatory Fish Schooling in Lateral Configurations* arXiv:1003.444lv1 [physics.flu-dyn] 2010

[55] P. Pujari *Energetics and Motion Planning for Free Deformable Hydrofoil in an Ideal Fluid* 2009

[56] M.S. Triantafyllou, G.S. Triantafyllou *An Efficient Swimming Machine* Scientific American, vol 272, p. 64-70 1995

[57] K. Morgansen, B. Triplett, D. Klein *Geometric Methods for Modeling and Control of Free-Swimming Fin-Actuated Underwater Vehicles* IEEE Transactions on Robotics, vol 23, No. 6, p.1184 2007

[58] J Kumph, MS Triantafyllou *A Fast-Starting and Maneuvering Vehicle, the Robopike* Proc. Int. Symp. Seawater Drag Reduction 1998

[59] K. Hirata *Development of experimental fish robot* Sixth International Symposium on Marine Engineering 2000

[60] J Aron *At Sea With the Pollution-Sniffing Robofish* New Scientist Elsevier 2012

[61] S. Kelly, P. Pujari *Propulsive Energy Harvesting by a Fishlike Vehicle in a Vortex Flow: Computational Modeling and Control* Decision and Control (CDC) 49th IEEE Conference on 2010

[62] Michini, Mallory, Larking, Hseih, Forgoston, Yecko *An Experimental Testbed for Multi-Robot Tracking of Manifolds and Coherent Structures in Flows* Proceedings of the ASME 2013 Dynamic Systems and Control Conference 2013

[63] Dazin, Dupont, Stanislas *Experimental Characterization of the Instability of the Vortex Ring. Part I: Linear Phase* Experiments in Fluids, Volume 40, Issue 3, pp 383-399 2006

[64] Richard, Van der Wall, Raffel *Application of PIV Techniques for Rotor Blade Tip Vortex Characterization* Notes on Numerical Fluid Mechanics and Multidisciplinary Design (NNFM) Volume 96, p. 446-453 2008

[65] Cuypers, Maurel, Petitjeans *Characterization of a Turbulent Vortex Using Phase Average PIV Data* Springer Proceedings in Physics, Volume 109, p.65-70 2007

[66] D. Holm, T Schmah, C. Stoica *Geometric Mechanics and Symmetry: From Finite to Infinite Dimensions* Oxford University Press 2009

[67] Cochran, Kanso, Kelly, Xiong, Krstic *Source Seeking for Two Nonholonomic Models of Fish Locomotion* IEEE Transactions on Robotics 25(5):1166-1176 2009

[68] G. Georgiou, J. Cooper, A. Robotham, A. Levers, P. Lunt *Numerical and Experimental Investigation of Aircraft Panel Deformations During Riveting Process* Journal of Manufacturing Science and Engineering, Vol. 137, No. 1 MANU-13-1417 2015

[69] Y. Arman, M. Zor, S. Askoy *Determination of Critical Delamination of Laminated Composite Plates Under Buckling Loads* Composites Science and Technology 2006

[70] L. Yang, Y. Yan, N. Kuang *Experimental and Numerical Investigation of Aramid Fibre Reinforced Laminates Subjected to Low Velocity Impact* Plymer Testing 32 (2013) 1163-1173 2013

[71] Y. Tang, Z. Zhou, S. Pan, J. Xiong, Y. Guo *Mechanical Property and Failure Mechanism of 3D CarbonCarbon Braided Composites Bolted Joints Under Unidirectional Tensile Loading* Materials Design, Volume 65, p. 243-253 2014

[72] Altair *MotionSolve 12.0 Users Guide, p 36* 2013

[73] S. Smale *Topology and Mechanics* Inv. Math., 10:305,331 1970

[74] J. Marsden and A. Weinstein *Reduction of Symplectic Manifolds with Symmetry* Rep. Math. Phys., 5:121 130 1974

[75] K. R. Meyer *Symmetries and Integrals in Mechanics* Dynamical System, p 259-273 Academic Press 1970

[76] R. Abraham and J. Marsden *Foundations of Mechanics* Addison-Wesley Reading, MA, second edition 1978

[77] M. Kummer *On the Construction of the Reduced Phase Space of a Hamiltonian System with Symmetry* Indiana Univ. Math. J., 30:281-291 1981

[78] J. Marsden and J. Ostrowski *Symmetries in Motion: Geometric Foundations of Motion Control* Nonlinear Science Today 1998

[79] R. Murray *Nonlinear Control of Mechanical Systems: A Lagrangian perspective.* IFAC Symposium on Nonlinear Control Systems Design (NOLCOS), p. 378-389 Tahoe City 1995

[80] P. Krishnaprasad and D. Tsakiris *G-snakes: Nonholonomic Kinematic Chains on Lie Groups* Proceedings 33rd IEEE Conf. on Decision and Control, p 2955-2960 Lake Buena Vista, FL 1994

[81] N. Leonard and P. Krishnaprasad *Motion Control of Drift-free, Left-invariant Systems on Lie Groups* IEEE Trans. on Automatic Control, 40(9):1539-1554 1995

[82] J. Ostrowski and J. Burdick *Control of Nonholonomic Mechanical Systems With Symmetry* Proceedins of the IEEE conference on Decision and Control, p. 4317-4320 New Orleans, LA 1995

[83] J. Koiller *Reduction of Some Classical Nonholonomic Systems With Symmetry* Archives for Rational Mechanics and Analysis, 118(2):113-148 1992

[84] L. Bates and J. Sniatycki *Nonholonomic Reduction* Reports on Mathematical Physics, 32:99 115 1993

[85] P. Krishnaprasad and D. Tsakiris *Oscillations, SE(2) Snakes and Motion Control* IEEE Conf. Decision and Control, p. 2806-2811 New Orleans, LA 1995

[86] R. Montgomery *Isoholonomic Problems and Some Applications* Communications in Mathematical Physics 138(3):565-592 1990

[87] J. Ostrowski and J. Burdick *The Geometric Mechanics of Undulatory Robotic Locomotion* International Journal of Robotics Research 1997

[88] B. Ahlborn, D. Harper, R. Blake, D Ahlborn, and M. Cam *Fish Without Footprints* Journal of Theoretical Biology, 148 p.521-533 1991

[89] H. Lamb *Hydrodynamics* Dover, New York 1945

[90] S. Childress *Mechanics of Swimming and Flying* Cambridge University Press 1981

[91] J. Osborne and D. V. Zendov *Steering the Chaplygin Sleigh by a Moving Mass* Proceeding of the 44th IEEE Conference on Decision and Control and European Control Conference, pp. 1114-1118 2005

[92] A. Borisov and I. Mamaev *The Dynamics of a Chaplygin Sleigh* Journal of Applied Mathematics and Mechanics vol. 73, no. 2, pp. 156-161 2009

[93] V. Arnol'd *Sur la Géometrie Differentielle des Groupes de Lie de Dimension Infinie et ses Applications a l'Hydrodynamique des Fluids Parfaits* Annales de l'Institue Fourier, Grenoble, 16(1) p. 319-361 1996

[94] J. Marsden and A. Weinstein *Coadjoint Orbirs, Vortices, and Clebsch Variables for Incompressible Fluids* Physica 7D, p. 305-323 1983

[95] V. Arnol'd *Topological Methods in Hydrodynamics* Springer-Verlag 1998

[96] N. Leonard and J. Marsden *Stability and Drift of Underwater Vehicle Dynamics: Mechanical Systems with Rigid Motion Symmetry* Physica D, 105 p. 130-132 1996

[97] Y. Ozcazanc *Dynamics and Stability of Spacecraft with Fluid-Filled Containers* Ph. D. thesis, University of Maryland 1994

[98] J. Koiller *Note on Coupled Motion of Vortices and Rigid Bodies* Physics Letters A, 120 p. 391-395 1987

[99] Sir. J. Lighthill *Mathematical Biofluiddynamics* SIAM 1975

[100] T. Wu *Hydrodynamics of Swimming of Fishes and Cetaceans* Advances in Applied Mechanics, vol II Academic Press 1971

[101] J. Newman and T Wu *Hydrodynamical Aspects of Fish Swimming* Swimming and Flying in Nature, p. 615-634 1974

[102] C. Hemelrijk, D. Reid, H. Hildenbrandt, J. Padding *The Increased Efficiency of Fish Swimming In a School* Fish and Fisheries 2014

[103] H. Smit, J. Amelink-Koutstaal, J. Vijverberg, J. Von Vaupel-Klein *Oxygen Consumption and Efficiency of Swimming Goldfish* Comparative Biochemistry and Physiology, Part A: Physiology, vol. 39, issue 1, p. 1-28 1971

[104] M. Ruffo *GhostSwimmer: Tactically Relevant, Biomimetically Inspired, Silent, Highly Efficient and Maneuverable Autonomous Underwater Vehicle* ONR STTR N08-030, US Navy 2010

[105] T. Dear, S. Kelly, M. Travers, H. Choset *Mechanics and Control of a Terrestrial Vehicle Exploiting a Nonholonomic Constraint for Fishlike Locomotion* ASME 2013 Dynamic Systems and Control Conference

[106] J. Marsden and T. Hughes *Mathematical Foundations of Elasticity* Dover Publications, New York 1983

[107] M. West *Variational Integrators* Ph. D thesis, California Institute of Technology 2003

[108] M. Leok *Foundations of Computational Geometric Mechanics* Ph. D thesis, California Institute of Technology 2004

[109] J. Arora *Introduction to Optimum Design* Elsevier Academic Press 2004

[110] Neimark and Fufaev *Dynamics of Nonholonomic Systems* Translations of Mathematical Monographs, 233 1972